UNIVERSITY OF SOUTHAMPTON

FACULTY OF ENGINEERING AND THE ENVIRONMENT

School of Engineering Sciences

Multiphase Computational Modelling of Particle-Flow Interactions in Plasma Spraying Processes

by

Konstantinos Koutsakis

Thesis for the degree of Doctor of Philosophy

May, 2017

UNIVERSITY OF SOUTHAMPTON

ABSTRACT

FACULTY OF THE ENGINEERING AND THE ENVIRONMENT

Computational Fluid Dynamics

Thesis for the degree of Doctor of Philosophy

MULTIPHASE COMPUTATIONAL MODELLING OF PARTICLE-FLOW INTERACTIONS IN PLASMA SPRAYING PROCESSES

By Konstantinos Koutsakis

The current work looks at the challenges of developing a computational solution for the modelling of the plasma spraying industrial process. A set of three 3D Computational Fluid Dynamics (CFD) models were developed and studied for this purpose. The first model that was implemented looks at the effects the electromagnetic properties have in the properties of the plasma flow in the nozzle of the spraying device. The second model studies the particle in flight atomisation after coding the thermal exchanges in the C++ framework and compares the results with experimental data. The third model studies the particle in-flight atomisation of molten metals and their resulting size distribution. The computational results from the first model agree with contemporary work analysing flows in nozzles of plasma spraying equipment. It also provides quantification of the additional energy exchanges that occur in the nozzle of a plasma spraying device, which are the ones that produce the gradients in velocity and temperature, which are met in plasma spraying processes. Finally, it looks into the effect the presence of dielectric may have on the plasma arc. The second model compares well with experimental data acquired by multiphase flows produced from plasma spraying devices and supports the finding that the Weber number is a good indicator of the deformation patterns of fluid particles, even liquid metal, where the density is much higher than regular liquids. The results of the third model in regards to particle size distribution show agreement with theoretical models of the distribution. The three models can be combined in the order presented, to provide a computational modelling solution which can cover the industrial application of the plasma spraying process, from the nozzle, to finer atomisation, to splat.

Table of Contents

List of Figures

DECLARATION OF AUTHORSHIP

I, Konstantinos Koutsakis declare that this thesis and the work presented in it are my own and have been generated by me as the result of my own original research.

Multiphase Computational Modelling of Particle-Flow Interactions in Plasma Spraying Processes

I confirm that:

1. This work was done wholly or mainly while in candidature for a research degree at this University;
2. Where any part of this thesis has previously been submitted for a degree or any other qualification at this University or any other institution, this has been clearly stated;
3. Where I have consulted the published work of others, this is always clearly attributed;
4. Where I have quoted from the work of others, the source is always given. With the exception of such quotations, this thesis is entirely my own work;
5. I have acknowledged all main sources of help;
6. Where the thesis is based on work done by myself jointly with others, I have made clear exactly what was done by others and what I have contributed myself;
7. Parts of this work have been published as:
   (Koutsakis, Gu, & Vardelle, 2013) (Koutsakis, Shrimpton, & Gu, 2016)

Signed: .....

Date:.....

Acknowledgements

I would like to thank my supervisor, Professor Sai Gu, for his invaluable support throughout my work in the University of Southampton.

My sincerest thanks to Professor Philippa Reed for her help, which played a catalytic role in the progression of this work. I would also like to show my deep appreciation to my examiners, Dr Tanvir Hussain from the University of Nottingham and Professor John Shrimpton from the University of Southampton.

The work towards this thesis, like all PhD theses, was a personal, long term commitment towards a scientific goal. The outcome and purpose of the goal was largely unknown during its inception. It has been a mini life journey with many actors and figures, most of which played an important part, be it out of good will, inadvertently, or by chance.

I especially appreciate Armelle Vardelle and Michel Vardelle who approached me in the University of Limoges and provided scientific input, help and encouragement with enthusiasm and genuine interest.

Thanks also extend to Kostas Papadikis, who during our time in the University of Southampton provided valuable insight on scientific matters. I would also like to extend salutations to all my friends and co-workers in room 1051, Building 25 in the University of Southampton: Jörn, Hani, Lindsay, Nanda, Nanhang, Ruben. Likewise, I am glad to acknowledge my colleagues at Lloyd's Register at the Global Technology Centre at Boldrewood Campus.

I would like to exclaim special recognition and a big thank you to my family, my mother in particular, for their endless support towards my career far from home. Additionally, my deepest appreciation and love to my inspiring partner, Shirley.

And finally, my biggest thank you to all my friends who have always been an invaluable support system in all respects.

Nomenclature

Dimensionless Numbers

Re	Reynolds Number
We	Weber Number

Greek

α	Volume fraction	$-$
α_t	Diffusion coefficient	m^2/s
$\boldsymbol{\delta}$	Unitary operator	
ε	Relative permittivity	$-$
κ	Curvature	m^{-1}
λ_D	Debye length	m
μ	Dynamic viscosity	$kg/(m \cdot s)$
μ_0	Magnetic permeability	NA^{-2}
ν	Kinematic viscosity	m^2/s
ρ	Volumetric mass density	kg/m^3
ρ_q	Charge density	C/m^3
σ	Surface tension	N/m
σ_m	Electric conductivity	$mA^2\Omega/N$
$\overleftrightarrow{\tau}$	Strain tensor	
φ_u	Compressible flow through the cell faces	kg/s
φ_E	Numeric electric potential	J/C
Φ	Numeric electric potential	J/C

ψ	Compressibility	s^2/m^2

Roman

A	Magnetic vector potential	$T \cdot m$
$\vec{B}$	Magnetic field	T
C_p	Specific heat capacity at constant pressure	J/K
d	Particle diameter	m
$\vec{E}$	Electric field	$kg \cdot m \cdot s^{-3} \cdot A^{-1}$
eV	Electron-volt	
$\vec{F}$	Force	$kg \cdot m \cdot s^{-2}$
$\overrightarrow{F_L}$	Lorentz force	$kg \cdot m \cdot s^{-2}$
$\overrightarrow{F_s}$	Surface tension	N/m
g	Acceleration of gravity	$m \cdot s^{-2}$
H	Enthalpy	J
$\vec{J}$	Current density	A/m^2
k_B	Boltzmann constant	$1.38 \times 10^{-23}\, m^2 \cdot kg \cdot\ s^{-2} \cdot K^{-1}$
KE	Kinetic energy	J
$\vec{n}$	Vector normal	
p	Pressure	$kg \cdot m^{-1} \cdot s^{-2}$
q	Electric charge	C
t	Time	s
T	Absolute temperature	K

$\vec{u}$	Velocity	$m \cdot s^{-1}$
$\overrightarrow{u_r}$	Artificial velocity	$m \cdot s^{-1}$

Subscripts

Ar	Of argon
Cu	Of copper
e	Of the electrons
i	Of the ions
lam	Laminar
n	Of neutrals
Rel	Relative quantity

Superscript

$\boldsymbol{T}$	Transpose

Acronyms

1D	One-Dimensional
2D	Two-Dimensional
3D	Three-Dimensional
APS	Atmospheric Plasma Spraying
CAPS	Controlled Atmosphere Plasma Spraying
CFD	Computational Fluid Dynamics
DC	Direct Current
FEA	Finite Element Analysis
FEM	Finite element method
FORTRAN	Formula Translating System
GPL	GNU Public License
GS	Gas Stabilised
HVOF	High-Velocity Oxy Fuel
LTE	Local Thermal Equilibrium
MHD	Magneto-Hydro-Dynamic
OpenFOAM	Open Field Operation and Manipulation
PHOENICS	Parabolic Hyperbolic Or Elliptic Numerical Integration Code Series,
PIC	Particle-in-cell
PIMPLE	PISO-SIMPLE
PISO	Pressure Implicit with Splitting of Operators

PSP	Plasma Spraying Process(es)
RF	Radio Frequency
SIMPLE	Semi-Implicit Method for Pressure-Linked Equations
Tokamak	Toroidal Chamber with Magnetic Coils
UDF	User Defined Function
VOF	Volume of Fluid
VPS	Vacuum Plasma Spraying
WS	Water Stabilised

Chapter 1: Introduction

1.1 Important Uses of Plasma Sprays

Plasma spraying is a branch of the industrial process of thermal spraying. Thermal spraying as a term is used to identify the industrial spraying process that is used to spray heated material onto surfaces in order to produce coatings with the purpose of attribute enhancement. It involves a spraying device which is called a spraying gun, the spraying gas, the sprayed substance and the surface to be enhanced. Similarly plasma spraying is the thermal spraying process which is used to deposit coating material on various surfaces where the working gas is considered to be in a plasma state. As an indication of its value, the sales of equipment, products and services to end users produced sales to the market of Direct Current (DC) atmospheric spraying only, that in 2004 reached $2.25 billion (Heiman, 2008).

Plasma spraying can have diverse materials as the spraying substance. Metal, composites, ceramics and polymers are, amongst others, the main types of materials used. The different types of materials which can be used demonstrate that plasma spraying can provide applications with diverse usability and scope and its flexibility has benefited the industry since it provides an adjustable and adaptable process that can enhance materials by engineering surface properties onto them.

By spraying the coating material on surfaces, the process can add new properties to the surface, enhance current properties of materials or simply alter them. The properties of interest can be thermal conductivity, reflectivity, biodegradability for biomedical applications, etc. The produced surfaces demonstrate properties which engineers can reproduce on an industrial level with consistency and without the

uncertainty of unpredictable new properties blending in. This is mainly based on the fact that most applications have already provided information, by research, modelling and experimentation, which helped establish methods and patterns for the industrial practice. Finally, on the mercantile level, the advantage of coating a thin layer on a surface rather than manufacturing the whole part from bulk provides a serious advantage in flexibility and economic viability of novel applications. Those three factors together have provided a basis for a strong industry which can also have the liberty of having a greenfield approach in scope each time a new controllable parameter is added into the picture.

Plasma Spraying refers to the Thermal Spraying technology in which the carrier gas is partially or completely in plasma state. The substrate enters the direction of the plasma gas flow, where it is melted (if not in a liquid state before), entrained and deposited on the surface to be coated. Any type of material with a well-defined melting point, like metals, can be used as a substrate. Common applications also include ceramic and polymer substances (Heiman, 2008). The substrate can be in powder or liquid form and its state and properties are characterised by the energy exchanges between substrate and spraying device. At the first stage, the energy transfer takes place from the potential electric field to the spraying gas, in the device nozzle. The electric potential field ionises the gas, which is set in motion by the spraying apparatus, up to the point where it is turned into plasma gas. This deposition of energy enables the gas to transfer thermal energy to the substrate, while kinetic energy is obtained mostly from the gas motion. Thermal and kinetic energy is deposited on the spraying surface which is coated gradually. The particles can be solid, molten or in semi-molten state when they reach the surface.

1.2 Modelling Plasma Sprays

One of the areas that was met with this increase in interest for modelling is the industrial application of thermal spraying since it could provide the industry with an insight to the inner workings of the different thermal spraying processes used and also help optimise the process itself. Optimisations are in fact actively sought, since thermal spraying processes in general, are considered effective at a deposition rate of 50%. Therefore, there is a clear indication that there can be plenty of room for improvement (Richard, 2011). Plasma spraying in particular was also the focus of academic and industrial research, where the more complex dynamics of a MagnetoHydroDynamical (MHD) system have been probed in order to give more details about how this process could be altered for more efficiency.

The present work looks into thermal spraying processes from a modelling approach with some special focus on plasma spraying. The details of parameters and interactions associated with such processes have been and will continue to be the subject of research; the present work tries to look into the process in parts by dividing it and as a whole, by recursively confirming agreement with the results from the sub-processes produced by division. In the end, it attempts to look into the usefulness of measuring the complexity of models for relevant systems. While it provides results and critique, it also provides information on the obstacles currently faced and how they can be lifted. In this introductory chapter, a basic overview of the plasma spraying gun technology is provided; the aim and the objectives of the research are set followed by the scope and structure of the text. A connection with past work is made with an overview of current applications of thermal spraying and its CFD approaches. It then moves onto the

current work that is done which is related to the field of thermal and plasma spraying. It then defines the scope of this thesis and finally it gives an overview of its structure.

The purpose of this work is to study the modelling of the plasma spraying process as a whole. With the use of similar, but diversified models, an attempt to cover different parts of the process is made with the aim to extract data which is useful for qualitative analysis of the inner workings. Since the quality of the process is measured by the quality of the coating, the sprayed substance behaviour is examined. Additionally, distinctive in the plasma spraying process is the use of gas brought in a plasma state and for this reason, the process is also examining the interactions in the nozzle. The targeted areas are the spraying nozzle of the plasma spraying equipment, the heat transfer in the sprayed particles and their entrainment and atomisation.

1.3 Basic Overview of Spray Gun Technology

Plasma spraying applications can be distinguished by the method of plasma generation into ones where the plasma is created by DC or Radio Frequency (RF) by coil induction. In terms of the medium which during the process obtains plasma attributes, it can be gas (Gas Stabilised), where usually noble gases with low atomic weight are used (Helium, Argon), or liquid, where water is used (Water Stabilised). In terms of the environment where the process takes place, it may be Vacuum Plasma Spraying, Atmospheric Plasma Spraying or Controlled Atmosphere Plasma Spraying where additional applications of high and low pressure are realised. These are explored further in Chapter 2. Finally, the way the substrate is added into the plasma provides additional capabilities and applications, where it can be liquid fed into the plasma flow, or powder that is heated, melted and entrained before deposition.

The main CFD suites or toolkits can be combinations of free, open source, closed source, commercial or proprietary. Some are mentioned here, in no particular order: Code Saturne, OpenFOAM, ANSYS Fluent, COMSOL Multiphysics, STARCCM+. Furthermore, other toolkits have been developed independently by research groups worldwide. Along with the adaptability of the thermal spraying processes themselves, research has been adopting and evolving to focus on current interests and has diversified to a level where only the basic methodologies regardless of the tools and approach are established. The particulars regarding the focus of research though, lie onto the decisions of each individual research group. So, based on their interests, they adopt and develop methods and tools, identify their particular fields of desired work, and concentrate on features of significance.

The previous approach of dealing with the modelling of the physical processes in thermal spraying applications has mainly been the use of simplified models and the focus on individual elements of the process. This is common, with examples of focus being the plasma arc stabilisation, the plasma creation, the characteristics of the plasma flow or the electrical energy transfer of the arc (Chang & Ramshaw, 1994), (Chang J. a., 1992), (Karthikeyan, Berndt, Tikkanen, Reddy, & Herman, 1997). 3D models have appeared later since it was initially difficult to couple and calculate some properties in space without approximations on many different levels. Generally the norm has been individual focus on small areas of interest and models covering theoretical approaches. While collective insight can be gained on various aspects of the process, it has not been easy to identify solutions with broad scope, such as the complete coverage of a thermal spraying process, for reasons explained in the final part of this chapter.

Current work attempts to gradually incorporate different quantifiable parameters to the modelling of thermal spraying. The aim is to produce a solution that enables the study of the process that can be adaptable in focus area and complexity. The additions of different elements that are taken into account each time are discussed and their effects analysed. Then, a comparison with experimental data and the potential validation is discussed and finally a model of greater complexity is introduced and studied. Finally, the effects of increased complexity are studied and the results are used to support the claim that the increased complexity itself is limiting with the current approach. The limitations though are also useful as they provide an insight into specific areas of modelling where complexity is reduced. This enables comparisons with results of previous modelling systems to be made and also indicates in which areas further work can focus, in order to improve the available tools. Finally it identifies what other changes the future is likely to bring that will make modelling of the process more scalable and complete without sacrificing in scope.

1.3.1 Components

In the past years many different plasma torches have been used for spraying, with the main differentiation being between RF and DC torches. Either, RF or DC, provide the extra energy required to turn the carrier gas into plasma state. This work is examining the nozzle of a DC plasma gun. RF torches will be briefly mentioned to present an alternative industrial method in plasma creation, but DC torches will be examined further. In a DC torch, the main components are the anode, the cathode and the nozzle. Figure 1.1 shows a schematic of this configuration.

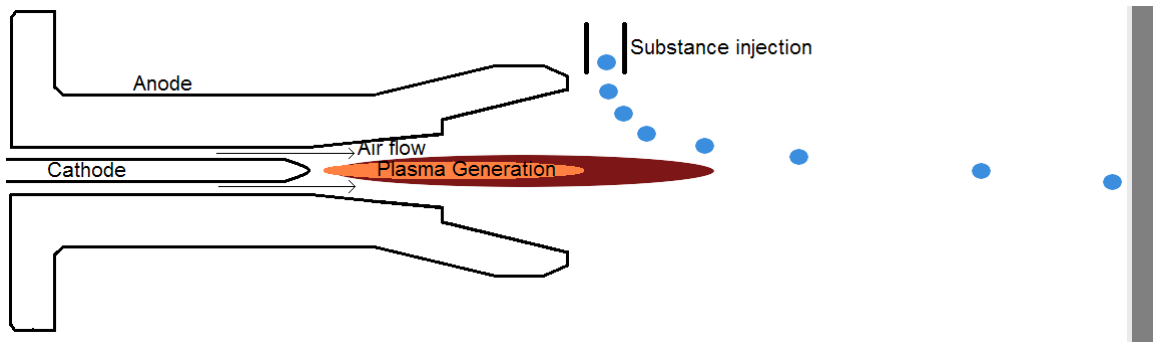

Figure 1.1: Schematic of a basic DC plasma gun configuration.

The main distinguishing principles in the plasma spraying application is bringing the working gas in a plasma state and use it to transfer energy rapidly into the sprayed substance in order to melt it. For this reason the torch configuration is engineered to deposit additional energy on the gas while it is accelerated in a nozzle.

1.3.2 Operation

The gas used in plasma spraying applications can be any, but noble gases are preferred for their capability of being inert and not interacting aggressively with the environment in a plasma state. The most commonly used gas Argon, due to the easier plasma creation and safety (Suryanarayanan, 1993), but combinations of Ar, He, H_2, N_2 are also used. An $Ar - H_2$ mixture is often used because hydrogen increases both the specific enthalpy and thermal conductivity of the plasma flow, especially in temperatures above $3000K$ (Fauchais, 2004).

In RF torches, the energy of the torch creates a glow discharge in a coil which becomes an arc discharge (Davis, 2004) where a glow to arc transition occurs in less than 10^{-7} seconds and voltage drops significantly while the gas absorbs the energy and turns into plasma. In DC torches the arc is created by two electrodes that form a part of the gun. They create the plasma which can have temperatures up to $20{,}000K$ (Dugdale, 1966). In RF torches, plasma is created inside the gun by an induction coil and then through a

nozzle into the environment where it entrains the particles which can either be in powder form or fed through wires of different potential which melt where they meet, normally in front or inside the nozzle. DC torches' electrodes are essentially a central cathode resembling a thick nail in the centre (Figure 1.1), which is surrounded by the anode that also plays the part of the nozzle. The voltage between them varies from $30V$ to $500V$ for power torches, with $50 - 80V$ around the average value and the torches can produce arc currents from $300 - 1000A$ (Fauchais, 2004). The gas enters the anode from one or two chambers that are positioned opposite to each other and once they flow at a minimum velocity specific to the torch, swirling of the gas around the cathode occurs, which is an important factor for the creation of plasma in the nozzle (Westhoff & Szekely, 1991). The gas then flows through the nozzle and meets and entrains the spraying substance which is usually in powder form at microscale and above and is fed to the plasma flow just outside the nozzle (Fauchais, et al., 1992). Another important aspect to the efficiency of spraying is the velocity of the powder and many commercial applications inject the powder through some secondary carrier gas so the particles can reach a velocity which gives between high deposition rates and entrainment efficiency.

1.3.3 Operational Challenges

The plasma spraying process is considered simple and versatile in its application in an industrial environment, but its main challenge lies in the quantification of the parameters and the complexity of the physical principles (Herman, et al., 1993). The parameters of the plasma such as temperature, heat capacity, velocity interdependently influence the process. In order to produce a coating with the required material properties, the plasma parameters, have to be carefully chosen and

applied. For this reason, automation of the process using robotics is often applied to reduce fluctuations of the parameters based on human factor (Heiman, 2008). Modelling of the process prior to its actual application is also employed, where the challenge is the modelling of the complex physical system in a way that correlates initial plasma conditions, to coating quality, which is the purpose of the current work.

1.3.4 Interactions and Unknowns

The plasma spraying process is an industrial, controlled process and as such the significant parameters are controlled by the engineered configuration. The controlling parameters are:

- Cathode to anode voltage controls the current between them.
- Cathode to anode current can control plasma temperature.
- Plasma gas temperature can be used to control the heat deposition on the particles.
- The nozzle shape and gas feed rate control gas velocity.
- Particle feed rate and size control heat rate deposition on it.
- The spraying distance can control in-flight particle time.
- Gas velocity also controls in-flight particle time.
- Gas velocity controls molten particle atomisation patterns.
- In-flight particle time controls whether the particle is in a molten or semi-molten state when it reaches the spraying surface.
- The state of the particle when it reaches the spraying surface controls if there will be a splat on the surface.
- The velocity and shape of the particle when molten controls the type of splat that will impact on the surface.

- The types of splat collectively, control the porosity and solidification of the sum of the sprayed material on the surface.
- The splat formation controls the quality of the produced surface.

1.4 Aim of Research

The aim of this work is to identify controlling parameters that can address industrial questions between the interactions of the dynamic system of plasma spraying. A simple dynamic system can have complex, even chaotic results, and for this reason there is a need to identify the controlling parameters and quantify the interactions between the layers of modelling sub-processes. The numerical analysis can produce results and evaluate them with the help of theoretical models to cover the unknown parameters. In this work, the domain of the system is split into three areas, so each model for the sub-process must produce useful results to provide initial and boundary conditions for the subsequent models.

The identified missing parameters from research are the plasma formation in the presence of a metal particle close to the plasma generation, the patterns of atomisation of molten particles and the particle size distribution of atomised particles when they reach the spraying surface. Combining these as a set of quantifiable models can provide information on optimising the procedure by using a minimal set of controlling parameters.

This work is using three Computational Fluid Dynamics solvers to study a generic plasma spraying system. The models are designed to be able to examine the energy creation and deposition on the particle, the heat transfer, the atomisation of particles based on heat transfer and the atomisation patterns of particles on the microscale.

1.5 Specific Objectives of the Research

The set of three models in this work was chosen and developed to be able to cover the plasma spraying process for a generic DC torch, gas and substance. It then can be used to model the process numerically providing results for the coating quality.

The first area of focus is the nozzle where the energy deposition, from the plasma arc, to the gas, creates very high velocities compared to other thermal spraying processes. The resulting velocities and temperatures will be used as initial conditions for the second model, which studies the atomisation of heated particles during their entrainment. This model also provides initial velocity conditions for the last model which looks at droplet break up pattern for the kinetic regime in that state. It becomes clear that one main objective of the research is to provide initial conditions for the subsequent multiphase models covering the whole plasma spraying process.

The second area of focus is the heat transfer on particles and their state and shape during entrainment. With the initial conditions covered in the first model, results for the atomisation patterns exhibited by droplets can be obtained. Additionally, the energy equation accounts for the heat transfer in the particles, so another objective of this work is to determine if particles are in a molten state.

The last area of focus is to validate the tools and expand the domain in order to cover an extended spraying distance. The Volume of Fluid (VOF) interface capturing method used is studied carefully and its iterative application produces results for the mesh refinement. Therefore a final objective of this work is to validate the tools and determine the mesh parameters for a domain that is able to cover atomisation patterns on the microscale.

1.6 Plan of the Thesis

This thesis focuses on the analysis of results of three different 3D CFD models that with valid hypotheses and sustainable assumptions try to provide useful information on the study of the plasma spraying process. It also pinpoints the current limiting factors and addresses why it is still not possible to have a cost effective modelling analysis of plasma spraying which could cover the totality of the process. It is common to use the phrase "nowadays, with the increase of computational power", but it is shown that with computational power increasing, model complexity increases equally and is pushed to the boundary. As a result, the researcher has still to balance between accuracy, domain size and amount of data produced.

From the computer science point of view, the computational tools used, provide valid algorithmic construction and solution for the employed numerical methods. Hence, the modelling solution is not a case of using computational power to brute force the results out of the model, but the proper algorithmic construction of the problem can be used to identify and highlight the limitations of current technology and systems implementation (Leiserson, Stein, Rivest, & Cormen, 2009). This is not an anathema, but a window to explore and appreciate alternatives or focus on specifics, which in themselves may give comprehensive vision of the inner workings or sub-processes of the studied process. It may also provide valuable information on the constructional elements of the parameters identifying the model.

The thesis is organised in 8 parts. The first part is this introduction. Following, is some theoretical background of Plasma Physics, useful in understanding the modelling of the plasma spraying process. Next, a critical review of the current literature and after that, the presentation of the work done towards modelling and studying the plasma

spraying process is presented. It consists of three different models, in their respective chapters, with an increasing number of parameters which are taken into account for each model. On the 7th part, the collective conclusions of the three models are presented. The limitations and obstacles into analysing the complete process are discussed on that part as well. Finally, on the last, eighth part, a summary is provided and areas of focus for future work are identified and proposed.

Chapter 2: Literature Survey

This part of the thesis is focused on the past and current literature regarding the plasma spraying process. It is believed that by separating the review of the literature in categories can help quantify the information and give a clear picture of the different permutations of the process that research has been carried through. This way, patterns can emerge and a clear view of the successes and challenges can be obtained.

2.1 Technological Background of Plasma Sprays

2.1.1 Common Plasma Spraying Parameters

Usually, three subsystems constitute the plasma spraying process, which researchers mostly examine separately:

- The plasma formation inside the plasma torch,
- the sprayed particles and their injection and their parameters' estimation (velocity, diameter, temperature, melting rate, size distribution) at impact,
- the splat formation, splat layering and the coating formation on the desired surface (Fauchais, 2004).

The elements that characterise the plasma spraying process are mostly common with small differentiations between different processes. The system is consisted of an electrical energy source the power of which can be controlled. At the same location, the gas through a feeder is put into motion by controlling the pressure in a nozzle. The combination of the two elements above is usually a nozzle of which the walls are wired to form an anode and a cylindrical interior protrusion which forms a cathode. The gas feed rate, the pressure and the nozzle shape control the velocity of the gas. The power

of the electrical energy source controls the plasma production rate and the temperature of the gas. The working substance is introduced at the flow at the exterior of the nozzle. Thus, it is heated, melted and entrained into the gas path. The velocity determines the atomisation of the molten substance and the resulting particles' entrainment, while the gas temperature determines the ratio of molten particles over the sum of particles produced by atomisation.

The gas used in plasma spraying applications is mostly Argon, due to the easier plasma creation and safety (Suryanarayanan, 1993), but combinations of Ar, He, H_2, N_2 are also used. An $Ar - H_2$ mixture is often in operation because hydrogen increases both the specific enthalpy and thermal conductivity of the plasma flow, especially in temperatures above $3000K$ (Fauchais, 2004).

An important aspect that determines the efficiency of spraying is the velocity of the powder. Some commercial applications let the powder drop into the flow via the gravitational acceleration. Many applications inject the powder through some secondary carrier gas so the particles can reach a velocity which compromises between high deposition rates and entrainment efficiency.

In the past years many different plasma torches have been used for spraying, with the main differentiation being between RF and DC torches. Either, RF or DC, provide the extra energy required to turn the carrier gas into plasma state. The research presented in the current work studies a DC Plasma spraying configuration. For the sake of completeness and establishment of the basic theoretical ideas behind plasma creation, RF plasmas will be mentioned. Additionally, different spraying configurations will be looked at to establish the research possibilities with the challenges for each approach.

2.1.2 DC Plasma Spraying

In DC torches the arc is created by two electrodes, a cathode and an anode, that form a part of the plasma spraying device. The electrical current that is created between the anode and the cathode creates the plasma which can have temperatures up to $20{,}000K$ (Dugdale, 1966). DC torches' electrodes are essentially a central cathode resembling a thick nail in the centre, which is enclosed loosely by a wall which is the anode. The wall, also serves as the exterior part of the nozzle. The voltage between them varies from $30V$ to $500V$ for power torches, with $50 - 80V$ around the average value and the torches can produce arc currents from $300 - 1000A$ (Fauchais, 2004). The gas enters the anode from one or two chambers that are positioned opposite to each other and once they flow at a minimum velocity specific to the torch, swirling of the gas around the cathode occurs, which is an important factor the creation of plasma in the nozzle (Westhoff & Szekely, 1991). The gas then flows out through the nozzle and meets and entrains the spraying substance which is usually in powder form at microscale and above and is fed to the plasma flow just outside the nozzle (Fauchais, Coudert, Vardelle, Vardelle, & Denoirjean, 1992).

2.1.3 RF Plasma Spraying

The energy of a RF torch creates a glow discharge in its coil which becomes an arc discharge (Davis, 2004) where a glow to arc transition occurs in less than 10^{-7} seconds and voltage drops significantly while the gas absorbs the energy and turns into plasma. In RF torches, plasma is created inside the spraying apparatus by an induction coil and then through a nozzle into the environment where it entrains the particles which can either be in powder form or fed through wires of different potential which melt where they meet, normally in front or inside the nozzle.

2.1.4 Controlled Atmospheric Plasma Spraying

Controlled Atmospheric Plasma Spraying is the plasma spraying method where the whole spraying configuration is located in a chamber where near vacuum pressures are maintained throughout its operation.

The modelling of controlled plasma flows provides the benefit of them being isolated in a sense that enables omission of parameters that would otherwise affect the process. Or sometimes, the extreme circumstances that are created by the control of the environment can create special cases where approximations can be made, that benefit the modelling approach. This is mainly supported by the atmospheric pressure of the environment being the one of vacuum (Zhao, et al., 2000). The advantage of the application is the simplicity of the environment which reduces the parameters under consideration enabling an easier to control procedure and process with easier to reproduce results. It also enables easier modelling where there is no need to consider multiphase gases and their interactions with the environmental air. Furthermore, the parameters of the isolated environment are measurable and dictate the parameters and initial conditions of the modelling environment. The disadvantages of the process are that it is difficult to set up as there is always a requirement for a physical barrier to be in place for the whole spraying system. There is also a requirement for additional equipment to be installed for the vacuum production. The above makes a Controlled Atmospheric Plasma Spraying challenging to produce, set up and transport.

2.1.5 Atmospheric (or Air) Plasma Spraying

The Atmospheric Plasma Spraying is the plasma spraying process where the configuration is operated in a controlled, but natural environment.

This is an expansion of controlled atmosphere modelling where the process happens in a natural environment where the carrier gas is atmospheric air. The benefit of this approach is that the ambient gas of this environment is studied extensively so the behavioural parameters can be easily obtained and several types of approximations and tested hypotheses are available to fit into the model. This process doesn't have the disadvantages of requiring a heavily controlled and moderated environment which utilises a physical barrier between the spraying configuration and the environment, therefore it is easier to set up and maintain. The atmospheric air effects are present, but they are usually considered minimal and neglected in modelling without considering multiphase flows, as it is assumed that the gas is not affected by the atmospheric air.

The current work will be looking at a DC plasma spraying configuration. This configuration demonstrates plasma creation directly via a current between the anode and the cathode of the plasma spraying device. The selected framework for the numerical solution enables a direct incorporation of a set of magnetohydrodynamics equations in the solution, derived from Maxwell's equations. The common element in the above is the electrical current which can be described theoretically, observed experimentally and solved numerically. It can also be a coupling element of the MHD with the fluid dynamics solution. This identification led to the selection of a DC plasma as the focus of this work.

2.2 Thermal Spray and Plasma Modelling

The plasma state is still under research as a physical state. Interest is high from both an experimental and modelling point of view, since all interactions have not been described in theoretical models until recently. Additionally there is still the need to

determine the extent of the various physical interactions in plasma creation on different scales. This makes modelling difficult since the analytical description of plasma interactions cannot be covered by a neat all-inclusive set of equations that can be streamlined easily into simple numerical methods. This creates the need in modelling, for large and fine domains, at which a solution of many complex and coupled equations is applied. A different route that one can take for the numerical modelling for each scale, is limiting the scope of the domain to focus on particular areas of the model. There is also the capability to apply different approaches to every possible different phenomenon of the deluge of phenomena present in plasma.

As a result, the first era of plasma simulations dealt with simpler problems, while the numerical modelling approaches were varying. Utsumi, Cunugi and Coga proposed a method for solving the Vlasov-Poisson equation in one dimension by numerically integrating on a grid cell, by using the distribution function and reconstructing the phase space (Utsumi, et al., 1998). Medlin, Morrow and Fletcher applied a pseudo-transient method for the calculation of the electric coronas on High Voltage power transmission lines (Medlin, Morrowb, & Fletchera, 1998).

From the early 2000s, CFD methods as we know them today started making their appearance on the study of plasma flows in the thermal spraying context. The work of Zhang, Gawne and Liu studied the in-flight behaviour of sprayed particles from a plasma gun and proposed methods for controlling the flow parameters (Zhang et al., 2000). In the same year, they linked the velocity and temperature of the nozzle accelerating a plasma jet, to the operational parameters of the spraying device at the outlet of their domain in order to avoid using a method that involves physicochemical

interactions (Liu, et al., 2000). Agreement with experiments which recorded similar outcomes provided validation to their results.

The globally on-growing value of the industrial thermal spray applications, along with the introduction of plasma spraying as a method and its proven effectiveness in practice, attracted more and more interest in its research. There were many technical challenges which needed to be addressed, from which some are named: the efficiency of the procedure, establishment of best practices, variations in spraying velocity, spraying substance, spraying environment, plasma gas, and plasma formation. Ideally, under challenges like these, one would be looking for tools that can help optimise the largest part of the process possible. As knowledge from research grows, and more complex systems for numerical simulations are being built, more parameters of the physical process are included in the model and the limitations make their appearance. The process though, even in analytical terms, is complex with many different factors affecting it synergistically (Heiman, 2008). Modelling every step of the process accurately would require infinite resources, so in that view, literature has been studying the process using approximations, simplifications and focusing on different areas or interactions of it. Computer power and disposable time are finite, hence the complexity and size of the domain pose a fundamental limitation on the depth at which the process can be examined. The next part will try to identify this separation of concerns in modelling plasma spraying, as it is believed that it will enable identification of the achievements and breakthroughs but also the recognition of the obstacles in modelling, while identifying the limitations that each method has.

2.3 Focus of Modelling Approach

The modelling of plasma spraying applications have to consider either multiphase flows for the plasma elements representation or the mixtures of gases. Another approach is to revise the equations of the flow regime to include plasma properties in order to factor for plasma attributes more accurately. MHD models use the latter where they introduce additional equations to solve for the electromagnetic interactions, coupled with the preexisting fluid dynamics system of equations. The gas interaction with sprayed substance is an additional enquiry, adding more complexity to the model (Meillot E. et al., 2013). If its calculation also requires the simultaneous study of the particle deformation, the VOF method can be used, but one of its limitations is that the VOF does not provide heat transfer on the phases, rather than on the densities per phase, so alterations on the VOF model should be considered. The additional solution for an interface tracking model is one challenge in CFD research for thermal spraying.

The literature on CFD simulations of plasma spraying puts the plasma spraying device in a domain solving for a set of equations with assumptions and approximations that enable the models to work while providing accurate results. The modelling applications also bear limitations in domain size or area of focus; hence many models cannot have a broad use, especially when they are designed specifically for a part of the total geometry. The literature trend in the 2010s is to present results more oriented in the electromagnetic properties of plasmas, which is especially the case in scientific journals focusing on Physics. In most models local thermal equilibrium (LTE) for the plasma is assumed, same notion as the plasma approximation, which is unknown if can be completely valid near the cathode tip because it is the area where the

electromagnetic energy exchanges originate from. For instance, recent publications assume LTE in thin argon plasmas and incompressible laminar flow, without any turbulence effects (Ghedin et al., 2003), (Chau et al., 2006), (Chen & Li, 2001), which demonstrates the types of assumptions that are considered in modelling. The assumption for LTE is the most common one, but it would be beneficial to establish the limits of the assumption for future research.

Many CFD plasma models are axisymmetrical or developed for two-dimensions (Ramshaw & Chang, 1992), (Garimella, Schlitz, & Chan, 1999), (Delalondre, Simonin, Kaddani, & Zahrai, 1999), (Chang & Ramshaw, 1994) or are solutions on the steady state (Mariaux & Vardelle, 2005). Axisymmetrical models extrapolate the solution in areas of the domain that have not been solved. For the full effect of the MHD forces, where the external product of quantities is ever present, a 3D solution should be better considered. Axisymmetrical, steady state and 2D solutions require a solid determination of where the results stop being useful. Producing a fully 3D, MHD solution is another challenge for plasma modelling research in both the foundation of the system of equations as well as for the computational time that will be required for each solution.

In 1992, Ramshaw and Chang published results of the two dimensional LAVA code to simulate the flow of multi component thermal plasmas. They included reactions of the components of the carrier gas, such as H, Ar, N_2 , N, O_2 and O, so as to be able to represent ionisation, dissociation, recombination and chemical reactions of the species (Ramshaw & Chang, 1992). The interactions between components were taken by generalised kinetics for the species. Eight years later, when computational power was adequate enough, Xiong et al. expanded the above model in three dimensions. They

considered one equation for the continuity of the ions in the plasma, and one of continuity, momentum and energy equations for the fluid mixture as a whole (Xiong, 2004). The generalised kinetics were used again. While the two dimensional models limit the representation of the phenomenon, as far as the three dimensional nature of Maxwell equations is considered for instance, they are extensively used and produce results that are acceptable for modelling as they can be compatible with experimental observations, or can deliver predictions that three dimensional models currently cannot. The coupling of the Maxwell equations with the transport equations adds more quantities to be calculated. Considering the coupling itself and the addition of several correctors on different quantities, it is clear that complexity is augmented and the problems of a diverging solution are potentially increased. This is further magnified when one adds another dimension to the model. Hence, two dimensional models are still considered regularly, even today with the large increase in computational power at disposal. Two dimensional models though, can be useful and can be in agreement to experimental data, thus complete in their own terms, especially when one considers only the flow regime and its progression at a point of view perpendicular to the surface at which it expands. The electromagnetic coupling has been achieved in many 2D models using a diffusion-type equation for the electric potential (Bolot et al., 2011), (Bolot et al., 2010), (Murphy & Kovitya, 1993). Other 2D models use other ways of electromagnetic coupling, introducing pseudo-densities (Chen & Li, 2001), or by introducing analytical functions for quantities such as the current from the anode to the cathode (Chau et al., 2006) that override the calculations in the CFD code.

Regardless of the assumptions implemented on the CFD code, researchers tend to use sinks and sources of various sorts, e.g. volumetric sink for radiative heat loss, or

momentum source or sink for the injection of particles as programming tools to help them model the phenomena better (Ramshaw & Chang, 1992), (Chang J. a., 1992), (Xiong, 2004). Similarly, Bolot, modelled the incompressible case of the wire arc spraying with a k-ε (Bolot et al., 2008) turbulence model. They used a mass source to inject particles of various sizes based on a distribution provided by interpolation of experimental data, which enabled them not to consider atomisation, while no electromagnetic model was used (Selvan & Ramachandran, 2009). The consideration of some quantities as external, in a way that can be represented with the addition of sources and sinks, is being done in order to overcome a lack of interaction knowledge (or an unusual interaction complexity) between factors. This challenge can be overcome with the introduction of factors external to the system, like sinks, but it predetermines a behaviour that would be better if it was researched on a greenfield basis.

Regarding the CFD code, most researchers tend to use the commercial package formerly known as FLUENT by ANSYS Inc. and is now called ANSYS, (Chau et al., 2006), (Xiong, 2004), (Bolot et al., 2011), (Bolot et al., 2010) (Selvan et al., 2009) which is numerically robust and can have external code added for the calculation of additional quantities, with the disadvantage of being commercial and closed source, so the balance of robustness and commercialisation does not allow several custom implementations such as boundary conditions, additional numerical schemes, modification of transport equations, additional phases introduced to the flow etc. OpenFOAM is open source and enables all types of custom implementations, by being a framework for CFD solutions. The current work used OpenFOAM for all solutions since it enabled coding additional elements that were identified for its pruposes.

In terms of the focus of research, researchers tend to divide the spraying process into many sub-processes. Extensive research focusses on the finer details of plasma creation in the torch (Chen & Li, 2001), (Bolot et al., 2011), (Bolot et al., 2010), (Murphy & Kovitya, 1993), (Selvan et al., 2009). This is the most challenging parts as the complex electromagnetic and flow phenomena taking place in the torch where plasma is created combined with the large voltage, current, pressure and velocity gradients make it interesting as well as demanding in terms of programming the model and computing the solution. In other pieces of literature the plasma flow and plume from the nozzle onwards is modelled and analysed separately assuming regular fluid flow characteristics for the plasma. The most complete solution, in terms of electromagnetic coupling and length of the domain, including both arc formation and flow at the exterior of the nozzle is considered the model of Trelles (Bolot et al., 2008), (Trelles et al., 2009).

As far as compressibility is concerned, many thermal spraying applications operate at conditions where compressible flows are present at the highest velocities reached. Some researchers have used modified incompressible solvers to model the flow, especially when near the limits of compressibility, in order to be able to introduce other elements such as heat transfer models (Mariaux & Vardelle, 2005). This approximation does not devalue the results or decreases their range, because high plasma temperatures enable a gas flow to be incompressible even at velocities at $1000m/s$ or more. Once again, the aforementioned modelling approach application was specific to a certain case and the assumptions for the specific case enabled a limited model to be applied. In a more generalised remark, one would say that CFD

platforms, as expected with every tool, have limitations. The challenges based on the limitations identified are:

- Interface capturing
- Local Thermal Equilibrium and its borders of effect
- Assumptions for the flow regime (incompressible, laminar, etc.)
- Steady state solutions
- Axisymmetrical domains
- 2D domains
- Sources and sinks
- Subdomains
- Compressibility

The limitations tend to be overcome by the introduction of additional tools each time. In this case, the additional tools range from boundary conditions, to sinks and sources as mentioned above, as well as additional calculation loops and parameter value alteration in order to use more accurate or easier to implement calculation of the quantities. By overcoming limitations with technical solutions, a complex model can give acceptable results with the available technology.

2.3.1 Current State of DC Plasma Modelling

A considerable amount of publications targets the modelling of plasma flows created by DC between a cathode and an anode on the thermal spraying device, as noted

further in this paragraph. The main characteristic is that they focus on arc formation and position and the effects on temperature and velocity. When heat transfer is used in those models, it is usually taken by using the enthalpy equation.

One of the first works regarding DC plasma formation in a CFD domain with focus to the thermal spraying process is in 2003 using a modified version of the LAVA solver. It uses Argon and Hydrogen for working gases in a Langrangian approach where the substrate is considered power, thus only the drag effects are taken into account. An interesting addition regarding previous CFD work on thermal spraying, but something enabled in the past by the use of LAVA, is the interaction of powder with the flame in order to study the resulting particle distribution, which agrees with experimental results (Ramshaw & Chang, 1992). The use of heat convection and thermal radiation also provides a temperature profile in the outlet, which also agrees with other individual experiments (Wan et al., 2003). PHOENICS can be also found mentioned in literature, in sporadic cases and it has been used for the optimal nozzle configuration of a plasma spraying assembly in a 2D cylindrical domain where a compressible two gas mixture was modelled in velocities up to 300m/s (Gedzevicius & Valiulis, 2006).

The pattern of focussing on the nozzle can be found in many pieces of literature. A well rounded article on the simulation of DC plasma is provided by Selvan, who worked in an incompressible 3D model with Argon and Nitrogen as the carrier gas in order to obtain the velocity and temperature distribution of the gas while 3D effects are captured. Their simulations seem to handle large gradients in temperature, but this may not be a problem in a domain of the size used as, from the scale of the whole process, only the cathode and nozzle are taken into account (Selvan et al., 2009). Another example of nozzle focus is from Bobzin et al. They employed a 3D model of

APS where DC (from three cathodes) plasma is formed and in a compressible Argon flow, they studied the temperature distributions comparing them to results obtained by computer tomography (Bobzin et al., 2011). This is an interesting case, as the method of computer tomography has not yielded other results in searches, but it may be promising in providing an interesting way of measuring plasma temperature, which can help quantify the macroscopic plasma properties in a way more useful for simulations.

Another example of localised model scope is the case where splats and their formation is studied. This cannot be a sufficient assumption in all cases of plasma flows, as in the distances usually travelled by sprayed substance particles, the plasma effects of the gas have vanished and the splats can be simulated by any reasonably sized interface capturing model without taking into account special considerations for the gas. Yet, one appearance in literature uses plasma spraying for splat formation and compares the resulting splat images with images from experiments and agreement is shown (Kang et al., 2011).

Recently, more 3D models started making appearance in literature where the methods are not using the coupling of a complete set of Navier-Stokes with other types of equations for the calculation of the electromagnetic properties of plasma, but the use of enthalpy again is dominant for the energy equation, for instance in the form of the total heat transfer rate (Guo et al., 2015). This work along with (Gu et al., 2015) show a new trend where very large gradients are handled by the solvers and velocity distributions are obtained, while the coupling of the Navier-Stokes equations with the Maxwell equations is more complete. In those two articles, the study of the current profile in the DC non-transferred arc is calculated, while 3D effects benefit from the

strongly coupled Maxwell presence. The parameters that cause the large velocity and temperature gradients seem to have been identified as well and their effect in divergence of the solution negated by imposing additional restrictions for them, such as relaxation factors. The restrictions are usually local and with valid physical assumptions behind them. A personal observation is that the reason for the approximation or restriction in the models studied the value of the approximate parameter(s) used is not easy to identify.

In plasma spraying, the substance for spraying can be either in solid state (powder form), or in liquid state, premolten. The substance being in solid state enables the focus on the entrainment of solid particles in a gas flow. This enables the modeller to focus on the gas phase only, omitting the effects of powder particles if they are considered very small, or enable the use of Langrangian/Eulerian approaches. Some studies though look into the phase change of particles in plasma flows, with the disadvantage of focussing on a small area of the domain where the process takes place, while boundary conditions are provided by approximations where the conditions of plasma flows are not themselves calculated for the particular domain, but are taken from other applications. If the sprayed substance is in liquid form, an additional fluid phase has to be added in the model. In that case any compressibility effects are difficult to incorporate, but it is not impossible. Another drawback is that the model has to be customised for the additional phases and the transport parameters of the flow overall will potentially be doubled, while the addition of the energy equation is not always the standard.

Coupling of multiphase flows with Electromagnetic equations has not been seen in literature until very recently. The MHD approach is often used for thermal plasmas

where the fluid is not as aggressively handled as in plasma spraying. The limitations and difficulties (maybe mention them briefly) of the production of a coupled MHD can be highlighted in a recent article of Wolfendale and Bluck, where the effects of the flow direction and angle with the magnetic field are discussed (Wolfendale & Bluck, 2015).

Code Saturne is used in many instances of modelling based on the MHD approach (Rehmet, Rohani, Cauneau, & Fulcherind, 2013) since it provides the benefit of a ready MHD solver. In the articles by Rehmet et al. and Lebouvier et al., the arc behaviour of DC plasmas is once again for the latter with good agreement with individual experiments, while the former studies an AC plasma torch. Both highlight the numerical challenges that arise with convergence in states where the plasma is not very stable. The transitions that take place affect convergence, since model design, by definition, cannot always take into account an enormous amount of parameters (Lebouvier et al., 2011).

2.4 Current State of Research in Drop Breakup

Interest in research in droplet atomisation is high for spray and fuel applications. The publications are either experimental or modelling approaches with results targeting final droplet sizes and distributions. The sizes used vary from centimetres to the microscale (Park et al., 2013), while the temperatures are from room temperature to plasma temperatures, thus making droplets in a plasma spraying regime the most challenging to research (Heiman, 2008).

Outside of the field of thermal spraying, the focus on atomisation research is mostly fuels. The experimental approach is mainly with the use of spray visualisation system

with the addition of droplet measuring system (Park et al., 2013) (Park et al., 2006). Phase Doppler Particle analysers are often employed for both purposes (Park et al., 2009). The studies generally try to determine the efficiency of fuel injection after atomisation for the resulting particle size distribution as well as combustion and exhaust emission characteristics for different distributions. The breakup patterns are also studied extensively, utilising the Weber number to quantify the atomisation regimen and study the resulting distributions (Zeng et al., 2012) (Park et al., 2006). The numerical approaches usually combine the Kelvin–Helmholtz model for the primary droplet breakup and the Rayleigh–Taylor for the secondary breakup patterns (Su et al., 1996) and this is incorporated in a CFD solution in the KIVA code (Park et al., 2009). Other approaches include the Taylor Analogy Breakup model which based on the droplets physical characteristics and forces acting on it determines its distortion (Ning, 2007). Finally the Volume of Fluid approach is very common in CFD applications for droplet atomisation.

Another important research enquiry, is the study of the effect of temperature in the resulting particle size distribution. Most fuel publications on atomisation tend to be isothermal, considering the physical properties in one ambient temperature (Park et al., 2006) (Park et al., 2009) (Zeng et al., 2012). Variations of the ambient temperature are also studied, but the only change here is a rerun of the model with different physical properties corresponding to that ambient temperature and no temperature changes happen in the model (Park et al., 2009).

Similarly, in thermal spraying, the particle breakup research is both experimental and numerical. Similar systems are used for the visualisation of the spray and the measurement of the resulting particle sizes (Fauchais et al., 2011). The Volume of Fluid

interface capturing technique is used more in non-plasma thermal spraying applications where it is less challenging to incorporate in a magnetohydrodynamics. For plasma spraying applications, models mostly incorporate the Kelvin–Helmholtz, Rayleigh–Taylor and Taylor Analogy Breakup solutions (Matsumoto et al., 2005) (Pawlowski L. , 2009). Volume of Fluid is not often considered since it is challenging to incorporate in a magnetohydrodynamics solution. This work identified the lack of Volume of Fluid publications in the plasma spraying area and utilised a VoF solution for the plasma spraying application.

2.5 Summary

Literature in DC plasma spraying focuses mostly on the arc creation and its behaviour. There is an abundance of experimental approaches where the phenomena take place and the outcome is recorded and measured with specialized equipment. The current work is looking into a numerical solution for the plasma spraying process and for this reason the limitations and challenges were identified as mentioned in paragraph 2.3. In general, a complete solution for the droplet atomisation in a plasma spraying regime using an interface capturing technique was identified to be lacking in literature. The identified solution was the production of a 3D, compressible, interface capturing, turbulent numerical model. The solution is split into subdomains, but the initial conditions for each subsequent model will be taken from the results of the previous domain for completeness and consistency.

Chapter 3: Introduction to Plasma Physics

For the understanding of the phenomena exhibited in the plasma spraying processes and in order to establish the limitations and the approach to counter them, some fundamental plasma physics terminology needs to be addressed. This section deals with the plasma state and notions associated with it, such as the “plasma approximation”, “quasineutrality” and the temperature exhibited by plasmas.

The properties of plasma expressed in physical quantities is the basis of modelling its motion and flow, so theoretical models and the quantification of plasma properties are the basis for modelling of the desired application or their parts. On this theoretical basis, experimental measurements of plasma properties can be added. The outcome is an overall structure of the model. The established physical models generally benefit the attempt to model the associated phenomena in CFD.

The hypotheses are based on a complete axiomatic system provided by classical atomic physics and nuclear physics. They are based on actual observations and are well established and devoid of unnecessary assumptions or oversimplifications, hence they can be used to build upon a complete theoretical formulation. Those theoretical parameters and their analytical generation provide value to the researcher and many different CFD models can be built to describe the phenomena, as will be explained in the next paragraphs.

3.1 Plasma State

Plasma is said to be the fourth state of matter, along with gas, liquid and solid state. A substance of matter is considered to be in a plasma state when it has the energy internally, to have its electrons separated by the nuclei of its atoms. This requires a

high amount of energy to be absorbed by the atoms internally. Therefore the substances first reach the gaseous state and subsequently, the plasma state. The electrons are still present, but not bounded to their atoms, so plasma is macroscopically neutral, but some proportions of the atoms of the gas have their electrons ionised. Thus, the plasma consists of electrons, ions and neutral atoms. The interactions between them can be ionisation, dissociation and recombination (Chang, 1992). Collisions between ions and neutral particles are apparent in plasma and they cause it to differ from the ideal gas kinetics. Usually, the Rutherford elastic scattering determines the effect and measure of differentiation, so in terms of modelling it may be considered if it shall contribute to the model or not (Restelloa et al., 2006). Glow discharge plasmas are the most common examples of plasmas to be found; they are created by the electric current that flows through a gas, i.e. when the gas is contained in a tube that bears an anode and a cathode on its ends. The current heavily ionises the gas and the dissociation and recombination of its electrons produce a glow discharge. In thermal spraying applications, glow discharge plasmas can be formed by the application of Direct Current (DC) or Radio Frequencies (RF) on the carrier gases (Heiman, 2008). DC plasmas are created by a cathode and anode with large potential differences between them and RF plasmas (or induction plasmas) are created when the carrier gas flows through a coil in which alternating in Radio-Frequencies current also flows through.

Plasmas can be characterised as thermal or non-thermal. The term thermal describes the fact that the heavier plasma species, which are neutrals and ions, have similar temperatures, thus energy levels, to the lighter ones, which are the electrons. Non-thermal plasmas are the ones where the thermal motion of electrons is significantly

higher than the heavier species' thermal motion so they can be characterised by two different temperatures for different weight species (Sturrock, 1994). The temperature in this case is determined by the thermal motion of each species and not by the thermal motion of its atoms as in more general applications. For this work, the term temperature will be used for the measure of the thermal kinetic energy per particle, for all particles.

3.1.1 Quasineutrality and the Plasma Approximation

Plasmas contain approximately the same number of positive charge as the number of electrons. This is due to the fact that electrons in the plasma are produced by the ionisation of its own, initially electrically stable, atoms. Therefore, plasmas are macroscopically considered neutral, but not in the same way the Niels Bohr model of the atom defines its neutral stable state. The inner electromagnetic properties of the plasma are not stable, because in closer examination the neutral and charged particles move in the substance, while electrons ionise and recombine with nuclei. The idea of quasineutrality is a hypothesis that helps to macroscopically quantify the plasma parameters, which are the number of electrons and ions in plasma. It states that plasmas are "quasineutral". This means that plasmas are macroscopically electrically neutral as long as the number of ions is approximately the same as the number of electrons:

$$n_i = n_e$$

The electrons and ions move freely enough so the electromagnetic forces of interest do not vanish completely. The scale that gives an indication of the distance at which those interactions are considered important is the Debye Length:

$$\lambda_D = \sqrt{\frac{\varepsilon k_B T}{{q_e}^2 \rho_{n_0}}}$$

Equation 3-1: The Debye length

Locally, in length scales near the Debye length (in glow plasmas is around $10^{-4}\ m$ (Hnat, 2015)), electromagnetic exchanges between atoms and their electrons do occur extensively, thus giving the plasma its unique characteristics.

The quasineutrality of plasmas and the plasma approximation, help to locally quantify the electric field in low collision frequencies between the species that compose the plasma. For the approximation to be established, a three-phase plasma is considered, where one phase is the neutral species, one is the ions and one is the electrons. If a local isothermal density rise is considered in some part of the plasma, there is a topical rise in the pressure gradient as well (Heiman, 2008). Additionally, the quasineutrality hypothesis states that the pressure gradient rise will be present for both electrons and ions (Belmont et al., 2013). The pressure gradient on the electron phase drives it away from the part where the density is increased creating a local increase of the number of positive charges. This creates an electric field which opposes to the electrons' motion due to the pressure gradient force. The electrostatic field that pulls electrons back is: $E = -\nabla\varphi_E$, where φ_E is the numerical electric potential (Heiman, 2008). As a result, any change in topical charge neutrality creates an electric field that opposes to the motion of electrons. From the scope of the complementary species, if the ions move, the electrons will follow due to this electric potential. So the plasma approximation refers to the fact that $\nabla \cdot E = 0$ combined with the fact that the number of electrons is approximately the same as the number of ions.

The plasma approximation's effect on the equation solving in MHD models is that the equation, $\nabla \cdot E = \rho_0$, shall not be used to calculate the charge density ρ_q, but the opposite should be applied, using the E calculated from the equations of motion (Chen., 1984). It must be noted that the plasma approximation has no effect when the electrons and ions move in very high frequencies, which means one species can move but the other one will not necessarily follow instantly, which is also accounted on the fact that ions are much heavier than electrons. The relatively slow transitions are denoted by the locally isothermal assumption made for the approximation. The electromagnetic forces propagate at a speed near the speed of light in gases and are of greater importance in lower velocity flows. However, when the flow's velocity is quite high, other parameters, such as viscosity and thermal conductivity, which are considered too slow to play a part in the electromagnetic view of slow plasmas, can also influence its behaviour (Chen., 1984). Examples of such highly energetic plasmas can be volcano cores or nuclear fusion where velocities are lower than the ones exhibited by plasma spraying processes. Thus, the plasma approximation can be valid for CFD modelling of plasma spraying where plasma is studied macroscopically. Ideal for this macroscopic study are the MHD models which also take into account flow parameters such as viscosity (Waelbroeck., 1998).

3.2 Mass and Momentum Conservation

The core of the numerical modelling of plasma flows is the models proposed to describe plasmas. The general MHD models' assumptions are applicable for laboratory scale plasma flows as described above, hence at the scale of plasma spraying application, and will be described here. Plasma as a fluid can be described by conservation equations for fluid dynamics, analogous to the hydrodynamics'

equations, but generally containing more and more complicated terms (Waelbroeck., 1998). The general distinction between the types of models proposed, which describe the motion of plasmas, is the distinction between multiphase models and a single-phase model. The proposed MHD models for plasma are usually one phase models, the equations of which are derived after combining the Maxwell equations with the Navier-Stokes equations for each species of the plasma and taking into account average velocities, total pressures and densities for each species. Again, the fluid is assumed to be quasineutral, so the plasma macroscopically is considered electrically neutral, but electromagnetic quantities are ever-present locally in the development of the flow, and in small scales. Several sets of MHD equations with the considered assumptions for plasmas have been given (Chen., 1984), (Choquet et al., 2007), (Sass-tisovskaya, 2009), (Heiman, 2008).

The equations considered are the equation of motion, the continuity equation, the charge conservation equation and the current equation. The parameters considered are mainly the velocity (u), the time (t), ρ the mass density, ρ_q the charge density, $\vec{j}$ the current density, $\vec{B}$ the magnetic field, $\vec{g}$ the acceleration of gravity, p the pressure, q_e the electron charge, n_i the number of ions (assuming quasineutrality) and sometimes p_e the partial pressure of the electron phase. Additionally, for the derivation of the set of equations for the model, two or more phases may be assumed, where one phase is assigned to the ions, one for the neutrals and one for the electrons (Choquet et al., 2007). This work considers the gas as one phase for consistency with the CFD models presented here that do not include MHD equations.

The definition for plasma given by (Rutscher, 1982) clearly indicates that a plasma gas, by definition consists of charged particles and this characteristic helps to define some

of its basic properties, which are useful in the analysis of the process. The moving charged particles induce a magnetic field $\vec{B}$ that is perpendicular to the direction of the electric field. The electric field is characterised by the current density $\vec{j}$. The current density gives the vector of the Lorentz Force $\overrightarrow{F_L} = \vec{j} \times \vec{B}$, which by definition is perpendicular to both $\vec{j}$ and $\vec{B}$. The Lorentz force in this instance an inward force that constrains the plasma around the central axis of the plasma jet. The confinement of the jet near the core accounts for a large concentration of gaseous mass that creates local large pressures. They can potentially expand rapidly to create a jet that often escapes the nozzle reaching velocities which in normal temperatures would be supersonic. The substrate particles, in powder form or liquid form, will be entrained by the jet and because of that they will be accelerated towards the surface to be sprayed.

Therefore, for a compressible plasma gas, the continuity conservation can be given as known:

$$\nabla \cdot \rho\vec{u} = 0$$

Equation 3-2

The momentum conservation equation for a plasma, needs to take into account the magnetic field force:

Momentum conservation normal arrangement:

$$\nabla \cdot (\rho\vec{u}\vec{u}) = -\nabla p + \nabla \cdot \vec{\tau} + \vec{j} \times \vec{B}$$

Equation 3-3

With $\vec{\tau}$ the strain tensor, $\vec{j}$ the current density in A/m^2 and $\vec{B}$ the magnetic field in T.

For the interface capturing, Rusche describes a method using an indicator function γ.

$$\frac{\partial \gamma}{\partial t} + \vec{\nabla} \cdot (\vec{u}\gamma) + \vec{\nabla} \cdot \left(\overrightarrow{u_r}\gamma(1-\gamma)\right) = 0$$

Equation 3-4: The transport equation for the indicator function (Rusche, 2002).

With the indicator function γ given below (Rusche, 2002):

$$\gamma = \begin{cases} 1, & for\ a\ point\ inside\ fluid\ a \\ 0 < \gamma < 1, & for\ a\ point\ in\ the\ transitional\ region \\ 0, & for\ a\ point\ inside\ fluid\ b \end{cases}$$

3.3 Plasma Temperature and Energy

Since a gas is composed of particles such as electrons and atoms and it is assumed to have thermal equilibrium, each particle can be independently moving with any velocity, but their velocities' distribution is determined by the Maxwell distribution. Hence, the average kinetic energy KE for a gas in three dimensions is: $KE = \frac{3}{2}k_B T$. This linear connection enables to characterise plasmas thermally, in terms of their energy instead of their temperature. For a $1eV$ plasma for instance, it is:

$kT = 1eV = 1.6 \times 10^{-19} J$.

Hence:

$T = 1.6 \times 10^{-19} / (1.38 \times 10^{23}) \cong 11,600K$ (Chen., 1984). A plasma gas can have two temperatures, as the electrons can have different Maxwell distributions than the ions. This can be caused by different collision rates between the ion-ion or electron-electron pairs and the ion-electron pair (Choquet, Lucquin-Desreux, & Degond, 2007). When the collision rate between same species is higher than the one exhibited by pairs of different ones, the plasma is characterised by two temperatures T_i and T_e for the ions and electrons respectively. This temperature difference is usually short lived though and the collision rates, as well as the temperature, soon equalise; this is the

reason they enable models not to take them into consideration in engineering plasma models.

Summarising the above, plasma is a state of matter that is characterised by the disassociation of electrons from atomic nuclei, which forms a medium which is macroscopically neutral electrically. A definition for plasma is given: “Plasmas are quasi-neutral multi-particle systems characterised by gaseous or fluid mixtures of free electrons and ions, as well as neutral particles (atoms, molecules, radicals) with a high average kinetic energy of electrons or of all plasma components, and a considerable interaction of the charge carriers with the properties of the system” (Rutscher, 1982).

The energy conservation equation as given by: (Heiman, 2008)

$$\frac{\partial}{\partial t}(\rho H) = -\nabla(\frac{\mathrm{k}}{\mathrm{c}_p})\nabla(\rho H)$$

Equation 3-5

The temperature is obtained from the specific heat capacity at constant pressure:

$$C_p = \left(\frac{\partial h}{\partial T}\right)_p$$

Equation 3-6

With T the temperature in $Kelvin$.

3.4 Key Non-dimensional Ratios

The parameter that quantifies the ratio of inertial forces over viscous forces and determines the type of flow is the dimensionless Reynolds number, which in the case of a plasma flow around a droplet of sprayed substance is given by:

$$Re = \frac{\rho_{Ar} u_{Rel} d_p}{\mu_{Ar}}$$

Equation 3-7

The Weber number is the parameter that quantifies the gas-liquid surfaces interaction, by the ratio of the inertial forces on surfaces compared to the surface tension.

Similarly, for a spherical droplet:

$$We = \frac{\rho_{Cu} \vec{u}_{Rel}^2 d_p}{\sigma}$$

Equation 3-8: The Weber number

A typical particle size in a plasma spraying process is $250\mu m$. For it, the Reynolds number in a 400m/s flow would be: $Re = 353$. For the same particle $We = 34.1$ and it indicates a bag deformation pattern for the particle.

3.5 Further Assumptions

For a quasineutral plasma gas, to be modelled, further assumptions are useful. One common assumption is that the plasma is in local thermodynamic equilibrium. This means that the energy exchange between the system of the plasma gas and external factors (such as the radiation of the plasma that is a significant factor towards the instability of its plasma state) do exist, but that the plasma overall is in a thermodynamic equilibrium for each area about any point of examination. Building on this, a plasma can be assumed to be optically thin overall, which means that radiation is not absorbed in the plasma itself.

3.6 Additional Equations for the Plasma State

In order to complete the MHD model for a plasma, the Maxwell's equations in potential formulation are given:

$$\nabla \cdot (\sigma_m \nabla \phi) = 0$$

Equation 3-9

With σ_m the relative permittivity and φ the electric potential.

$$\nabla^2 A = \sigma_m \mu_0 \nabla \phi$$

Equation 3-10

Where A is the magnetic vector potential in $T \cdot m$ and μ_0 the magnetic permeability in NA^{-2}.

Chapter 4: Numerical Methods

4.1 Overview of Methods for Plasma

In general, CFD methods started being used as soon as frameworks capable of solving for them were developed. As a result, they have been used to model systems by using frameworks that were unique at the time. This time was an era where computer systems with capabilities of solving for those models were limited to large organisations and universities and it was more expensive than today to spend time and effort on solutions for this process. The first supercomputer, Electronic Numerical Integrator and Computer - ENIAC, in the 1940s is now considered to have run code for a CFD solution. The code was based on the algorithms developed by Lewis Fry Richardson, who used numerical methods to determine meteorological patterns and weather prediction, amongst others (Hunt, 1998). It was structured in a different way than today's solutions. It was not using the Navier-Stokes equations, but it assumed that the space was constructed by a finite number of cells where fluids moved. By the finite differences in quantities between them, the flows were determined (Hunt, 1998).

It was not until 1985 that the first mention of a structure for what was then known as a Finite Element Machine was first mentioned and it was deployed by NASA to study problems of Finite Element Analysis (FEA), a methodology very close to the one of CFD. This machine was carefully architectured and deployed for the study of a "complex but narrowly defined family of algorithms" whose purpose was to provide fast solutions for problems in structural engineering (Lawrence Snyder, 1985).

The first mentioned use of CFD as we know it today though, was around 1955 in the Los Alamos National Lab by Frank Harlow and his team (Harlow, The Particle-in-Cell

Method: A combined Eulerian-Lagrangian computing method that is suitable for solving multimaterial problems involving large fluid distortions, 1955), (Harlow F. H., 1957). By using the "Particle-in-cell" (PIC) method (Harlow F. , 1963), (Butler, 1964), (Harlow F. , 1964), (Amsden, 1966), they used numerical methods to quantify the aspects of various problems of fluid dynamics.

The PIC method was also used in simulations that provided results for systems in which plasma interactions were taking place. It is not difficult to understand that there is excessive interest in the development of a reactor where effective thermonuclear fusion takes place. Furthermore, plasmas have always been a subject of astronomy research as stars and intergalactic regions are areas where plasma is created naturally and contributes greatly to their physical behaviour. The need of physical models to describe the phenomena taking place in stars and intergalactic regions has been the reason behind the initial interest and active study of plasma systems. The modelling of those systems initially differed greatly from the approaches taken today, but all of them were trying to explain basic plasma characteristics in a flow in order to predict its behaviour. This would provide a basis for extrapolation or establishment of the validity of assumptions that would be applied in reactors, tokamaks, for thermonuclear fusion (Kortshagen, 1998). Tien and Moshman run a 1D simulation of 1 particle for the study of an electron gun in order to determine the produced current (Tien & Moshman, 1956), and J.M. Dawson provided the first 1D model for plasma (Dawson, 1962), which was also studied by C.O. Eldridge and M. Feix (Eldridge & Feix, 1962). The majority of those simulations were 1D and they focussed on one localised part of the system studied. This can't be overlooked, neither it can be looked at with today's standards, as they were major breakthroughs in all four fields of software and systems architecture,

CFD and the study of plasmas (either in a flow or outside of it). But it makes clear that with limited technological resources; they set the bases for today's modelling approaches. As a result, on one hand the growing interest in CFD and on the other hand the interest in plasma, mainly for fusion, gradually shaped the methods and procedures used, creating unique architectures (Oran, 1992) for the numerical analysis of plasma and providing invaluable research input for future researchers.

The domain of the problem in this work includes representation and interactions of the nozzle of a plasma-spraying device, the anode, the cathode and the sprayed substance. An aim of the work is to study atomisation of the substance. For this reason the analysis method was selected to be FVM, because it produces a solution of fluxes and based on the fluxes, interface solutions can be applied. The applicability of particle and control volume methods was the reason behind selecting FVM for the solution.

4.2 Overview of Methods for Interface Tracking

Particle methods, or Langrangian methods, solve for independent particles consisting a multiphase flow. Each particle has properties assigned to it (such as location and velocity) and based on the solution for the properties around them, their new properties are calculated for each step of the solution.

Volume control, or Eulerian methods, solve the solution for each volume of the domain and the properties of each point in the domain are defined as fields. Therefore, one can get the field properties for any location of the domain, at any given time for which the solution exists.

The solution for the current work was aiming to study atomisation patterns of molten metal droplets, therefore a solution for free surfaces was required. The Volume of

Fluid method provides modelling for freely moving interfaces and can be incorporated in an Eulerian solution, so it was considered an ideal element to incorporate in the modelling solution for the scope of this work.

4.3 Solution Toolbox Selection

In this part, a brief overview of the computational tools and packages that can be useful for CFD research will be given. A special mention has to be given to LAVA framework, developed by NASA which was specifically designed to deal with aerodynamics, but was also adopted in order to deal with plasma flow models (Moini-Yekta et al., 2013). The University of Limoges has also developed individual code packets for the simulation of plasma flows (Fauchais et al., 1992), (Fauchais P. , 2004), (Pawlowski, 1995), (Trelles et al., 2009). This approach is much customised and looks promising in for future if large research teams are assembled with smaller groups working on a particular subject. The University of Limoges has benefitted from that, as well as the LAVA framework. However, approaches such as this need general direction in architecture and design. The code base should be continuously enhanced and remain current since in technological fields, such as scientific software development, standards change rapidly and it is difficult to support solutions without constant maintenance.

From commercial packages, FLUENT and later ANSYS, provide a solid proprietary CFD suite with solvers that usually provide good overall convergence and the ability to add User Defined Functions (UDFs), where new parameters can be added and their values calculated by writing code in C (SAS IP, 2013). It also benefits from good documentation regarding the dynamics of fluids in general. Another proprietary suite that enables adding custom code is PHOENICS, where the user can add custom code in

FORTRAN, while it can deal with FEM solutions along without particular focus on CFD (CHAM Ltd., 2005). Code Saturne is a package licensed under the GNU Public License (GPL), hence it is free and can run on Linux environments. The user can simulate compressible and incompressible flows adding flow properties such as heat transfer and turbulence parameters according to their needs (EDF R&D, 2015). Star-CCM+ is another proprietary suite with a client-server architectural design, focusing on efficient user interaction in the visualisation of models. The simulations are run on powerful servers, but the user visualises the results locally as a client. It handles compressible 3D flows with heat transfer (CD-Adapco, 2015).

Finally, OpenFOAM, is an open source package and it was chosen as the software basis for the current work. By being open source and providing a way of coding the conservation equations that resembles the analytical representation, the researcher can add main equations to the solution and set up appropriate parameters, units, their values and mathematical relations between them (OpenCFD, 2010). This tool on the other hand, lacks in official documentation and while it has gradually improved with time, familiarisation with it is a steep learning curve, which requires a solid knowledge of aspects of computer science and software engineering (i.e. algorithmic formulation, abstraction and inheritance in C++). The fact that the developer is able to write custom code and use pre-existing libraries in the whole CFD package, or alter them at will, were the factors that led to it being used for the present work.

The OpenFOAM version at the time the simulations for this work were carried through provided a framework with various fluid dynamics solvers and specific independent elements in the form of libraries which together could be combined programmatically to produce an independent and new solution. Useful for this work were the

compressible solvers, the Volume of Fluid solution and the ability to use thermophysical properties' tables in a standardised data format. As in a framework, the elements that had to be combined to produce a complete solution were:

- a compressible Volume of Fluid solution,
- a newly written expression for the heat transfer conservation for each model in this work,
- the magnetohydrodynamic equations and their incorporation in the solution.

4.3.1 The VoF Model Method Used

The Volume of Fluid method used is the one implemented in OpenFOAM and its high accuracy in the microscale along with the visualization toolkit available were the reasons for its selection for this solution. It benefits from a multi-dimensional limiter for explicit solution which is called MULES (Multidimensional universal limiter with explicit solution). MULES is a computationally costly solution, but it is fundamentally explicit with strict limit on the time step limit based on the conditions of the flow and is proven to be a very effective method of guaranteeing boundedness in the phase/mass-fraction fields (Greenshields, 2014).

The VoF in OpenFOAM can solve accurately for compressible flows since it is employing a bounded method which enables it to take into account the compressibility of the interfaces. The discretised momentum equation includes a correction loop where it introduces an artificial velocity term u_r. This term is only active in the thin interface region and does not significantly affect the solution outside of it. This way the velocity field is calculated for each control volume, by taking into account the

maximum velocity magnitude in the interface and using its vector normal to determine the magnitude of compression (Rusche, 2002).

4.4 Summary

For the scope of this work, the OpenFOAM toolkit was identified as most suitable and expandable due to its open source nature. The base framework was OpenFOAM in a compressible solution with the VoF interface capturing method. The existing code of the compressible multiphase solver was to be expanded by the addition of heat transfer equations and suitable numerical schemes as described in the following chapters. For the solution of Chapter 5, a set of magnetohydrodynamics equations was also required to be coded in. A local Git repository was set up for versioning control. The compiled solvers were tested locally on a 16 core computer at 2.53GHz and when testing was successful they were recompiled on Iridis 3 and 4, the computational clusters of the University of Southampton (Iridis, 2015). For the Iridis solutions, the domain was decomposed in 128 parts and the solution was recomposed for local analysis. It was found that the decomposition and recomposition added to the time cost of the solution, but in general the benefit of using a computational modelling cluster significantly reduced the time cost of each solution.

Chapter 5: 3D MHD Study of Plasma Spraying Device Nozzle

5.1 Objectives

The general aim of this work is to provide a set of models that describe adequately the plasma spraying process for industrial purposes. As mentioned in Chapter 3, in the DC plasma spraying processes the area where the arc is formed is the nozzle where the cathode and anode are usually placed. Since the arc formation dictates the plasma formation and therefore determines the plasma gas acceleration, it is vital to model the plasma fluid properties at the area where it is formed, i.e. the nozzle. By modelling the plasma flow at the source of its creation, a first step for modelling the complete plasma spraying process is taken. The benefit of isolating the modelling in that area is twofold:

- First, the domain of the process is shortened to focus on a small area where the extreme variations in the fluid properties take place, thus enabling consistency of the numerical solution which is crucial for successful modelling.
- Second, the information provided by the model can provide boundary conditions for a subsequent model that will focus on the next area of interest: outside the nozzle. There, the plasma generation does not have a significant effect, and the modelling can focus on different elements of importance, like the interactions between the gas and the liquid working material.

The modelling in this chapter studies the nozzle area fluid flow in a compressible regime with the addition of electromagnetic equations for the study of the electrical properties that result in plasma generation. An additional phase through a Volume of

Fluid solution (4.3.1) is also added to study the effect of the droplet presence in the arc formation. This model enables the study of the effects of the Maxwell equations on heat generation and velocity. With the subsequent models described in this thesis, it can give an integrated overview of the plasma spraying process.

The model enables the study of the effect of the electromagnetic interactions in the fluid dynamic properties of the plasma gas and the effect of the presence of the dielectric of metal on the current, the arc distance, the temperature and the establishment of the flow regime for the whole process.

5.2 Domain and Mesh

The domain for the simulation is the nozzle of an F4 plasma spraying torch by Sulzer Ltd., Switzerland (1.3.1). The nozzle contains the cathode, with the anode being the surrounding, exterior wall. In the modelling domain, the nozzle from the cathode tip onwards was used. The larger base of the conical frustum, that is the convergent part of the nozzle, was the flow inlet (1.3.1). This truncated cone leads to a cylinder of radius equal to the radius of the smaller base of the nozzle and the cylinder base that is not attached to the truncated cone was set as the flow outlet. The exterior of both conical and cylindrical parts which form the boundary of the domain were set as wall.

The mesh of each base was created by a square half the cylinder base diameter, the diagonal of which extends to the circumference of the base, thus partitioning it into four quadrants. The extension of the interior square diagonal leads to a curvilinear grid expanding to the exterior circle. The meshing of the edges of the inner square can have the same number of points as the arc of the outer quadrant, resulting in a structured mesh. Then, by extruding the mesh towards the next cylinder base and

scaling for the base radius difference progressively, a structured mesh of hexahedral cells can be created. The resultant mesh is shown in Fig. 6.1. It is consisted of $6{,}250{,}000$ structured hexahedral cells. The cylindrical and conical features with coinciding axes, enables the technique of the square with extended diagonal to be used for the construction of the mesh. The domain was chosen to have a large number of cells in order to counter numerically the steep gradients that appear in plasma flows. The cells for the tip of the cathode and the high conductivity area were set independently, by their location.

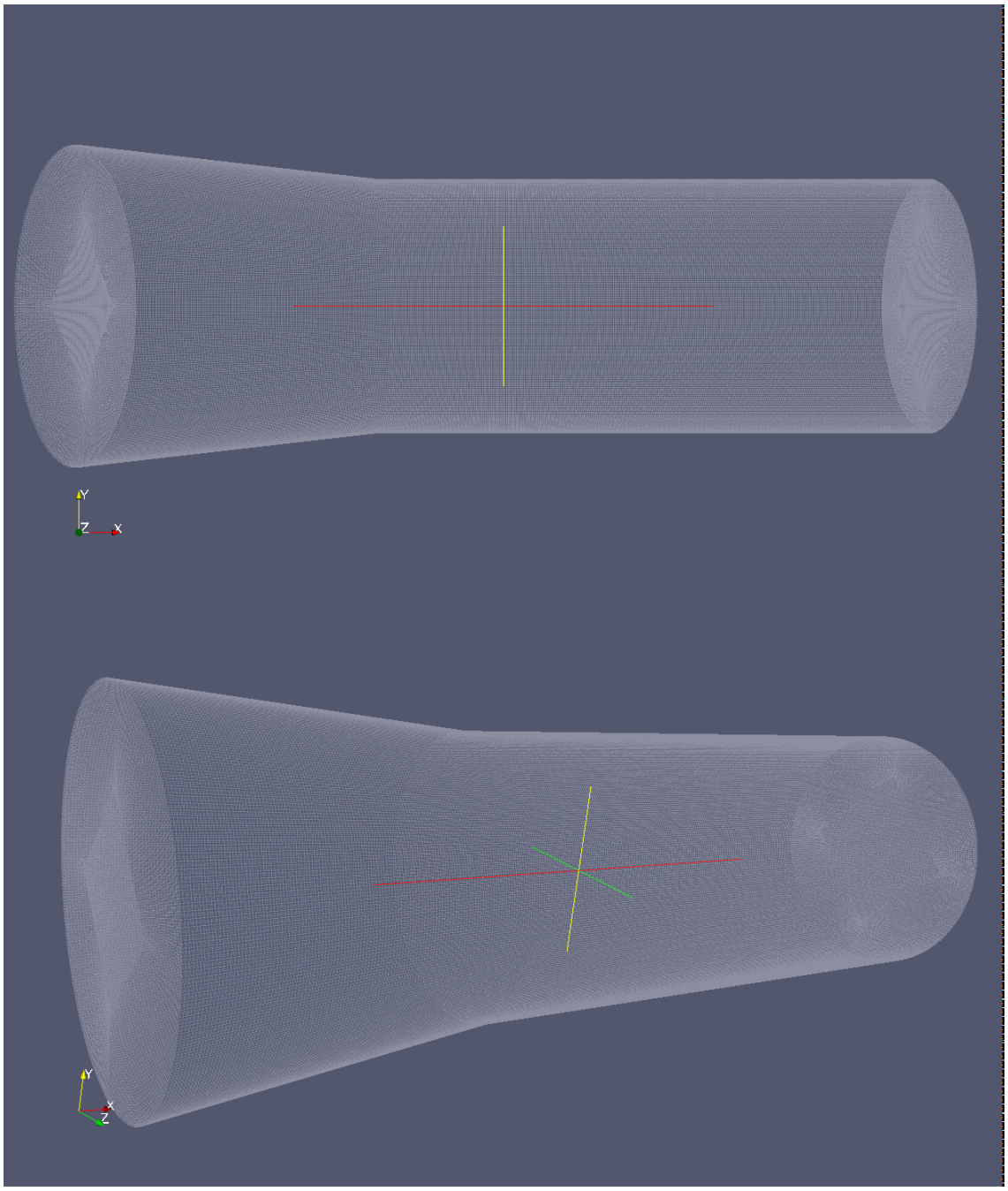

Figure 6.5.1: The mesh used for the model.

5.3 Boundary Conditions

The cathode, the converging part of the nozzle and the cylindrical part are the walls of the nozzle, therefore they were set as `noSlip` boundary condition for the simulations. In this boundary condition, the velocity is set to (0, 0, 0) for the directions (x, y, z) respectively. The inlet around the cathode is the base with the larger diameter

of the conical frustum was set as `fixedValue` for the velocity inlet where the velocity was set to a constant speed for the x direction and set to 0 for the y and z. The pressure outlet was the unattached base of the cylinder at the limit of the domain and was set as `zeroGradient` where the normal gradient of the quantities is calculated as equal to zero. The pressure at the inlet and the wall was set to `zeroGradient`. For the magnetic vector potential, `zeroGradient` was assigned in all patches, except the outlet where it was set to zero. The electric potential was set to zero at the anode and `zeroGradient` at the outlet.

5.4 Initial Conditions and Modelling Parameters

The electric potential was set to the predefined current density values at the inlet and the cathode. The temperature was set to $3000°K$ at the domain. The inlet velocity was set to be $330m/s$.

The density of Argon for temperatures up to $20000K$ was taken from (Sass-tisovskaya, 2009), which is a combination of (Rat, Pascal, Aubreton, Fauchais, Elchinger, & Lefort, 2001) and (Rat, Pascal, Aubreton, Elchinger, Fauchais, & Vacher, Transport coefficients including diffusion in a two-temperature argon plasma, 2002). The attributes for temperatures higher than $6000K$ were added to modified Janaf tables and they were used for the solver to reference values of the thermodynamic properties of Argon and Copper. Additional transport properties were given by (Colombo, Ghedini, & Sanibondi, 2008). The electrical permittivity of copper ε_{Cu} was calculated from (Matula, 1979). The current was set to $600A$ for the simulations.

5.5 Physical Assumptions

Based on the discussion in section 3.1.1, the following assumptions are made for this model:

- The plasma is a Newtonian fluid
- The plasma is in a Local Thermodynamic Equilibrium
- The plasma is optically thin
- Viscous dissipation is negligible.
- A small area strip on the anode with high electrical conductivity of $10^4 S/m$ is considered.
- The electric field by induction is considered very low compared to the plasma field.
- The transport of electron enthalpy is considered negligible (Sass-tisovskaya, 2009).

5.6 Mathematical Model

The governing equations are given below:

The continuity equation is as given in section 3.2.

The momentum conservation from Eq. 3-2 can be rearranged for use in OpenFOAM (Sass-tisovskaya, 2009):

$$\frac{\partial}{\partial t}(\rho \cdot \vec{u}) + \nabla \cdot (\rho \vec{u}\vec{u}) - \vec{u}\nabla \cdot \rho\vec{u} + \nabla \cdot \left(\mu(\nabla\vec{u} + (\nabla\vec{u})^T)\right) - \frac{2}{3}\mu_{Eff}(\nabla \cdot \vec{u})\boldsymbol{\delta}$$
$$= -\nabla p + \vec{j} \times \vec{B}$$

Equation 5-1: Rearranged momentum conservation equation

With δ the unitary operator, $\vec{j}$ the current density in A/m^2 and B the magnetic field in T.

The energy conservation can be rearranged from Eq. 3-3 to (Sass-tisovskaya, 2009):

$$\frac{\partial}{\partial t}(\rho H) + \nabla \cdot (\rho \vec{u} H) - H\nabla \cdot \rho \vec{u} - \nabla \cdot (\alpha_t \nabla H) = \nabla \cdot (\vec{u} p) - p\nabla \cdot \vec{\mathrm{u}} + j \cdot E$$

Equation 5-2: Rearranged energy conservation

With H the enthalpy and $\vec{E}$ the electric field.

The temperature is obtained from the specific heat capacity at constant pressure is given in section 3.4.

The Maxwell's equations in potential formulation as given in Eq. 3-5 and 3-6 complete the system of equations for the model.

5.6.1 Discretisation Schemes

For the equation terms in this paragraph, the discretisation schemes used are given: for the compressible flow through the face surface (φ_u) divergence product with velocity, a second order Gauss linear upwind discretisation based on the velocity gradient was used. For the electromagnetic properties Gauss linear schemes were used. For divergence and gradient terms containing enthalpy, the Gauss upwind scheme was used.

5.7 3D Simulation for the Calculation of the Gas Motion Properties

The first results obtained from this model were from simulations run without an additional liquid phase present and they focus on velocity and temperature.

The inclusion of the electromagnetic properties is expected to provide a more aggressive flow regime than regular compressible flow through a nozzle. The inwardly directed Lorentz force at the cathode, compresses the plasma near that area, creating pressure gradients and accelerating the gas rapidly as can be seen in Figure 6.2. The acceleration stabilizes and stops at around 140mm where the nozzle also ends, hence it stops contributing to pressure hot spots that would increase the rate of velocity change. For a spraying system with relatively low inlet velocity and a simple nozzle, very high outlet velocities can be exhibited with the maximum velocity magnitude for an inlet velocity of $330m/s$ reaching around $3300m/s$, which agrees with findings from (Guo, et al., 2015), (Guo et al., 2015). As can be seen in Fig. 6.3, the highest velocity is $3200m/s$ reaching a peak near the convergent area of the nozzle and starts slowly declining until it reaches $1800m/s$ at the outlet.

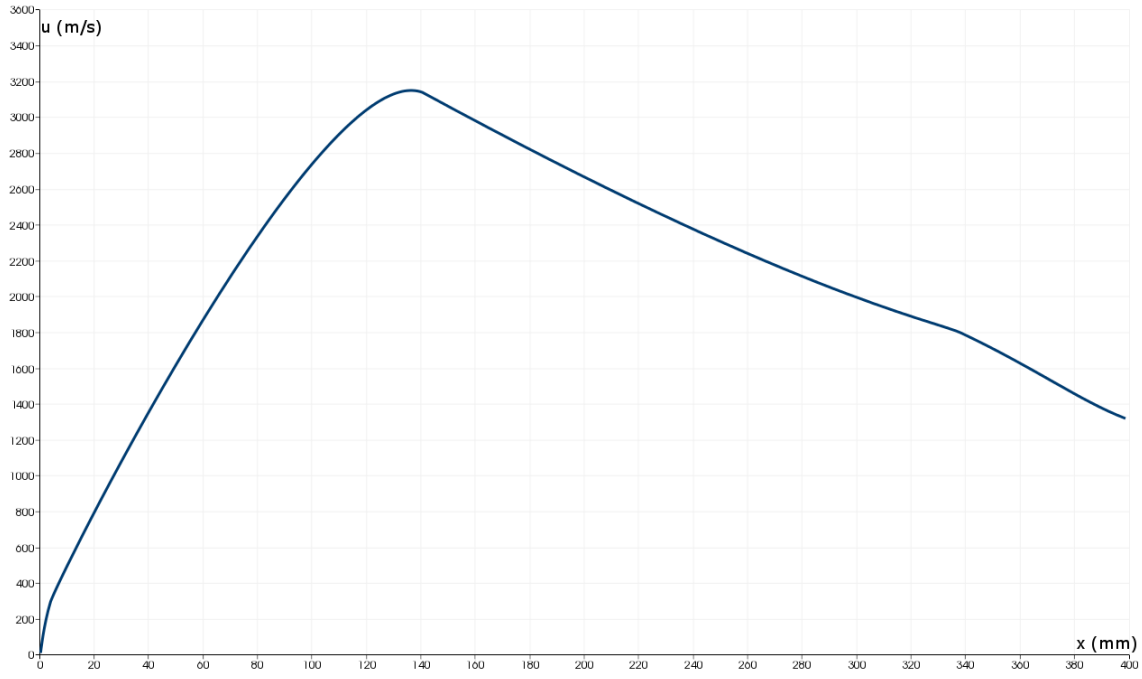

Figure 6.5.2: Velocity in the centreline

The contribution of the electromagnetic properties leads to a very steep temperature gradient in the domain which can be seen in Figure 6.3. As will be demonstrated in the

next chapter, omission of the electromagnetic properties in this model leads to a high ceiling for temperature of $2500K$, whereas in this model the transformation of the electrical energy of the arc, and its conversion and deposition onto the working gas, makes it reach temperatures up to $20000K$ in the nozzle area of the gun.

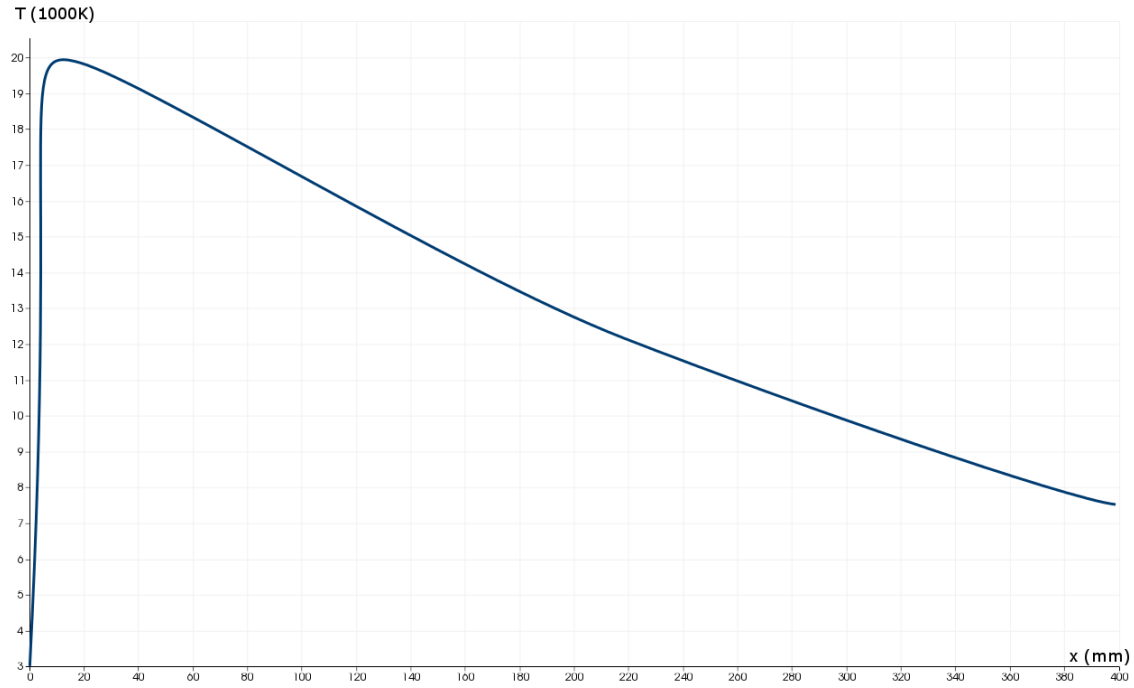

Figure 6.5.3: Temperature at the centreline.

Since the results of this model will provide information on the initial conditions of the following model covering the atomisation of metal substance with heat transfer, the velocity and temperature profiles at the nozzle exit were plotted in Figure 6.4. The radial profile for temperature is nearly flat at 8000K, with a tiny shift towards 9000K near the cathode. Taking into account the temperature drop rate and the distance from the nozzle where the droplets will be placed in the next model. The temperature at 400mm from the tip of the cathode drops by approximately 11000K and a common distance where the externally fed working substance is free of substrate is 0-5cm from the nozzle exit. So assuming a 2.5cm distance where the working substance is fed, to ensure molten state, the inlet temperature for the next model should be set at 2000K.

Similarly, the velocity drops by 1600m/s from 180mm from the cathode tip to 400mm where the nozzle exit is located. Based on that rate, the velocity at 2.5cm from the exit should be considered around 400m/s.

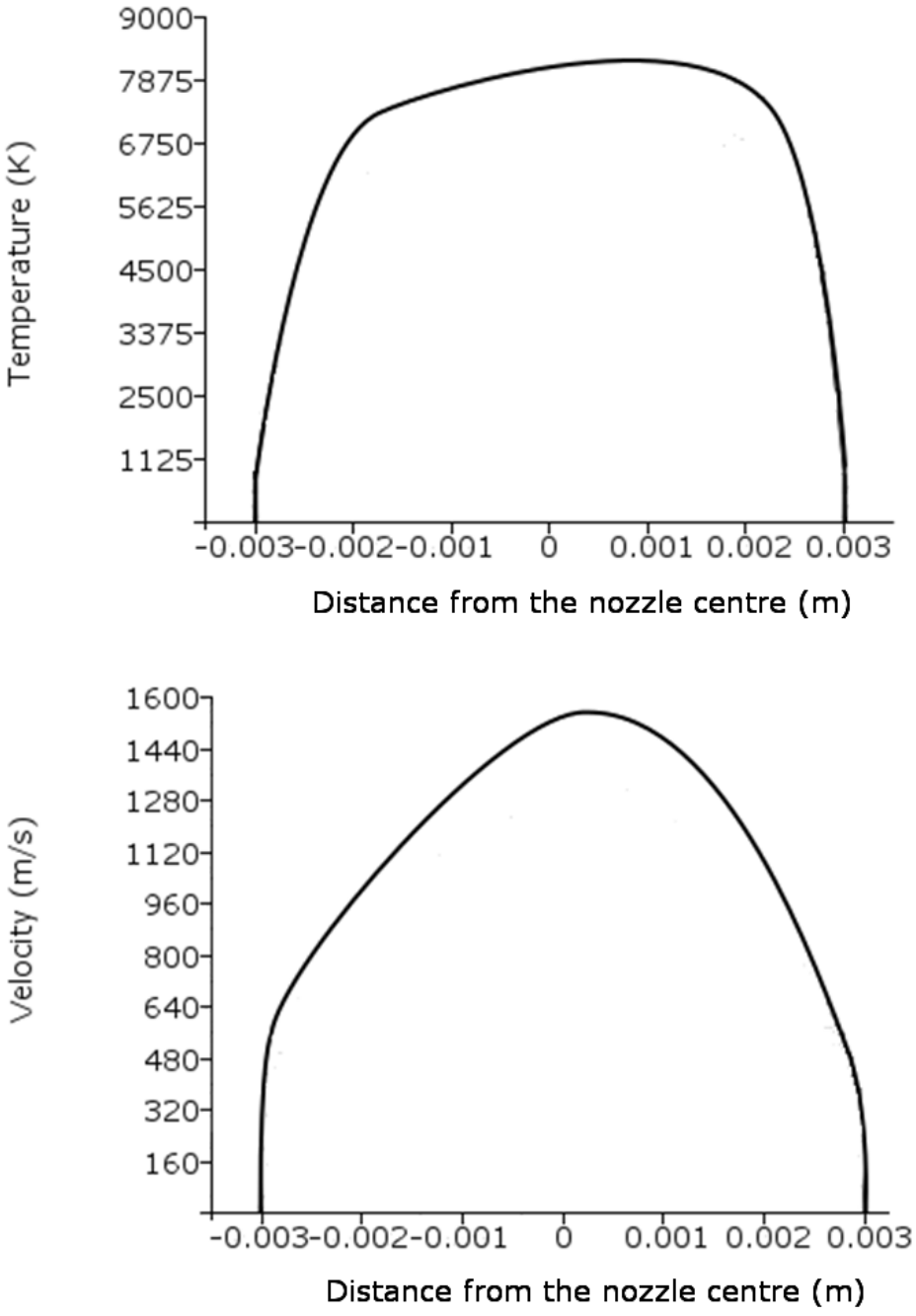

Figure 6.5.4: Temperature and Velocity radial profiles at the nozzle exit

5.8 3D Simulation with Presence of Metallic Substance

This part of the simulation is looking at the effect of the presence of the dielectric of copper in the electrical current flow. The copper may affect the frequency of the fluctuations of the arc and may also have an effect on the arc properties such as the length and its radius, both of which will be investigated in this paragraph. Studying the length and shape of the arc is of importance since in practice the arc length and shape determines the amount of energy which can be effectively invested into the working gas to form plasma.

The simulations were run by setting the current steady with a current density of $1.5A/m^2$. A droplet was placed in the nozzle and the solver was run on a steady state in order to examine if its presence has any effect on the plasma arc. The droplet was set in increasing distance from the inlet. The plasma arc distance and radius were measured for different positions and sizes of the droplet and the results are shown in Fig. 6.5, 6.6 and 6.7.

The presence of the copper droplet seems to have a minor effect on the plasma arc, with the arc length increasing as the droplet distance increases, while the arc radius decreases as the droplet distance increases. This provides and indication that the presence of the metallic working substance is not close enough to the plasma generation areas to provide a significant increase to the electric potential field lines.

As far as the droplet size is concerned, the arc length increases as the size increases, while the arc radius decreases as the droplet size increases. This gives indication that the radius becomes more concentrated with the presence of the dielectric.

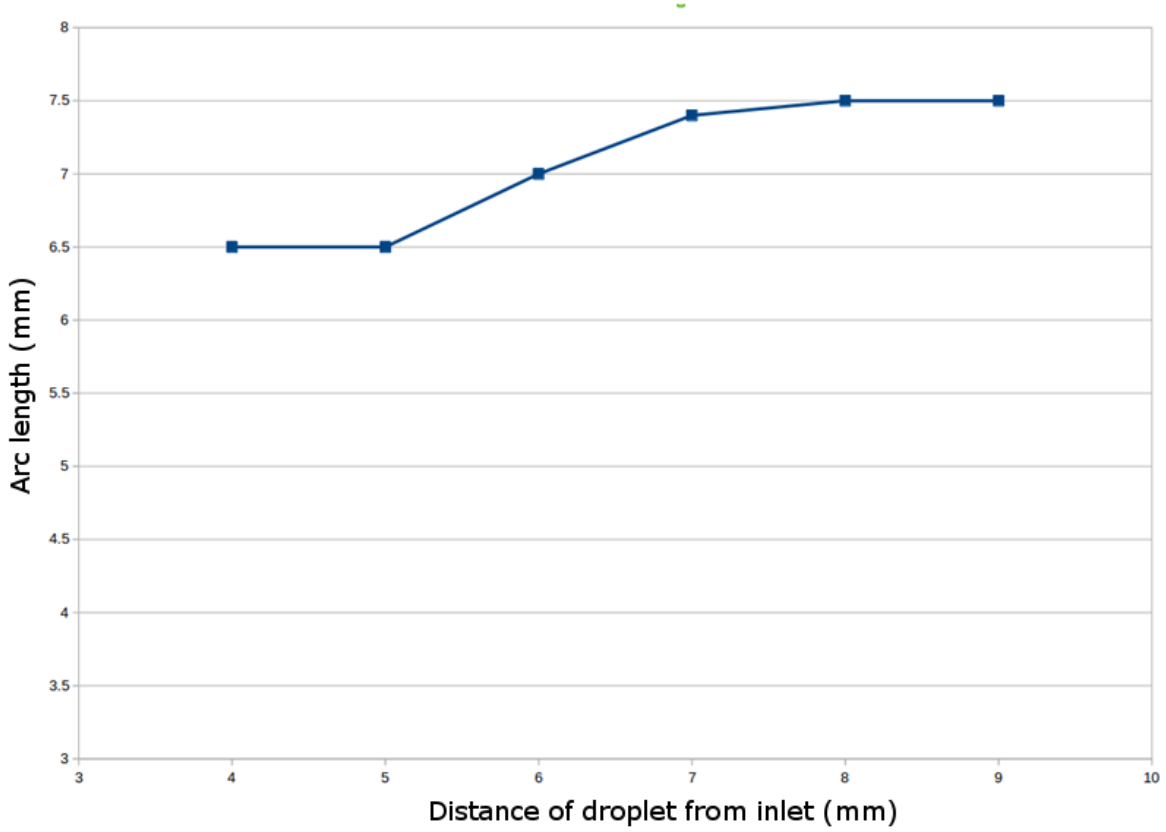

Figure 6.5.5: Arc length plotted over the distance of the droplet from the inlet.

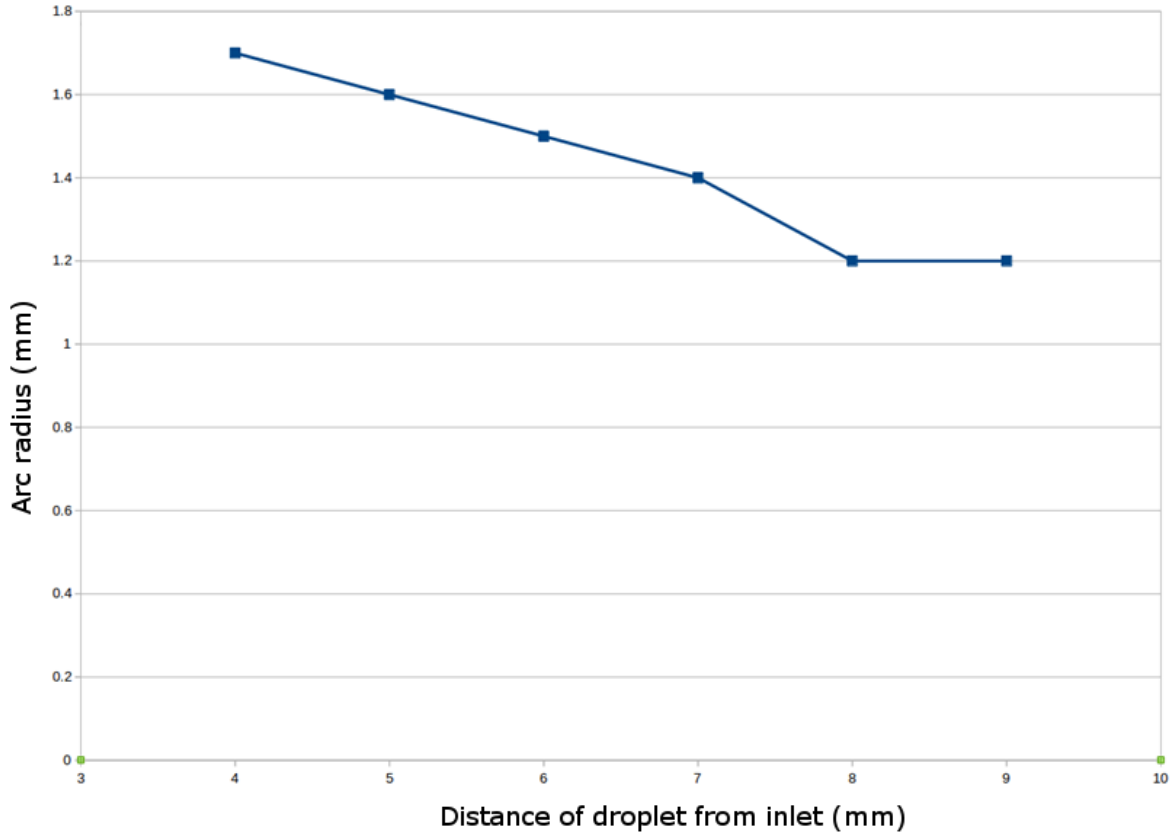

Figure 6.5.6: Arc radius plotted over the distance of the droplet from the inlet.

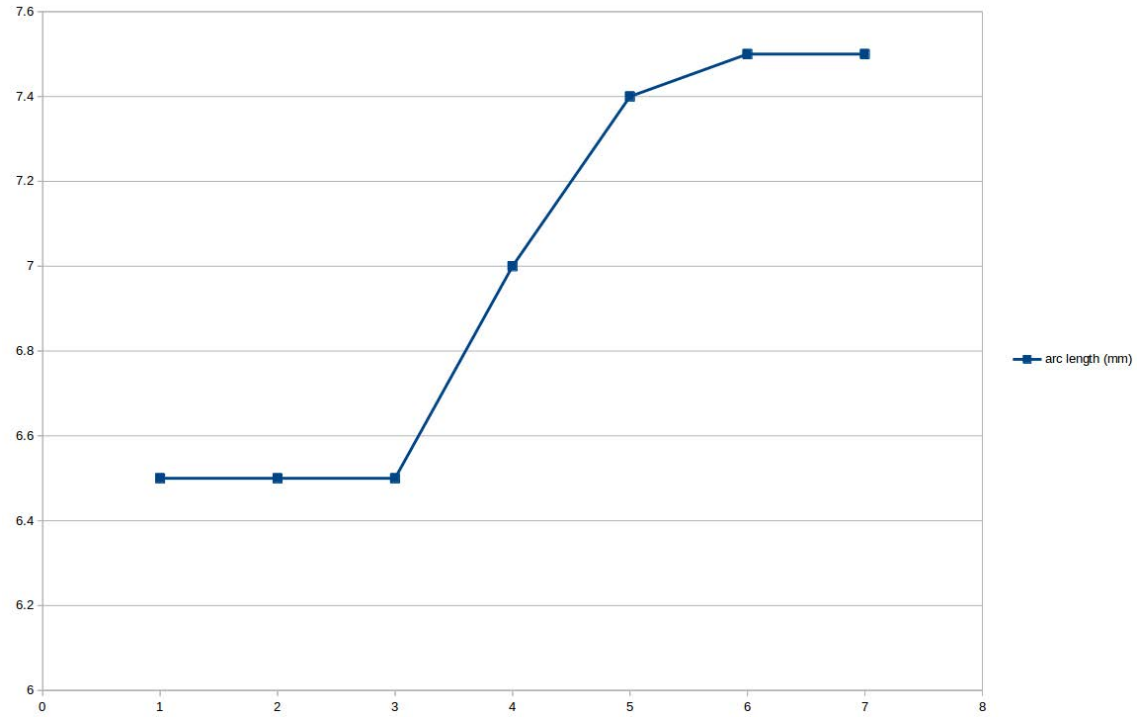

Figure 6.5.7: Arc length plotted over the size of the droplet.

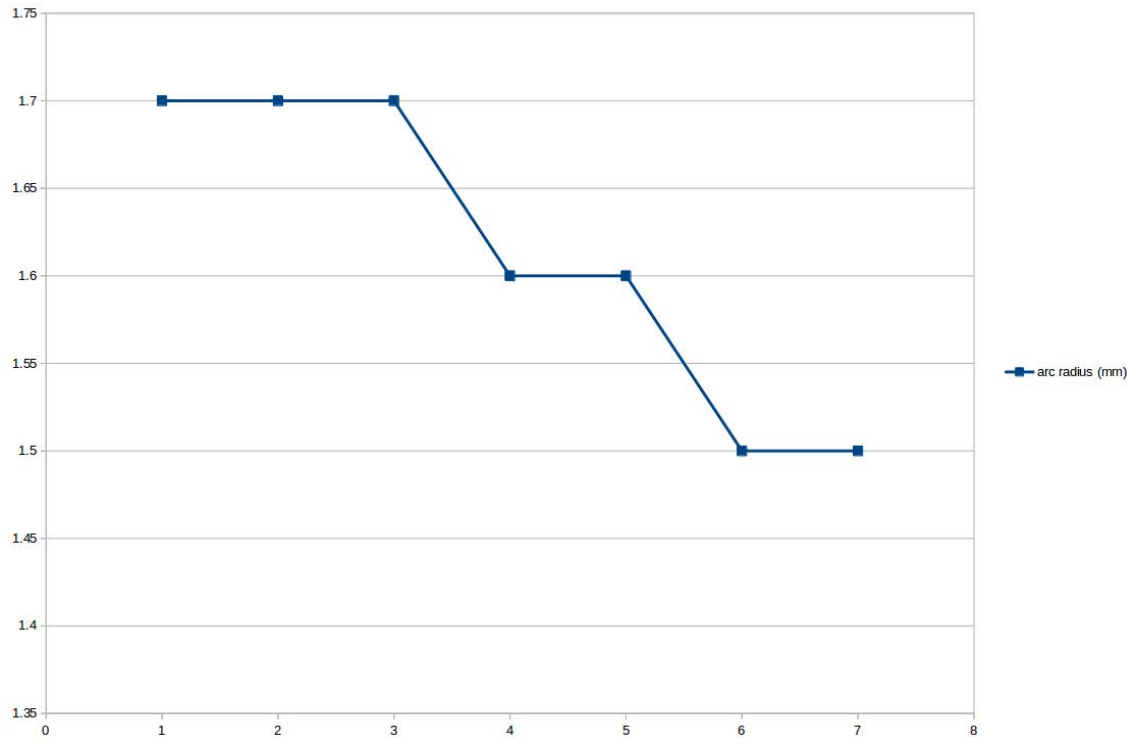

Figure 6.5.8: Arc radius plotted over the size of the droplet.

5.9 Summary

The model in this chapter showcases its capabilities in calculating fluid mechanics properties of the working gas with the presence of electromagnetic forces in a 3D domain with or without the presence of a liquid substance. It can provide calculations that can be used to measure the effect of the electromagnetic properties of the model on the working gas velocity and temperature. These properties are of highest importance in the industrial process of plasma spraying, as they determine the entrainment velocity and heat transfer between gas and working substance. The work in this thesis aims in covering the whole plasma process with different models for different areas of focus. This first model covers the first stage of plasma spraying, focusing in the nozzle area and provides results for the internal processes for plasma generation, gas transport and heat transfer. This information can be used for the subsequent models, where the resulting parameters determine the subsequent hypotheses, since the regime and the applicable type of forces can be extracted based on the current results. Additionally, the initial conditions for subsequent models can be determined and the next two models' regime, hypotheses and initial conditions base their choices in the results of the current model.

The drawback of this model is long simulation times and heavy CPU core utilisation. Compared to the next models, the simulations take almost three times the time to run and keeping in mind that subsequent models are also demanding for simulation times and core utilisation, especially with a very fine mesh. The model's resulting temperatures and velocities at the outlet provide an extrapolation equation for the initial conditions. Since they are at the same order of magnitude of the following

model and agree with modelling and experimental results, it can be considered that it provides safe hypotheses for the following model's initial conditions.

Further study should include the addition of different phases, either as more gaseous phases as a mixture to argon, or as demonstrated in the previous models, the sprayed substance with their electromagnetic and transport properties in order to study if its presence has any effect on the plasma generation and arc for transferred and non-transferred arcs. Furthermore, with the solver of this model, more localised studies on the process can be obtained, with focus being either on the plasma generation (voltage, current) near the nozzle or the velocity and heat distributions at the exit of the spraying device. The data obtained can be combined with the previous solvers enabling a more complete modelling of the process. For instance, velocity, pressure, particle and gas temperature data can be obtained at the exit of the nozzle and the same data can be input as a next step, to study further atomisation and particle size distribution and since the solvers capture the interfaces, detailed analysis up to the level of splat formation can be derived. The most hindering limitation is computer time, so focus on different local sub-processes with the appropriate solver should be advised.

The large gradients of velocity and temperature are localised near the nozzle which hosts the anode and cathode. After expansion of the flow outside of the cathode, the velocities are towards the lowest end of the gradient velocities, but the presence of the initial steep gradient plays a big role in increasing the overall velocity of the flow in the levels exhibited by plasma spraying applications.

Differences in temperature between this model and the next two show the large contribution that the additional energy parameters from the electromagnetic terms have in the energy flow characteristics.

Chapter 6: 3D Molten Metal Atomisation Simulation with Thermal Properties

6.1 Motivation

A multiphase model with heat transfer was considered to provide a more complete overview of the liquid and gas interactions in the flow regime for processes such as plasma spraying where the spraying substance can be liquid metal, suspensions of nanoparticles or microparticles in solvents, or metal salts solutions (Huang, et al., 2010) (Meillot, Damiani, Vincent, Caruyer, & Caltagirone, 2010) (Meillot, et al., 2012) (Caruyer, S., et al., 2010) (Caltagirone, et al, 2011) (Marchand, et al., 2008). The analysis can be expanded to include generic liquid precursor spraying which uses feedstock in liquid form in general. Splitting the process into sub-processes and the model into sub-models is one of the main themes of this thesis and the application of this theme in this chapter is the focus of the model in the interactions between gas and particles (Marchand, et al., 2008). The working conditions of this model and the interactions can be exhibited by either plasma spraying at the spraying phase that is outside the gas flow controlling nozzle or by liquid precursor spraying assemblies. By adding the heat transfer, the final particle size distribution, the axial velocities and the axial temperatures are produced by the model solution.

Since the goal of this thesis is to provide a set of CFD models that combined can produce useful results for the industrial application of plasma spraying, it would lack completeness without the introduction of the energy conservation in the flow. For this reason, heat transfer was introduced and several models were studied in order to identify a workable solution that could be applied. The previous model provided

results that had enough information for the finer details of molten metal atomisation near the microscale and this was encouraging and guided interest towards heat transfer between droplets of working substance and working gas.

Heat transfer in the gas and liquid phases was described by diffusion which is considered appropriate for this work as they interact with each other by conduction. This way the thermal effect of argon in the substrate can be examined. Additionally, a model which provided information on the aforementioned interactions, combined with the fact that mass sources for the liquid phase could be introduced without affecting the numerical foundations of the model, could be made to enable the study of the gas-droplet interactions produced by processes such as liquid precursor plasma spraying. This notion was further supported by the fact that in conference 5RIPT in 2011, the author participated with a presentation on this matter, which won the award for Best Presentation. Further benefit was the collaboration with Arnelle Vardelle who provided experimental results for validation of the current numerical study. One simulation of the current models was subsequently run in conditions similar to the working conditions that researchers from the University of Limoges used, and was shown to provide very good agreement in deformation patterns and atomisation results.

For the current model, a CFD simulation for the copper atomisation was produced, with different inlet velocities with argon as the working gas that atomises the substrate, at an initial temperature of $2000°K$. The comparison with the experimental data showed agreement with the CFD model and provided support on the notion that such a model for plasma spraying using liquid precursor, or not, can provide information on the control of the process and the quality of the produced surface.

6.2 Mathematical Model

The solution used for the current model employed a modified version of OpenFOAM's compressible VOF solver which adds the energy conservation and appropriate parameters to it. The complete set of governing equations for this domain is given:

$$\frac{\partial \alpha}{\partial t} + \nabla \cdot (\alpha \vec{u}) + \nabla [\alpha(1-\alpha)\vec{u}_r] = 0$$

Equation 6-1: The VOF equation as discussed in sections 3.2 and 4.3.1.

The artificial velocity term $\overrightarrow{u_r}$ is in m/s. Its purpose is to act only on interfaces, which is translated into acting on cells where both phases are present. The velocity term accounts for the compression of the interface. By the use of the magnitude of compression, it adds a velocity field acting on a thin area of the interfaces (Rusche, 2002).

The continuity equation is given in Equation 3-2.

$$\frac{\partial}{\partial t}(\rho \vec{u}) + \nabla \cdot (\rho \vec{u} \vec{u}) = -\nabla p + \nabla \cdot \left[\mu \left(\nabla \vec{u} + \nabla \vec{u}^T\right)\right] - \vec{F}_s + \rho \vec{g}$$

Equation 6-2: The momentum equation

Where t is the time, in s, the pressure p in Pa, the acceleration of gravity, g, in m/s^2 and the surface tension of the interface F_s in N/m which is calculated with the following equation:

$$\vec{F}_s = \sigma \kappa(x) \vec{n}$$

Equation 6-3: The surface tension with the curvature κ(x) in m^{-1} given by:

$$\kappa(x) = \nabla \cdot \vec{n}$$

Equation 6-4: The curvature of the surface of the mass fraction interface in each cell

$$\vec{n} = \frac{\nabla \alpha_{Cu}}{|\nabla \alpha_{Cu}|}$$

Equation 6-5: Vector $\vec{n}$ is a vector that is the normal to the interface of the mass fraction measured in m.

$$\rho = \alpha_{Cu}\rho_{Cu} + (1 - \alpha_{Cu})\rho_{Ar}$$

Equation 6-6: The density equation is calculated by (Ubbink & Issa, 1999) With the density of copper ρ_{Cu} is in kg/m^3, u_{Rel} and d_p as above and σ the surface tension of copper in N/m.

$$\mu = \alpha\mu_{Cu} + (1 - \alpha)\mu_{Ar}$$

Equation 6-7: The equation of the local viscosity μ is given by (Ubbink & Issa, 1999)

$$\frac{\partial \rho H}{\partial t} + \nabla \cdot (\rho \vec{u} H) - \nabla(\alpha \rho_{Cu} \alpha_{tCu} H) - \nabla((1 - \alpha)\rho_{Ar}\alpha_{tAr} H) = \frac{\partial p}{\partial t} + \vec{u}(\nabla p)$$

Equation 6-8: The energy conservation equation

6.3 Domain

As in the next model, the mesh is cylindrical as the in flight droplet atomisation patterns are under examination. Each end of the cylinder is the boundary, with one being the inlet and the other being the outlet. The bases are meshed with the use of a central square where each diagonal is extended towards the circle consisting the base of the cylinder until it meets the edge of the domain. This enables the creation of a mesh with structured hexahedral cells that avoid angles with skewness that should be avoided. The projection of this base of the cylinder to the other base completes the meshing that is in total consisted of 9 million cells. Same procedure for mesh refinement was followed as in the first model for full retainment of the mass fraction of the initial liquid substance.

The spherical copper droplet had a diameter of 1mm and was placed at a distance of 5mm from the inlet of the domain which had a length of 200mm. Two simulations were run, one with inlet velocity of 230m/s and one with velocity 400m/s.

6.3.1 Boundary Conditions

The velocity inlet was assigned an `inletOutlet` boundary condition, the same as the pressure outlet. The outlet boundary was assigned a zero gradient velocity field and the walls were assigned slip boundary conditions for the velocity and pressure, in order to remove wall effects. The outer surface of the cylinder was assigned slip boundary conditions for all fields. The solver used the PISO algorithm operating on the pressure based solution algorithm in a PISO loop. The volume fraction for the copper phase was taken from the MULES algorithm explicitly with second order upwind schemes for the velocity and pressure (Rusche, 2002)(4.3.1).

6.3.2 Modelling Parameters

For argon, the diffusion coefficient was taken as: $\alpha_{t_{Ar}} = 0.00015\ m^2/s$ (Devoto, 1973). The compressibility ψ is calculated from the ideal gas law: $3 \cdot 10^{-6}\ s^2/m^2$, as well as the density, which at the operating pressure has a value of $\rho_{Ar} = 0.30966\ kg/m^3$. The kinematic viscosity: $\nu_{Ar} = 2.83 \cdot 10^{-4}\ m^2/s$ from Maitland & Smith (1972).

For the copper, the diffusion coefficient value used was $\alpha_{t_{Cu}} = 0.002318\ m^2/s$, extrapolated from (Kuper, et al., 1956), the compressibility $\psi = 1.4 \cdot 10^{-8}\ s^2/m^2$ from (R. Turner, 1973), the density value $\rho_{Cu} = 7500\ kg/m^3$, from (Brillo & Egry, 2003) and the kinematic viscosity was calculated as $\nu_{Cu} = 1.56 \cdot 10^{-7} m^2/s$ from (Konstantinova, et al., 2009). The surface tension $\sigma = 1.128\ N/m$ was calculated

from (Matsumoto, et al., 2005). All values correspond to an initial temperature of $2000\ K$ and an initial operating pressure of $1atm$.

6.4 Results

The resulting particle sizes were collected at the pressure outlet of the cylindrical domain. The width of the metal phase can be obtained at the pressure outlet by examining the timestep when the atomised substance has reached that point and plots of the location where the phase was found over two lines. The line was parallel to the surface of the outlet but not on it, enabling a minimal distance to be present between the particles and the outlet. The reason for this was to avoid measuring the same particle twice, as the build-up of copper volume fraction on the outlet could have that effect. The line was dictated by the orientation of the particle elongation and was always in the direction of the largest elongation on the outlet in order to give the atomised particle length. The same process was followed for the shortest length. For the temperature and velocity, the particles were simply coloured by velocity and temperature and their values at the minimal distance from the outlet was obtained.

The velocities and temperatures for the respective profiles were taken at the same position as the resulting particle sizes. The comparison of the atomisation pattern for the droplets of the same Weber number showed agreement with the experimental results.

The particle size distribution obtained from the $230m/s$ run is shown on Figure 7.1 and the results for the $400m/s$ run are shown on Figure 7.2. The distribution graphs for both particles show little difference between them and the distributions agree with relevant publications (Huang, et al., 2010) (Karthikeyan, et al., 1997) (Shan, et al.,

2007). There is no difference in the atomizing pattern as per the Weber numbers ($We = 29$ for the $230m/s$ flow and $We = 44$ for the $400m/s$). Subsequently, the particle size distributions for the two simulations exhibit similar qualities. In a precursor spraying environment, the particles entering the gas flow are expected to be of similar size, so the atomisation of each particle should yield similar results, as observed from the simulations. The control of the initial droplet sizes in the flow of the original precursor is vital in order to achieve uniform particle sizes entering the flow and uniform atomisation patterns, which eventually leads to uniform sprayed surfaces. It is becoming once again clear that with careful application of some simple principles, thermal spraying processes can be controlled in order to produce desirable particle sizes for the appropriate application (Huang, et al., 2010).

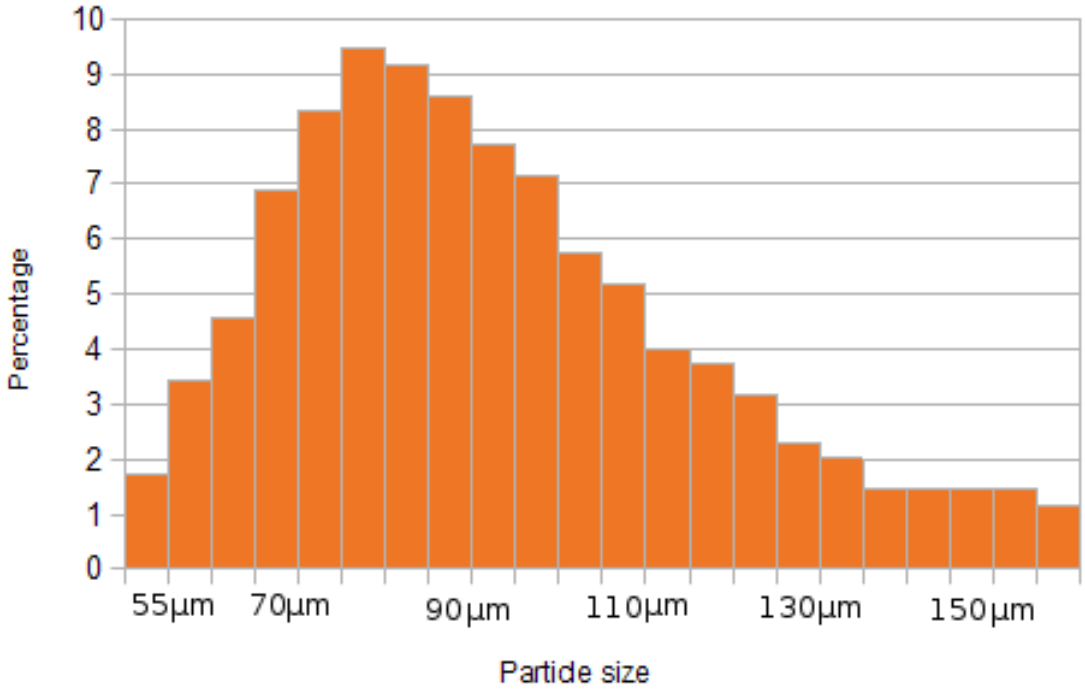

Figure 7.1: Resulting particle distribution for the 230m/s simulation (Koutsakis, Gu, & Vardelle, 2013).

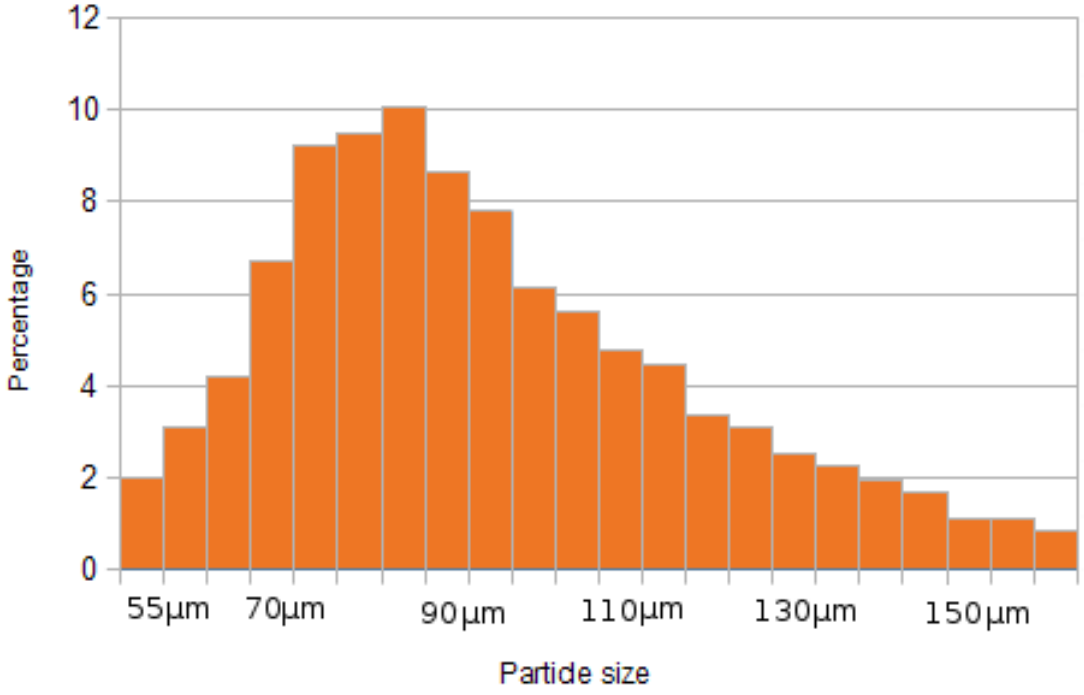

Figure 7.2: Resulting particle distribution for the 400m/s simulation (Koutsakis, Gu, & Vardelle, 2013).

The axial velocity bands at which the particles impact on the substrate are shown in Figure 7.3 and 7.4 for the 230m/s and 400m/s respectively. Both diagrams have two peaks, where the second peak with the higher velocity is in both slightly lower in particle percentage than the peak with lower velocity. The higher velocities in the outlet are mainly by the smaller particles which are entrained fast by the flow and moved to the outlet. The larger particles have a higher mass and are slower to reach higher velocities, but the higher mass accounts for a steady momentum build up, so they accelerate steadily throughout.

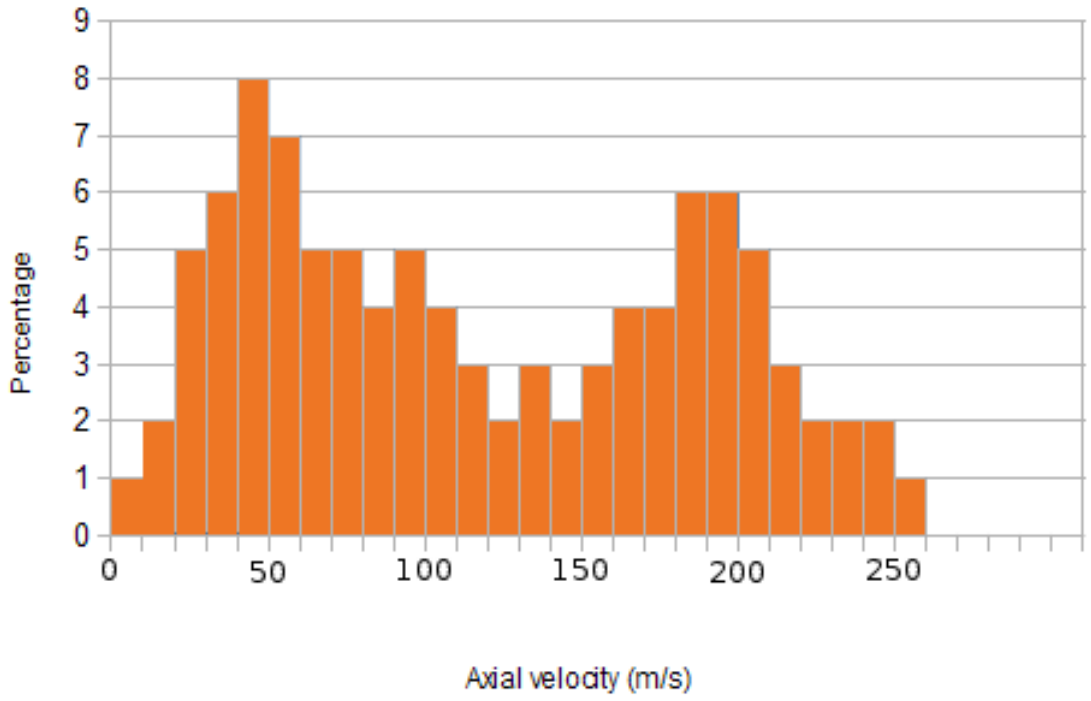

Figure 7.3: Velocity distribution for the resulting particles in the 230m/s flow (Koutsakis, Gu, & Vardelle, 2013).

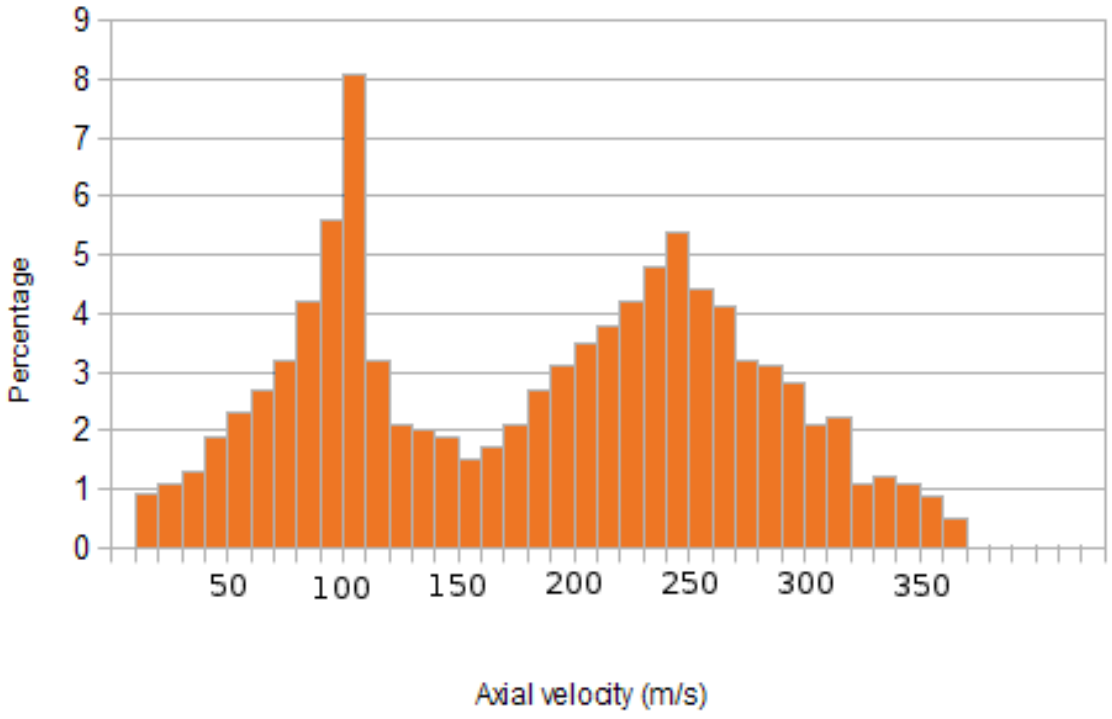

Figure 7.4: Velocity distribution for the resulting particles in the 400m/s flow (Koutsakis, Gu, & Vardelle, 2013).

The temperatures that the particles exhibited are shown in Figure 7.5 for the 230m/s simulation and in Figure 7.6 for the 400m/s simulation. The temperature at the outlet was found to be at $400K$-$500K$ for $30-40\%$ of the particles collected. A further 20% is at temperatures above $1300K$. For copper, with a melting point of $1358K$, nearly 20% of the particles is in a molten state throughout the flight. The gas temperature used ($2000K$), was relatively low, so it is fair to suggest that with higher temperatures from plasma flows in the liquid precursor spraying, the particles can sustain a much higher percentage of them in a molten state, which can enhance the quality of the spray and the control of the resulting surface.

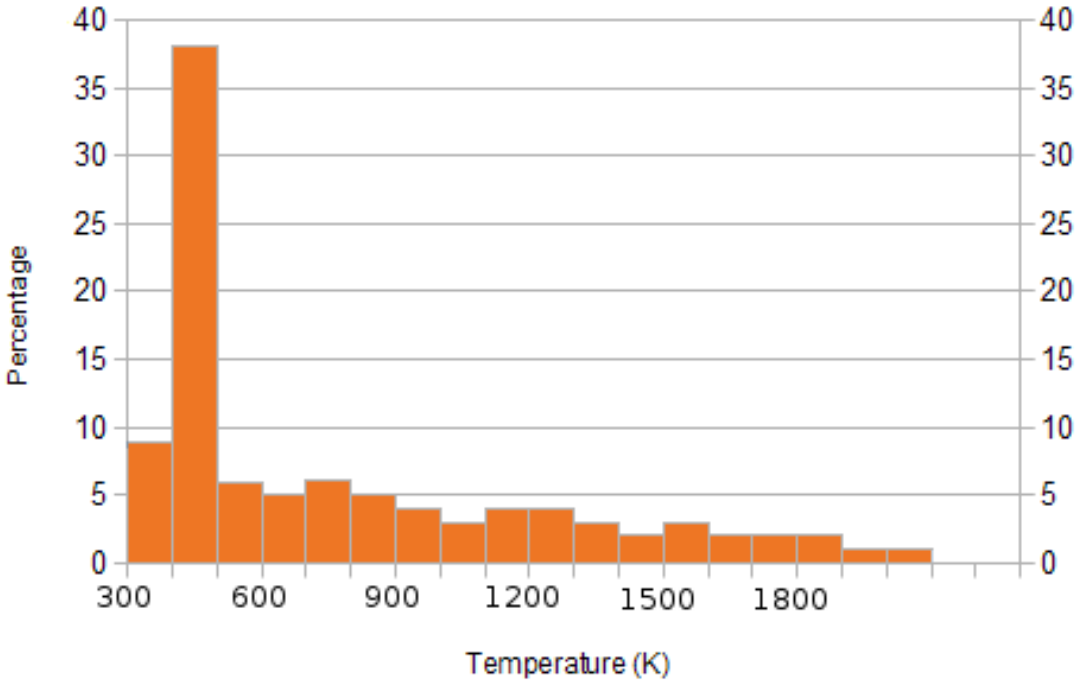

Figure 7.5: Temperature distribution for the particle in the 230m/s flow (Koutsakis, Gu, & Vardelle, 2013).

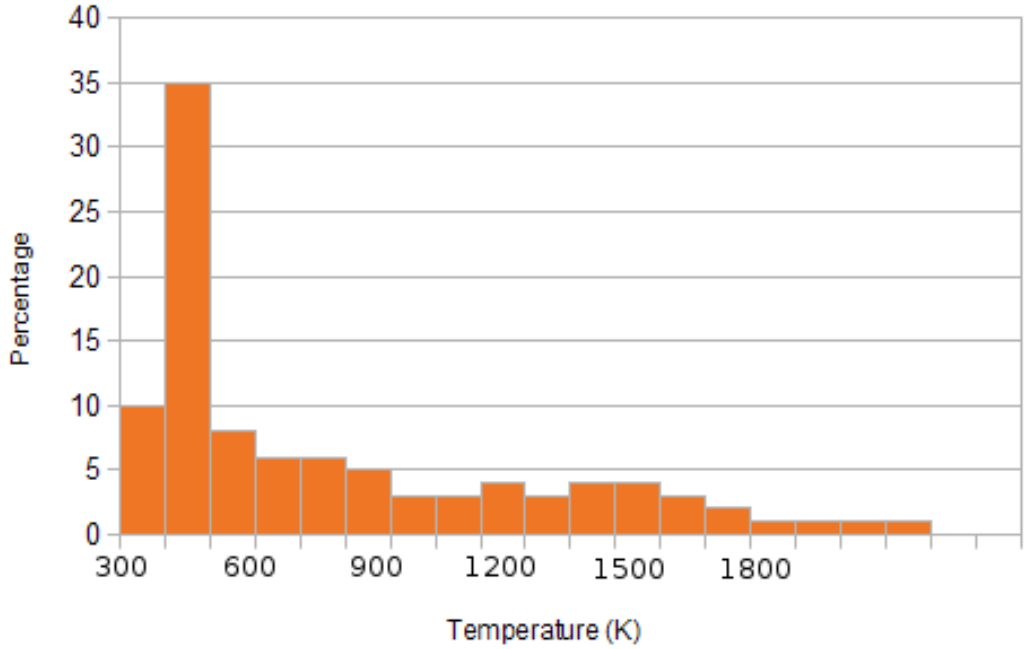

Figure 7.6: Temperature distribution for the particle in the 400m/s flow (Koutsakis, Gu, & Vardelle, 2013).

The atomization patterns for the two simulations are shown on Figure 7.7 and 7.8, while comparison of the $230m/s$ case with experimental results is shown on Figure 7.11. The Weber number can be a single indicator of the atomisation pattern a substance may have. The deformation pattern agreed with the expected one based on Weber number for the secondary atomisation (Zeoli & Gu, 2006) (Park, et al., 2006). For both of the particles studied, the deformation type was expected to be the bag deformation, as both have a $We < 80$. For the particle in the argon flow with an inlet value of $400m/s$, there is $We = 44$. The deformation it followed started from the outside, while the particle in a flow of $230m/s$ started stripping from both the edges and the middle.

The stripping of the particle which is already in bag deformation in the higher velocity flow starts from its outer layer. Much of its mass starts expanding in the direction of the flow forming strips that detach off the particle, resembling atomisation patterns in

primary jets. The particle in the flow with the lower velocity does not exhibit the same stripping effect that atomises most of its mass instantly, like the first particle does. After the initial bag deformation, the mass fractions start being atomised from the particle from a central area of the droplet's mass. The patterns, again, resemble the primary atomisation patterns of liquid jets, up to the point where they completely break down into smaller particles that do not subject to further size reduction before they reach the outlet (Nasr, et al., 2002).

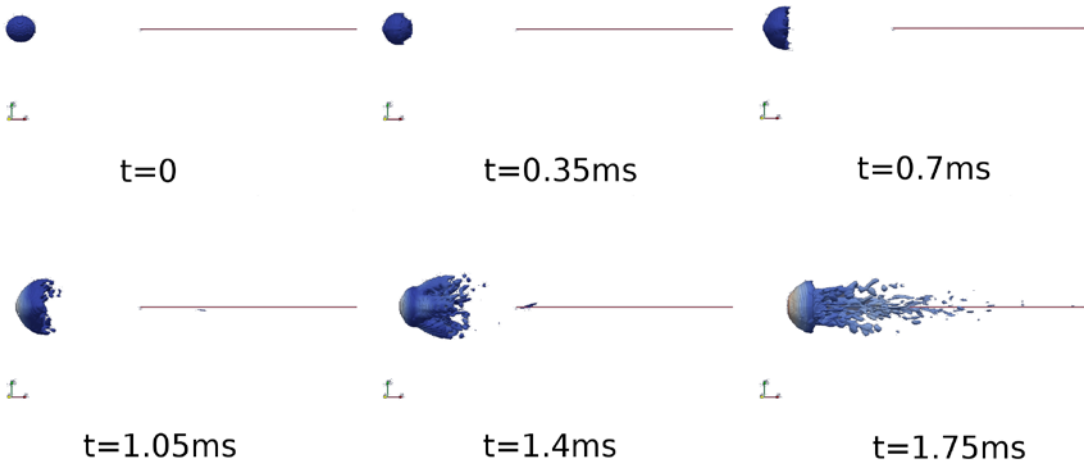

Figure 7.7: Deformation profile of the particle with inlet velocity at 230m/s (Koutsakis, Gu, & Vardelle, 2013).

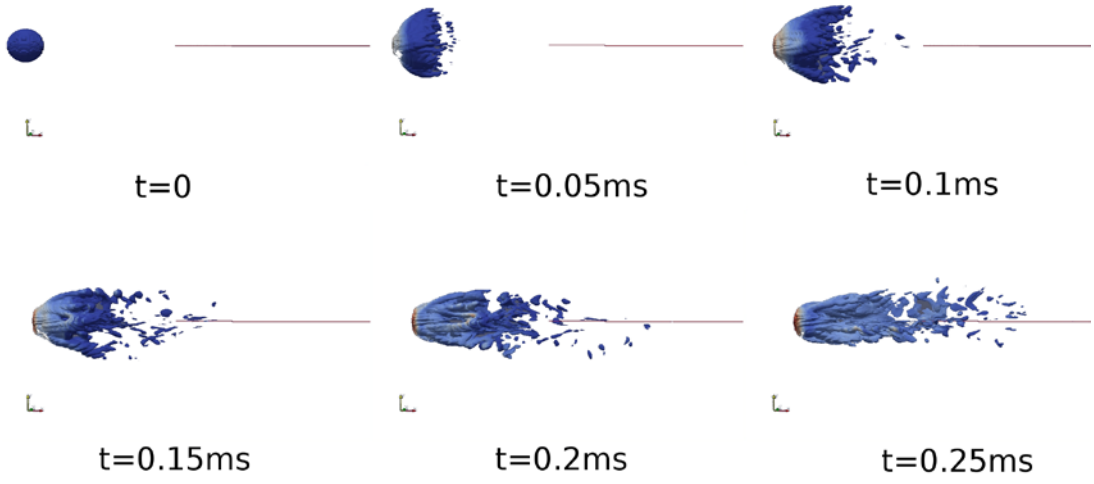

Figure 7.8: Deformation profile of the particle with inlet velocity at 400m/s (Koutsakis, Gu, & Vardelle, 2013).

Tables 7.1, 7.2 provide information on the velocity and temperature and the velocity of the atomised particles. The atomised particles were examined at the exit by colouring the mass fraction by velocity and temperature. This way, the velocity and sizes of particles that are in a molten state can be determined. The molten particles are towards the middle of both velocity and size bands for both simulations. The total particles examined for each case can be seen in Figures 7.9 and 7.10.

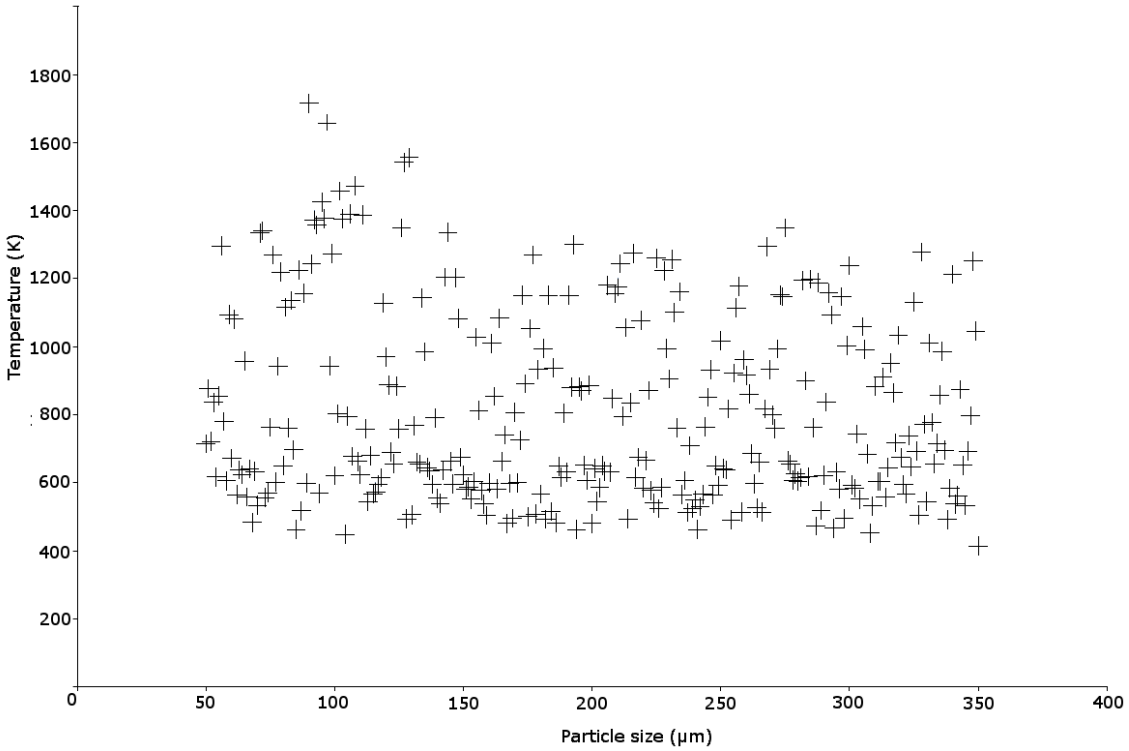

Figure 7.9: Resultant particles and their temperature for the 230m/s simulation.

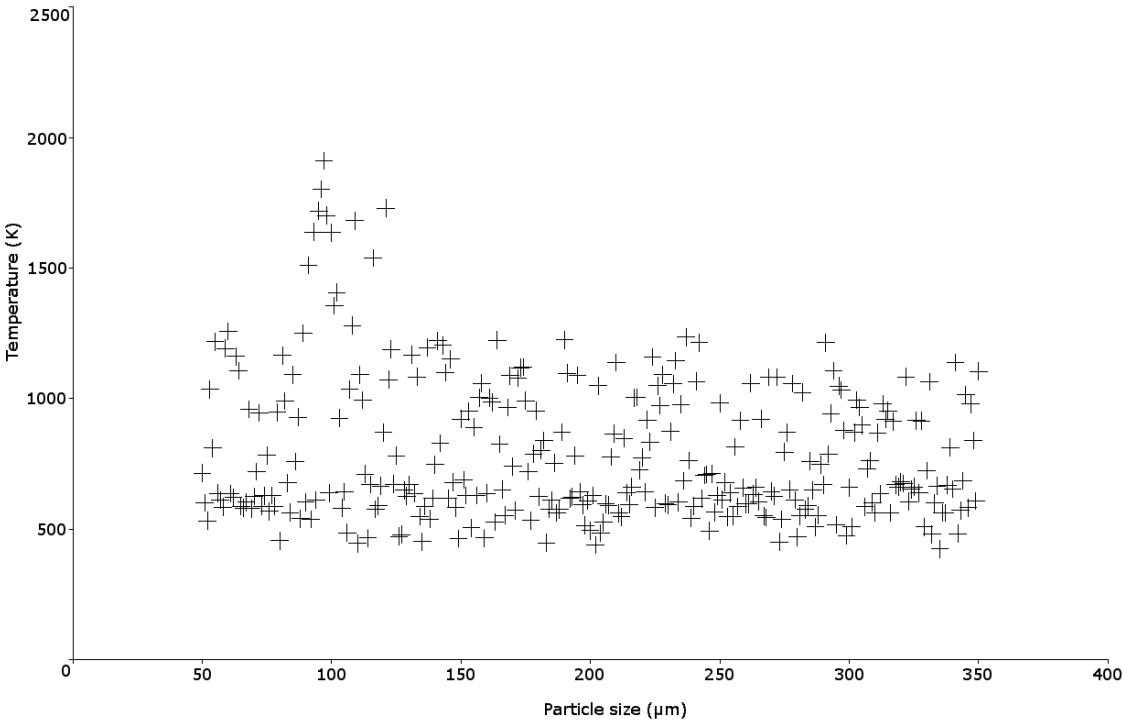

Figure 6.10: Resultant particles and their temperature for the 400m/s simulation.

Velocity	Molten particle count		Size	Molten particle count
0-10	0		55-60	0
10-20	0		60-65	0
20-30	0		65-70	0
30-40	0		70-75	0
40-50	0		75-80	0
50-60	0		80-85	0
60-70	0		85-90	0
70-80	0		90-95	3
80-90	0		95-100	3
90-100	0		100-105	2
100-110	0		105-110	2
110-120	0		110-115	1
120-130	2		115-120	0
130-140	2		120-125	0
140-150	4		125-130	2
150-160	2		130-135	0
170-180	1		135-140	0
180-190	1		140-145	0
190-200	1		145-150	0
200-210	0		150-155	0
210-220	0		155-160	0
220-230	0			
230-240	0			
240-250	0			
250-260	0			
Sum	13			13

Table 7.1: Velocities and sizes of the particles that are completely in a molten state for the 230m/s simulation

Velocity	Molten particle count		Size	Molten particle count
0-10	0		55-60	0
10-20	0		60-65	0
20-30	0		65-70	0
30-40	0		70-75	0
40-50	0		75-80	0
50-60	0		80-85	0
60-70	0		85-90	0
70-80	0		90-95	3
80-90	0		95-100	4
90-100	0		100-105	3
100-110	0		105-110	1
110-120	0		110-115	0
120-130	0		115-120	1
130-140	0		120-125	1
140-150	0		125-130	0
150-160	0		130-135	0
170-180	0		135-140	0
180-190	0		140-145	0
190-200	0		145-150	0
200-210	0		150-155	0
210-220	3		155-160	0
220-230	2			
230-240	4			
240-250	3			
250-260	0			
260-270	1			
270-280	0			
280-290	0			
290-300	0			
300-310	0			
310-320	0			
320-330	0			
330-340	0			
340-350	0			
Sum	13			13

Table 7.2: Velocities and sizes of the particles that are completely in a molten state for the 230m/s simulation

6.4.1 Comparison with Experimental Data

The results of the numerical simulation were compared with experimental data that was produced by liquid precursor spraying in flow produced by a plasma gun, at the University of Limoges, conducted by Armelle Vardelle. This provided validation for the results produced by the 230m/s droplet which exhibited the same breakup pattern as the experimental data. Experiment and simulation, both exhibit the same Weber number We=29, which is indicative of the atomisation pattern and for a droplet of similar size between them, the primary atomisation occurring is that of an elongation of the body of the droplet with the part of it that is not directly facing the flow start expanding in parallel with the flow. Finally, smaller droplets expand as streams with patterns resembling the primary atomisation of liquid jets which quickly break down into small particles that become entrained in the flow.

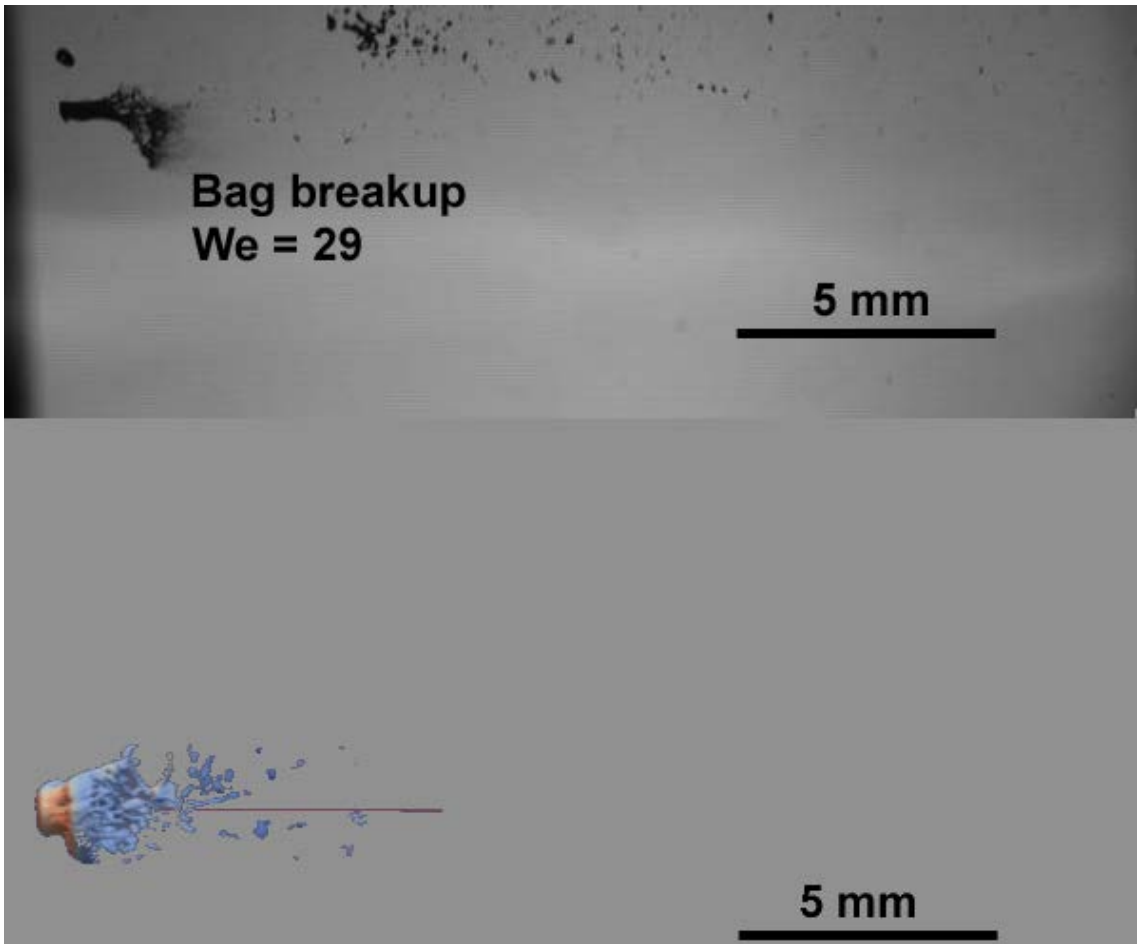

Figure 6.11: Comparison with image obtained from an experimental set up, provided by A. Vardelle (Koutsakis, Gu, & Vardelle, 2013).

6.5 Discussion

The results of this model agreed with previous work on the field of droplet atomisation by gas flow that were either numerical or experimental (Huang, et al., 2010) (Marchand, et al., 2008) (Zeoli & Gu, 2006) (Park, et al., 2006) (Karthikeyan, et al., 1997) (Shan, et al., 2007). A run of simulations of the current model, once validated can provide a great amount of detail in the study and can provide information on finer details than what the experimental study can give, with more control of the views and the progression of the atomisation pattern. It is becoming clear that primary atomisation patterns are also present in secondary atomisation of droplets, where after the initial droplet deformation, strips of substance are produced which may eventually be broken down to smaller droplets, but until that time, the elongation of the substance in the strip, from the main mass of the droplet, is similar and sometimes identical to atomisation patterns of liquid jets. Finally, supported once again is the idea that with careful control of the identified important properties of the flow, the organization of industrial sessions for spraying can lead to good control of the resulting surfaces, with optimised cost.

Chapter 7: A Model for the Particle Distribution of Molten Metal Droplets after Atomisation

7.1 Motivation

With the motivation to produce numerical models using CFD for the determination of properties for the plasma spraying process, the properties that are meaningful and useful for the industrial process were identified. In the industrial context, one of the factors with significant impact on the process and its sustainability is the economic factor, which relies heavily on the actual substance used and the coverage of sprayed surface the substance can achieve. With this in mind a CFD model was developed that would quantify properties of molten metal particles such as the atomisation of an initial amount of metal, the sizes and distribution of the resulting particles and the spraying surface coverage they can achieve. Finally, it can provide the final sub-model of the plasma spraying process breakup.

Since the model is solved numerically and is time dependant, it provides data for the entirety of the sub-process of particle flight and deposition. It can individually and additionally focus on the final part of a thermal spraying process, which is particle collision with the surface, and splat formation.

For this model, droplets with the transport properties of molten copper were placed in a domain with a compressible, isothermal fluid flow of Argon in velocities exhibited by plasma spraying guns. This work can be complementary with subsequent PSP models, as the part of the PSP where the particle is in flight and under atomisation can be separated from arc generation, as the flow establishes outside the nozzle (where the anode and cathode are) and most atomisation happens outside the nozzle as well. The

model provides results for the deformation patterns of the droplets, the resultant particle size distributions and the coverage at the outlet. With this data for copper and comparison with modelling and experimental data of the literature, validation of the model can be provided, thus ensuring validity for other metals of which the kinetic properties in liquid form are known.

The difficulties that arise while trying to model thermal spraying processes have been already discussed to an extent. The use of more than one working gases for particle entrainment may be easy for industrial or experimental applications, as the spraying device will spray whatever it is fed to it, and inert noble gases are not a rarity. But for a CFD model, each gas introduces another phase for the solver. For this reason, multiphase solvers have usually been incompressible, with an emphasis on the mixing of the gases and without the working substance present, or compressible with the VOF interface capturing approach, but with the lack of slip velocities between the interfaces. The drawback of the latter is its inability to deal with other types of phenomena, such as phase changes. There are also thermal spraying models where the operating conditions are traditionally described with compressible solvers, or are at the limits between compressible and incompressible flow. However, such models employ an incompressible solution for the numerical modelling, since it enables it to incorporate other elements easier, such as heat transfer (Mariaux & Vardelle, 2005). Another approach is the introduction of a Lagrangian framework that considers the drag as the main force and the particles solid.

With the motivation that literature up to the time of writing has not found to demonstrate samples studying the atomisation process of molten metal using CFD, the attempt was to produce such a model which could be of benefit to industrial

applications where the particle size distribution for the working materials in question is of importance.

Since two distinct phases of a gas (working gas for the spraying device) and a liquid (working substance) can be considered separate, and at temperatures where phase changes are not predicted to happen, the model was thought to benefit from a VOF approach, with a fine mesh that would enable interface capturing in detail. The open source toolkit of OpenFOAM provided the framework based on which a 3D CFD simulation of the atomisation of copper droplets of various sizes was carried through. The resulting deformation and atomisation patterns were then studied and comparison with the Rosin-Rammler distribution showed agreement.

Additionally, the large gradients appearing in such processes combined with the small particle sizes and the sizes of such installations, makes their modeling highly grid dependent. Very long grids with large resolutions can be extremely demanding in terms of CFD modeling and even inapplicable with the technology currently available.

Although a model can never be complete in terms of describing a whole process in total, it should provide an accurate representation up to a desirable point for the processes it is going through. Most models describe processes by selectively omitting effects or sub-processes, making compromises as long as they are justifiable and the final model predicts accurately the aspects of the process it is designed for. Therefore, the thermal spraying processes are usually modeled as sub-processes of the whole application introducing approximations and sometimes having limitations, resulting from the difficulties described above.

Atomisation is the process of reducing the size of an amount of a substance into smaller particles. In the air spray atomization, the means to atomize is a substance in the gas phase with a much higher relative velocity than the substance to be atomized. The Rosin-Rammler distribution is used to estimate particle size distributions produced from processes such as grinding and fragmenting Rosin & Rammler (1933) and on the present work it is used to validate particle size distributions derived from atomisation (Rosin & Rammler, 1933).

The present work focuses on modelling of the molten copper deformation and atomization in flow conditions that can be derived by the operating conditions of thermal spraying processes such as plasma guns. The deformation patterns of the atomization process and results complement other works pieces of research which focus on modeling or describing such flows and interactions as the type of atomization the model demonstrates.

Generally there are many difficulties which prevent thermal spraying processes being modeled completely using a single model. Many applications use several gases to entrain the substances to be sprayed which introduces another phase for each gas, plus one for each substance to be sprayed. Furthermore, the multiphase solvers available are either incompressible emphasizing on the mixing of phases, or compressible using a VOF interface capturing approach which lacks the slip velocities between interfaces and it cannot readily deal with phenomena such as phase changes.

7.2 Mathematical Model

The VOF used in this Model is the one discussed in sections 3.2, 4.3.1 and solves for Equation 6-1. It provides a CFD interface capturing method which solves one continuity equation and one momentum equation for the domain. The density and the viscosity are not constant at each cycle of the solution, but they represent the density and viscosity of the phases that constitute the multiphase flow. The mathematical formulation of a total phase α of 1 enables the mathematical model to assign each phase on a cell and for the phases that are present in each cell, it computes the movement of each phase by the continuity and momentum equations. It obtains the density and viscosity gradients and the influence they will have in the flow and it determines the shape and movement of each interface. The initial shape and resulting flow determine the shape functions that will act on the interfaces and what the resulting shape will be. For two phases, like in the current mode, the total volume fraction α will be 1, so in this case, the volume fraction of one phase, can be expressed by the volume fraction of the other one. Choosing α_{Cu} as the volume fraction of the copper phase, and setting it to the generic α, the volume fraction of argon is expressed as $1 - \alpha$.

The equation sets for the model were Equation 6-1 to Equation 6-8, excluding the energy equation which is not present for the isothermal solution.

7.3 Domain

The objective was to study deformation and atomisation patterns, and for this reason a very fine grid was required in order to observe the finest deformations and resulting particles. The model was shown to be heavily grid dependent as observed in the initial tests of the solver, where it ran on smaller grids compared to the final grid used. In modern VOF solvers, the alpha is summed at each timestep and the resultant alpha is normalised to one. Without this normalisation, the total alpha was found to be declining throughout the simulations, which meant there was phase loss due to the domain being unable to capture the finer interfaces. Ergo, the domain mesh was continuously increased in cell size and tested, until there was no observable reduction in the alpha for the copper phase. This procedure can also play the role of a guide for heavily grid dependent meshes providing a direction of when the mesh refinement can stop. The model was run for a cylindrical grid of 9 million hexahedral cells, shown in Fig. 8.1 and Fig. 8.2. The refining process was followed for all particle sizes used in the simulations and the domain was scaled for each different particle diameter used in order to maintain the same level of accuracy for all simulations.

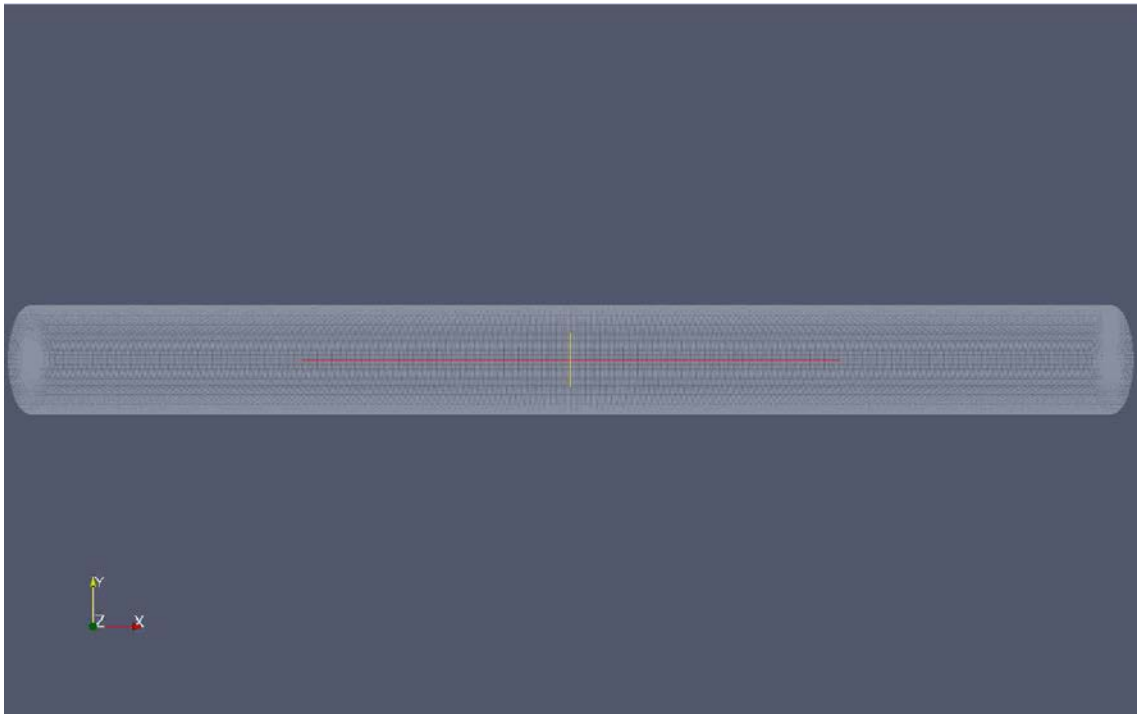

Figure 7.1: The domain used in the first model

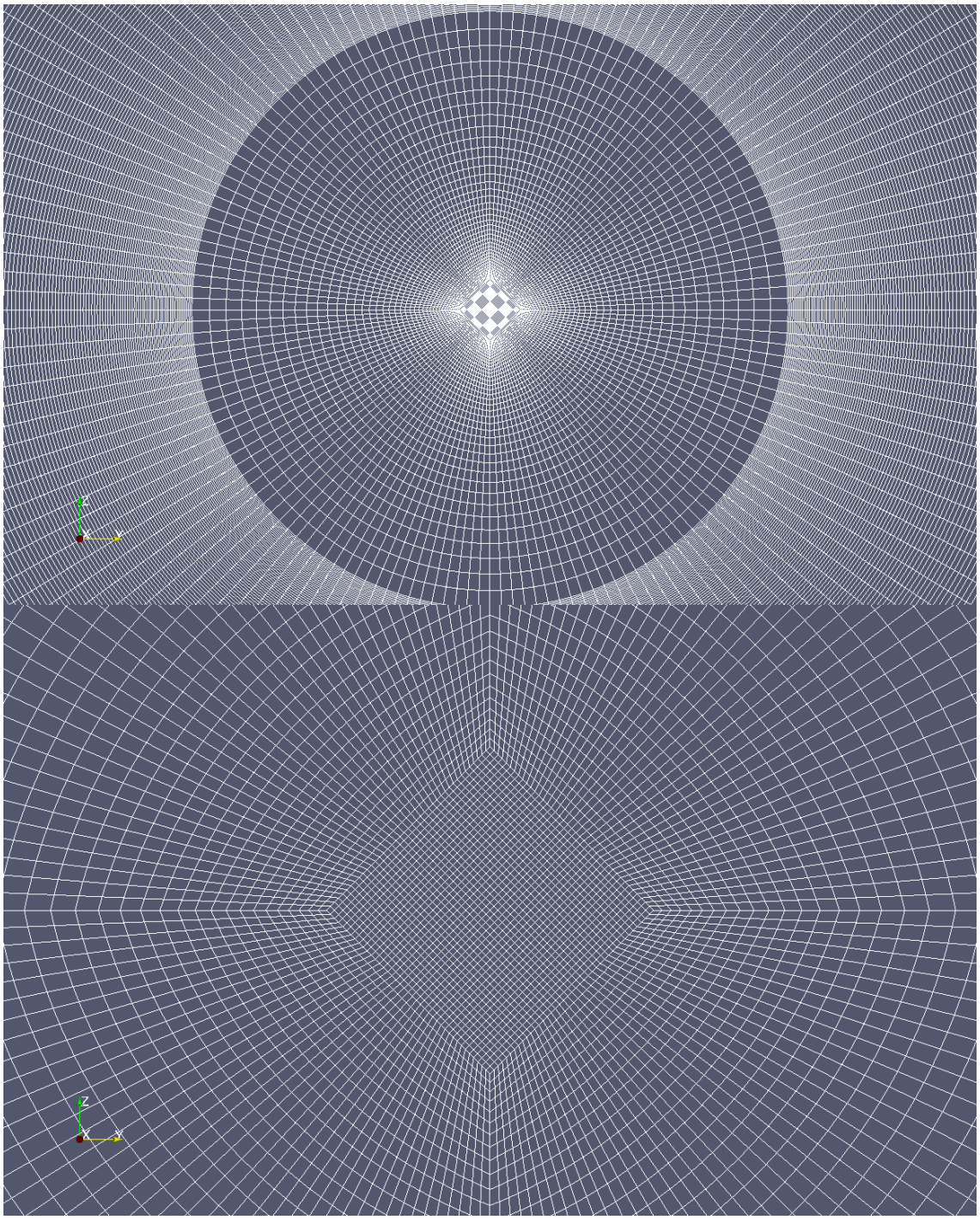

Figure 7.2: Meshing of the inlet with closeup.

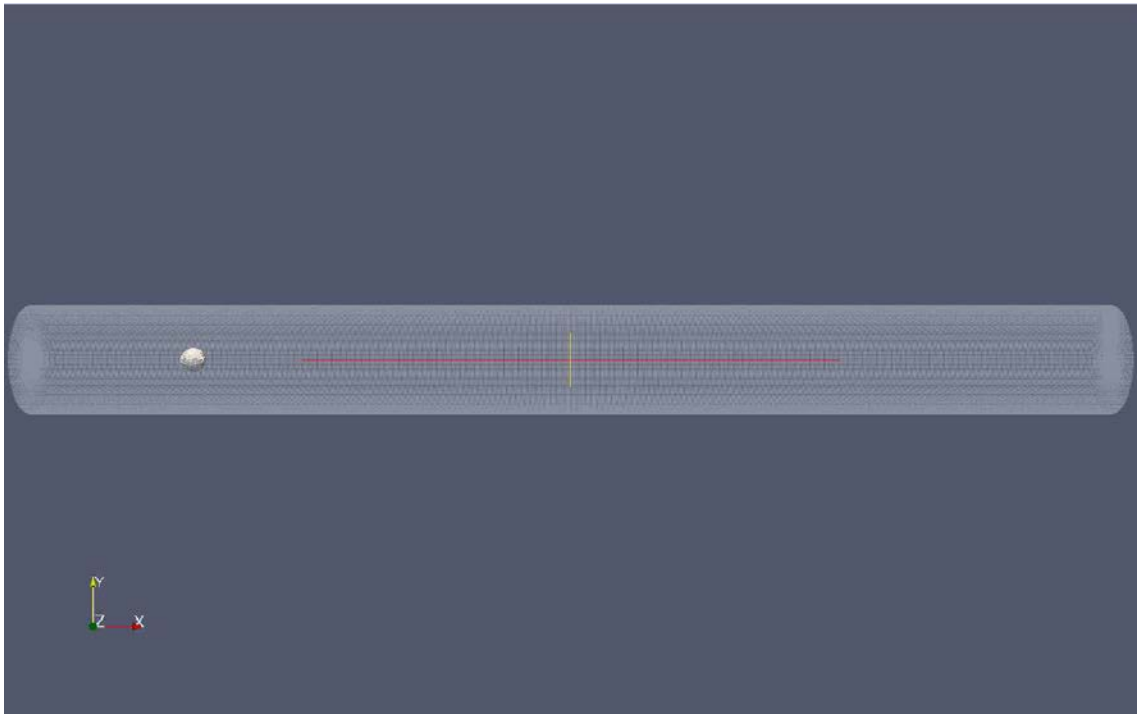

Figure 7.3: The copper droplet in the domain.

7.3.1 Boundary Conditions

The domain was designed as cylindrical. One inlet and one outlet were considered, which were the opposite bases of the domain cylinder. For the inlet boundary field, a `VelocityInlet` boundary condition was specified and its value was set to $400m/s$ parallel to the x axis.

The Mach number for this flow is $Ma{\sim}0.5$, and for this reason a compressible multiphase solver was used. The outlet boundary field was set to `inletOutlet` boundary condition of OpenFOAM. This boundary exchanges pressure and velocity boundary conditions between the fixed inlet value and a zero gradient velocity field, according to the direction of the velocity on each cell face (OpenCFD, 2010).

The curved surface of the cylinder was set to `Wall` but it was assigned a `Slip` boundary condition for the velocity. This was chosen so as the wall effects that would normally appear in such a narrow grid were not present.

The VOF solver of that version of OpenFOAM used (2.0.0), employed a PISO loop for the pressure based solution algorithm. The multiphase solution employed the MULES explicit algorithm with second order upwind schemes for the velocity and pressure (Rusche, 2002). The turbulence model used was the LES model (Smagorinsky, 1963).

For the pressure, a zero gradient field boundary condition was assigned in the inlet and outlet and a slip condition to the walls to complement the corresponding velocity boundary condition for the avoidance of wall effects.

The copper phase was set to be spheres for all runs of the simulation. Three different radii were used for the particle: $250\mu m$, $500\mu m$ and $1mm$. For each run, the initial position of the particle was ten times its radius. This was established after several tests, were the flow was not building up correctly and the positioning of the particle very close to the velocity inlet was causing very large gradients to appear. Once the particle was moved away from the inlet, no obstruction to the inlet was observed and the study of the deformation and atomisation became feasible. For each simulation, the domain length is 100 times the particle's diameter.

The values of $y+$ for the $250\mu m$ ranged from 10^{-8} to 50, with an average of 1.2 for the first time step. They gradually rose as the flow progressed, to an average of 5.5. Similar $y+$ values were exhibited by the other two particles.

7.3.2 Modelling Parameters

For argon, the diffusion coefficient: $\alpha_{t_{Ar}} = 0.00015 m^2/s$ (Devoto, 1973). The

compressibility ψ is calculated from the ideal gas law: $3 \cdot 10^{-6} s^2/m^2$, as well as the density, which at the operating pressure has a value of $\rho_{Ar} = 0.30966 kg/m^3$. The kinematic viscosity: $\nu_{Ar} = 2.83 \cdot 10^{-4} m^2/s$ from (Maitland & Smith, 1972).

For the copper, the diffusion coefficient value used was $\alpha_{t_{Cu}} = 0.02318 m^2/s$, extrapolated from (Kuper, et al., 1956), the compressibility $\psi = 1.4 \cdot 10^{-2}\ s^2/m^2$ from (Turner, et al., 1973), the density value $\rho_{Cu} = 7500 kg/m^3$, from (Brillo & Egry, 2003) and the kinematic viscosity was calculated as $\nu_{Cu} = 1.56 \cdot 10^{-7} m^2/s$ from (Konstantinova, et al., 2009). $\sigma = 1.128\ N/m$ was calculated from (Matsumoto, Fujii, Ueda, Kamai, & Nogi, 2005). The turbulence model used was the 3D Smagorinsky LES model (Smagorinsky, 1963), with the cubic root of volume set as filter width.

7.4 Results

The simulation produces data for the particle deformation patterns and the resulting particle sizes can be obtained by collection at the pressure outlet of the cylindrical domain. Similarly to the previous chapter, the width of the metal phase was obtained at the pressure outlet for two lines on the shortest and longest elongation axes on the particle. Most particles were spheroids, for this reason only two axes were needed. The resulting surface from the projection of the spheroid to the ellipse was calculated and finally the equivalent circle diameter was obtained. The diameters were grouped into size bands, thus the particle size distributions were produced.

All three particles demonstrate good agreement with the Rosin-Rammler distribution (Figs 3-5), while larger droplets tend to produce more atomized particles that are larger than the predicted count for these sizes.

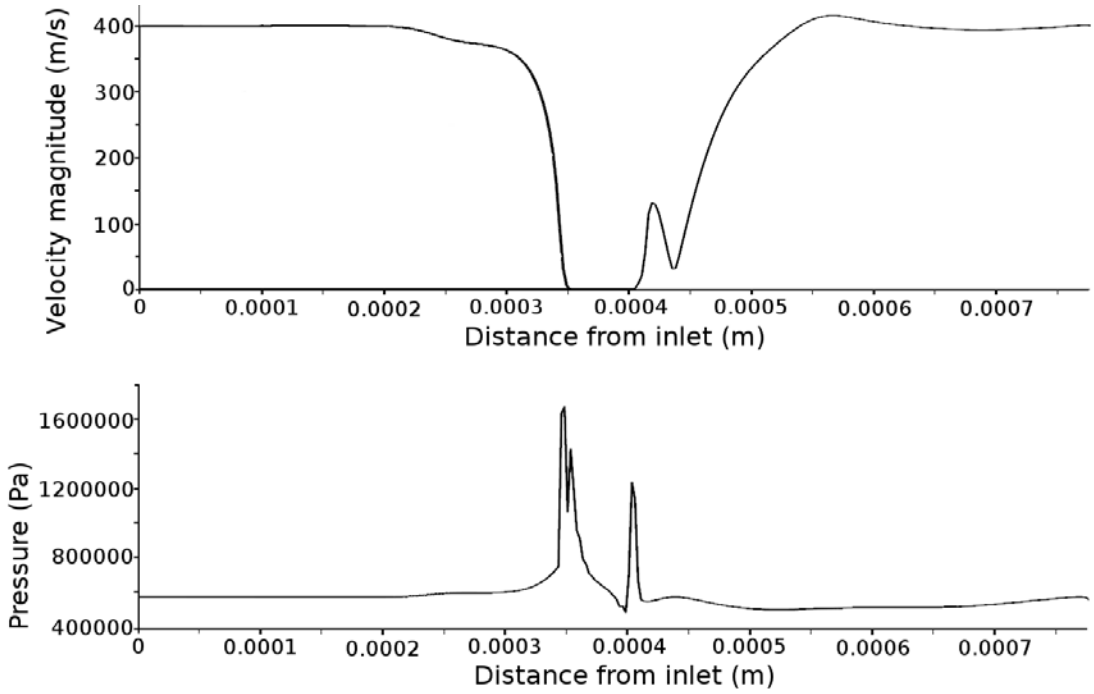

Figure 7.4: Velocity and pressure of the 250µm particle at t=2E-6 s (Koutsakis, Shrimpton, & Gu, 2016).

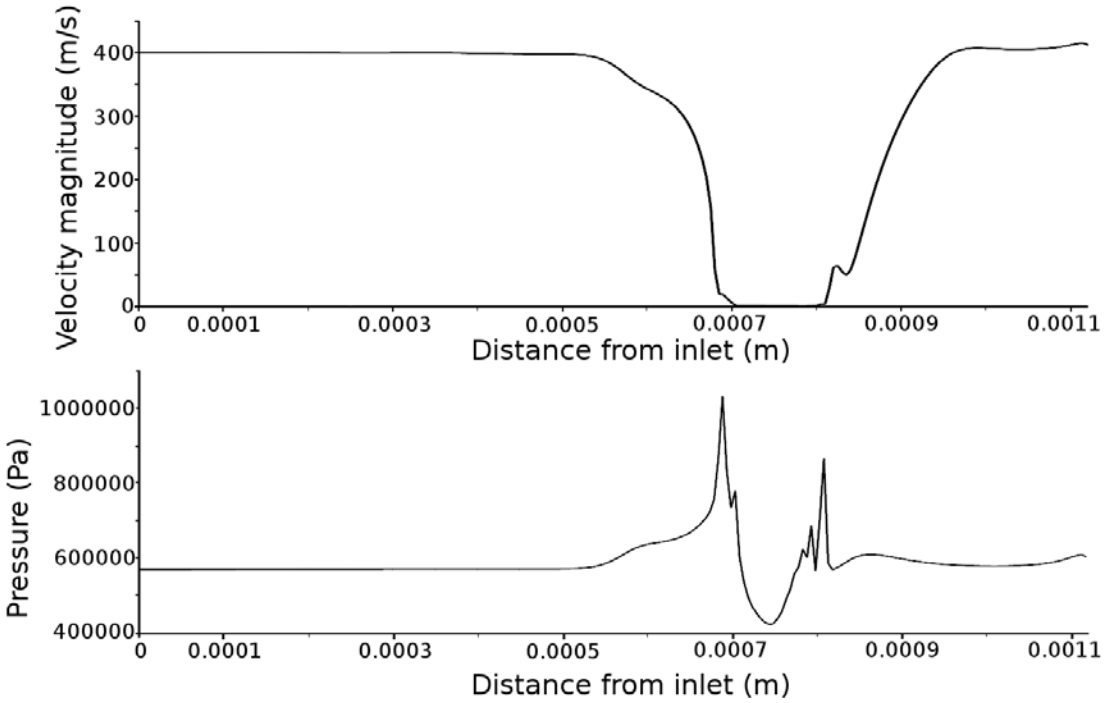

Figure 7.5: Velocity and pressure of the 500µm particle at t=4E-6 s (Koutsakis, Shrimpton, & Gu, 2016).

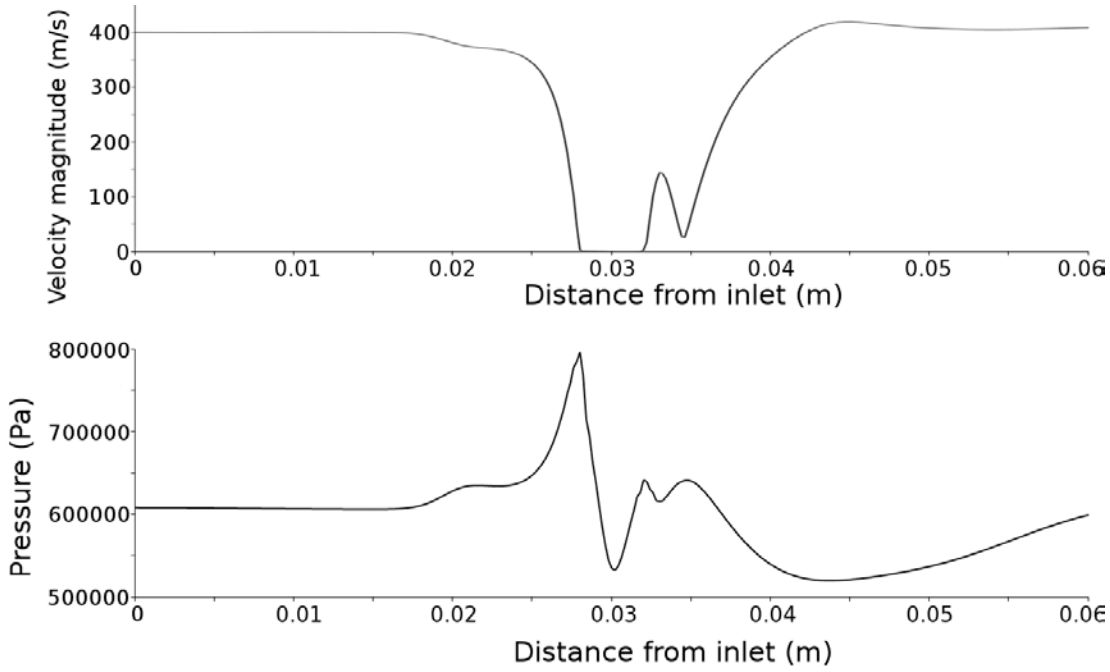

Figure 7.6: Velocity and pressure of the 1000µm particle at t=1E-4 s (Koutsakis, Shrimpton, & Gu, 2016).

7.4.1 Atomisation Patterns

All atomization patterns fall closely into the boundary layer stripping breakup pattern (Ranger & Nicholls, 1972), with the particles stripped throughout their surface. The pattern is well known and exhibited in many gas atomization applications and can be found in other modelling or experimental works such as (Marchand, et al., 2008) which applies a model to explain experimental results from water droplets in an $Ar - H_2$ plasma, as well as (Ranger & Nicholls, 1972) which studies larger particles with similar Weber numbers to the ones exhibited herein. Additionally, the patterns show good agreement with the experimental results in (Joseph, Beavers, & Funada, 2002) which were carried through with similar Weber numbers, though reaching values up to $We = 168.6 \cdot 10^3$.

The $250\mu m$ particle initially follows a stretching and thinning breakup pattern (Zeoli & Gu, 2006), which is initially deforming to a shape that resembles a half sphere with the curved area towards the velocity inlet with a crown on the other side (Fig. 6), the latter being the source of the initial atomized particles. The specific shape the particle assumes during atomization shows very good agreement with the experimental observations on $300\mu m$ particles by (Marchand, et al., 2008). The particle Reynolds number for the $250\mu m$ particle is $Re = 353$. The type of deformation it demonstrates on the simulations is expected by the Weber numbers for the particle, $We = 34.1$, where the inertial forces dominate the surface tension forces on the droplets. In the simulations the particle cannot be entrained by the argon flow (Rein, 2002), but starts accelerating very slowly obtaining an initial velocity of $5.6 \cdot 10^{-2} m/s$ when the flow has completely covered it. Although not entrained, the particle is affected by the high velocity and pressure gradients (Fig. 7) that develop in its boundary, producing large

shear stresses, and it starts deforming. The particle inertia combined with the high velocities that flow around it causes the crown deformation demonstrated on all three particles of the simulation. This causes the particle to start atomizing from the tips of the crown, which also exhibit patterns of primary atomization which takes place in round liquid jets of low to medium Reynolds and Weber numbers (Nasr, Yule, & Bendig, 2002). These patterns can be seen in Figs. 6, 8 and 10, in longer strings of copper mass that are produced by the tips of the crown pattern. After about half of the droplet mass is left unatomised, the remaining flattened copper surface is broken into smaller pieces of comparable sizes and shortly each one is atomized according to the pattern observed in the whole particle, in a smaller scale.

The $500\mu m$ particle (Fig. 8) follows the same pattern as the $250\ \mu m$ particle. Its particle Reynolds number is $Re = 707$. The pattern is almost identical to the smaller droplet, but for longer tips on the crown in proportion. Its Weber number is $We = 68.1$, still indicating the observed atomization pattern. The velocity and pressure gradients on each side of the particle in the direction of the flow (Fig. 9) also accounts for the boundary layer stripping pattern. The dominance of inertial forces against surface tension provides an explanation to the deformation pattern and breakup of the droplet, with the boundary layer stripping throughout and crown tips that atomize following patterns of primary atomization.

As for the $1\ mm$ particle (Fig. 10), it follows a pattern which starts with boundary layer stripping but more of its mass is quickly stripped and the deformation is more extended. Its particle Reynolds number is $Re = 1413$ while $We = 136.3$. Large parts of the droplet are stripped away from its main mass and long crown tips produce a not so common atomization shape, but the prevalence of inertial forces against surface

tension is obvious in the breakup. The crown deformation is still apparent initially and later, the patterns similar to primary atomization patterns are easily visible, as the crown tips are more in number and longer in length.

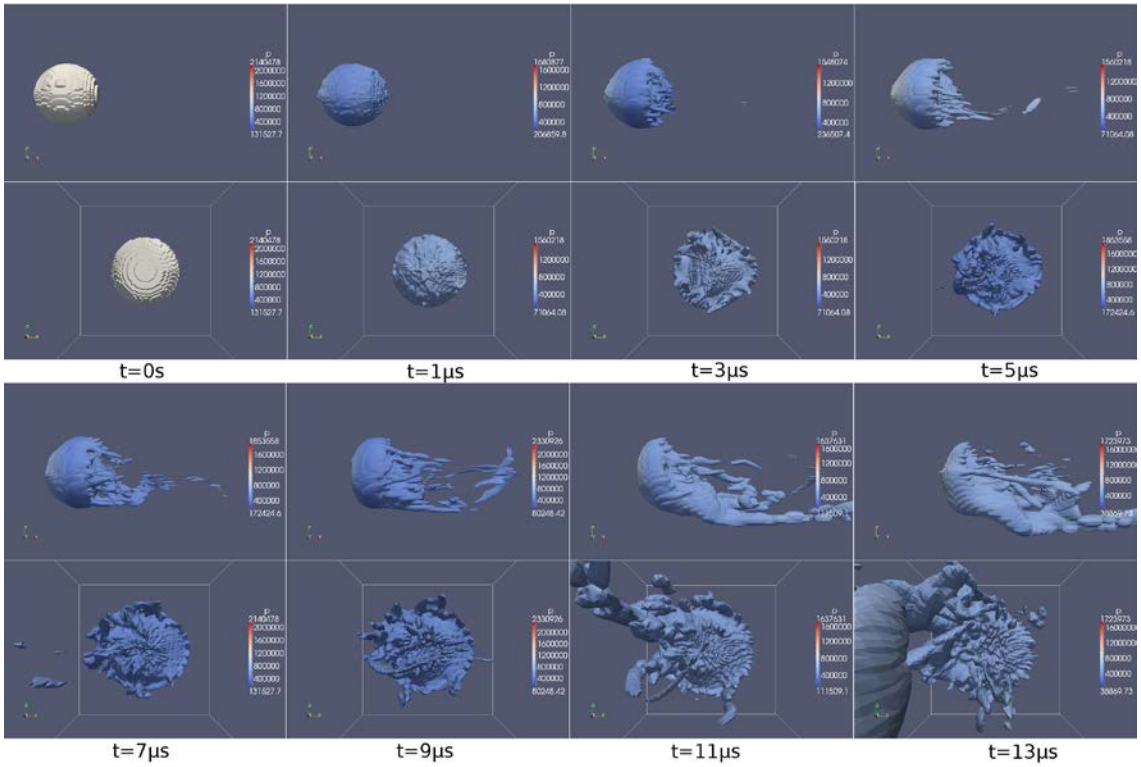

Figure 7.7: Atomisation profile of the 250µm particle (Koutsakis, Shrimpton, & Gu, 2016).

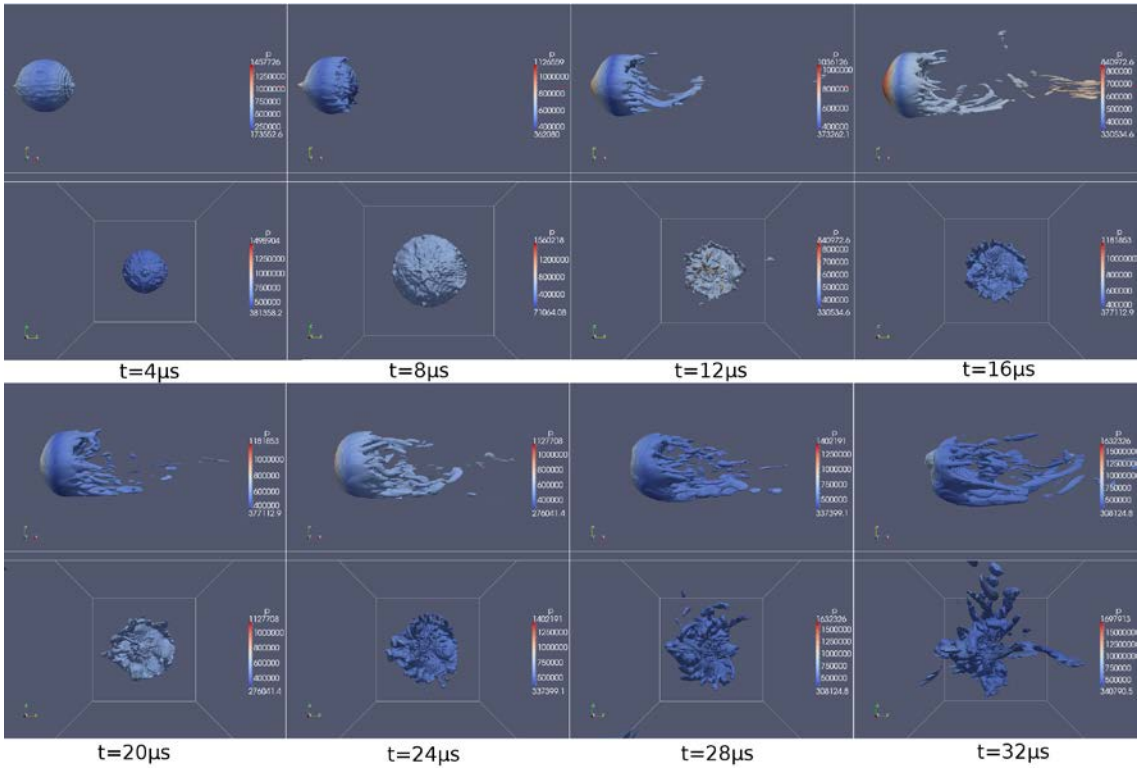

Figure 7.8: Atomisation profile of the 500µm particle (Koutsakis, Shrimpton, & Gu, 2016).

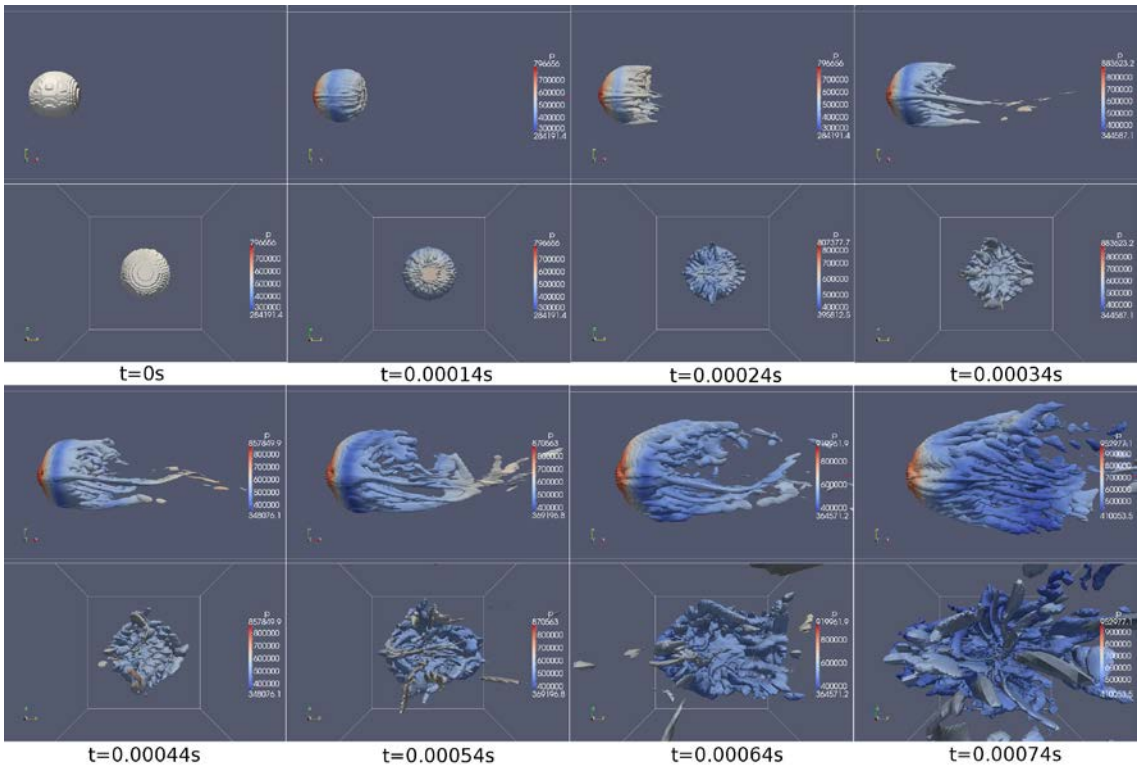

Figure 7.9: Atomisation profile of the 1000µm particle (Koutsakis, Shrimpton, & Gu, 2016).

7.4.2 Particle Size Distributions

The simulations can provide information for both particle sizes as well as particle shapes. In Tables 8.1-8.3 the type of spheroid the observed atomised particles exhibit. Similarly to results from the previous model, most spherical particles concentrations are observed in the smaller particle sizes. This is due to the fact that after entrainment and effect of atomisation patterns of liquid jets in the oblate spheroids, the final atomisation results in finer particles. Additionally, prolate particles are across the flow, so the effect of the velocity front will atomise them across, resulting in smaller more spherical particles.

The tables 8.1-8.3 can provide useful input data for splat formation using combined splat sizes, even by using the same model. The input can be a window of splat sizes in random locations that can be re-run in batch and can provide results for splat coverage by setting the outlet as wall.

Size range	number of particles	oblate spheroid	prolate spheroid	sphere
0-2 e-06	6	3	1	2
2-4 e-06	12	5	3	4
4-6 e-06	19	6	3	10
6-8 e-06	29	11	4	14
8-10 e-06	33	10	10	13
10-12 e-06	32	15	6	11
12-14 e-06	31	14	8	9
14-16 e-06	28	16	5	7
16-18 e-06	25	14	5	6
18-20 e-06	21	11	6	4
20-22 e-05	18	9	5	4
22-24 e-05	17	9	4	4
24-26 e-05	16	8	3	5
26-28 e-05	15	8	3	4
28-30 e-05	14	7	2	5
30-32 e-0.5	13	7	1	5
32-34 e-05	12	4	1	7
34-36 e-05	11	5	0	6
36-38 e-05	11	4	1	6
38-40 e-05	10	3	1	6
40-42 e-05	10	2	1	7
42-44 e-05	8	2	1	5
Sum	391	173	74	144

Table 8.3: Observed particles for the 1000µm initial particle simulations and their shape

Size range	number of particles	oblate spheroid	prolate spheroid	sphere
0-1.5 e-06	6	0	1	5
1.5-3 e-06	12	2	4	6
3-4.5 e-06	16	8	4	4
4.5-6 e-06	20	10	6	4
6-7.5 e-06	26	11	7	8
7.5-9 e-06	32	15	8	9
9-10.5 e-06	33	14	8	11
10.5-12 e-06	34	17	10	7
12-13.5 e-06	34	16	9	9
13.5-15 e-06	32	16	8	8
15-16.5 e-06	28	14	7	7
16.5-18 e-06	26	12	7	7
18-19.5 e-06	25	12	6	7
19.5-21 e-06	24	10	6	8
21-22.5 e-06	22	8	6	8
22.5-24 e-0.6	21	6	5	10
24-25.5 e-06	19	5	5	9
25.5-27 e-06	18	5	6	7
27-28.5 e-06	15	4	5	6
28.5-30 e-06	14	4	4	6
30-31.5 e-06	10	3	3	4
31.5-33 e-05	9	3	2	4
Sum	476	195	127	154

Table 8.4: Observed particles for the 500µm initial particle simulations and their shape

Size range	number of particles	oblate spheroid	prolate spheroid	sphere
0-1 e-06	1	0	0	1
1-2 e-06	2	0	0	2
2-3 e-06	6	2	0	4
3-4 e-06	12	5	1	6
4-5 e-06	15	7	3	5
5-6 e-06	20	8	3	9
6-7 e-06	22	9	4	9
7-8 e-06	25	9	6	10
8-9 e-06	26	10	8	8
9-10 e-06	28	10	8	10
1-1.1 e-05	26	11	7	8
1.1-1.2 e-05	25	8	7	10
1.2-1.3 e-05	23	6	8	9
1.3-1.4 e-05	22	6	10	6
1.4-1.5 e-05	17	5	6	6
1.5-1.6 e-0.5	15	4	6	5
1.6-1.7 e-05	14	3	6	5
1.7-1.8 e-05	12	3	5	4
1.8-1.9 e-05	11	2	5	4
1.9-2 e-05	10	2	6	2
2-2.1 e-05	9	1	5	3
Sum	341	111	104	126

Table 8.5: Observed particles for the 500μm initial particle simulations and their shape

Finally, worth mentioning is that each initial particle when atomized can cover a surface up to 4.8 times the cross section area at its diameter, which is the total cylindrical mesh's diameter.

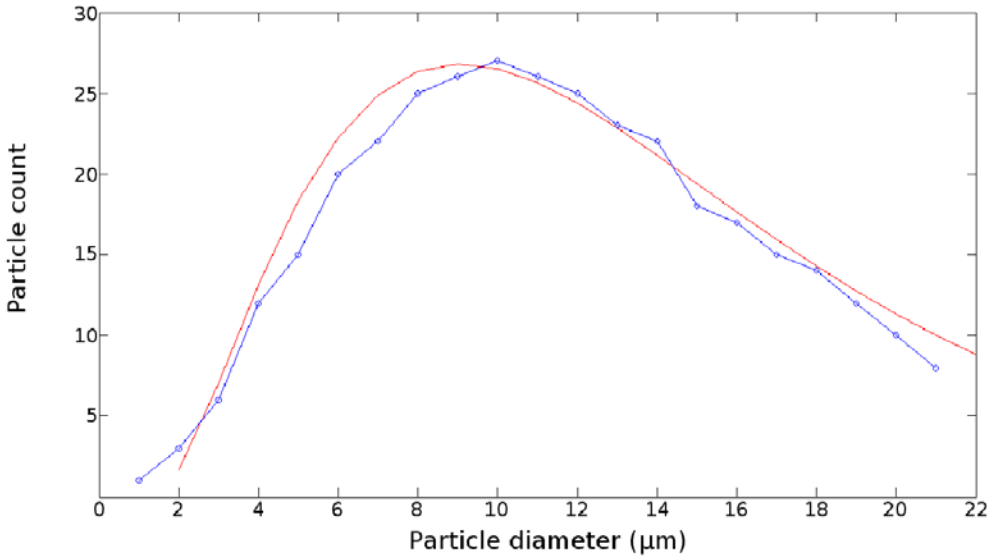

Figure 7.10: Distribution of resulting particle diameters from the 250µm particle (Koutsakis, Shrimpton, & Gu, 2016).

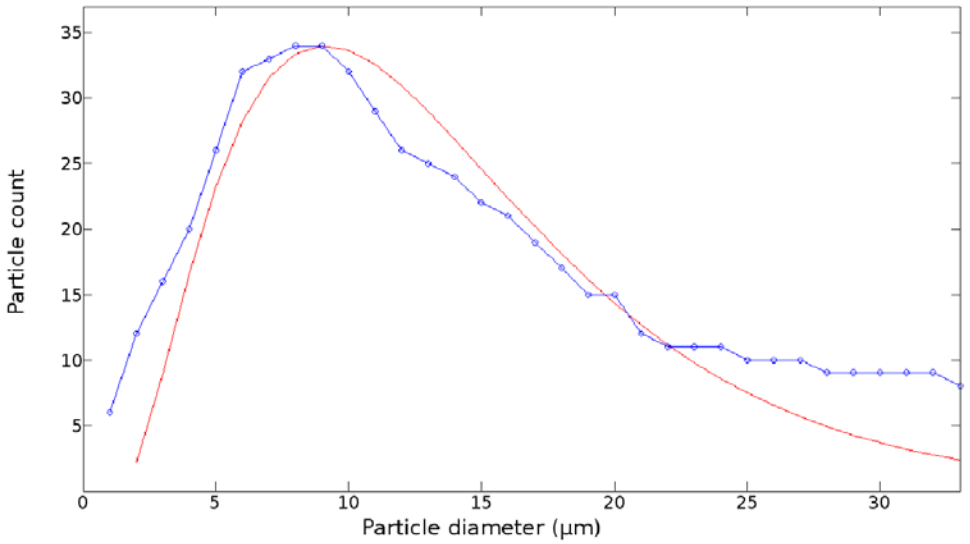

Figure 7.11: Distribution of resulting particle diameters from the 500µm particle (Koutsakis, Shrimpton, & Gu, 2016).

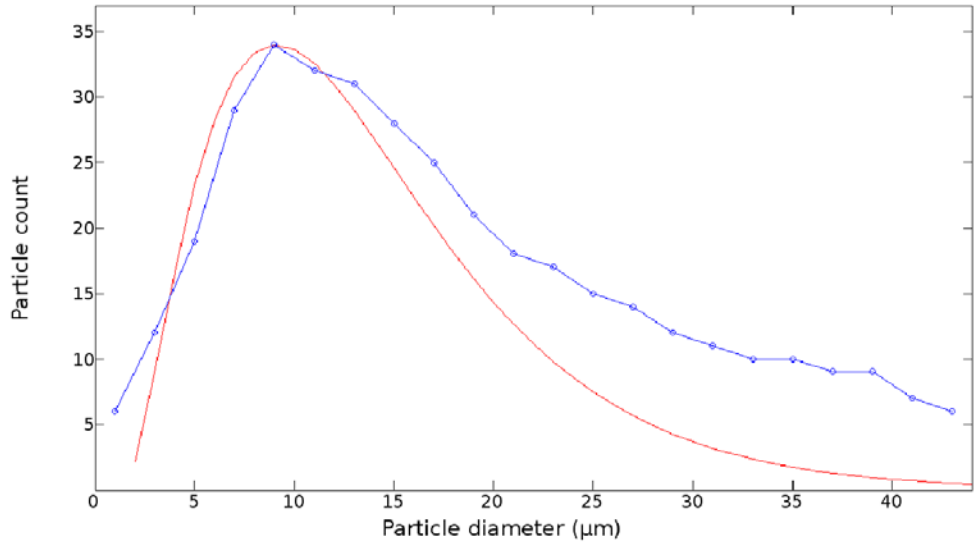

Figure 7.12: Distribution of resulting particle diameters from the 1000µm particle (Koutsakis, Shrimpton, & Gu, 2016).

7.5 Discussion

The copper particle is always stationary in the starting time of the simulation, while the argon flow has a velocity of $400m/s$, hence the Particle Reynolds numbers for the simulation are at the scale of 10^3 to 10^2, where the drag coefficient is smaller (~ 0.4) compared to cases with a lower Re. The particles exhibit Weber numbers that indicate boundary layer stripping atomization patterns, which is the case in the simulation as well. This in one hand is explained by the high Reynolds numbers and on the other hand by the very large differences in the viscosities and densities of each phase. The particles are deformed and stripped by the flow, while as a whole they move slowly and smaller atomized particles with lower Weber numbers are entrained and reach the outlet quickly. Also, the primary atomization patterns observed are explained by the fact that the velocity drops significantly behind the particles, as their surfaces act as obstacles to the flow (Figs. 7,9,11). This enables them to demonstrate boundary layer stripping and the long crown tips resulting from the stripping have lower velocities and smaller diameters, so patterns of primary atomization of round jets are expected and indeed observed. Another aspect which is essential to the establishment of the particular atomization patterns is the fact that the particles are not entrained by the flow as they do not move, as a whole, as fast as the gas phase towards the outlet. This fact combined with the fact that pressure gradients appear before and after the particle, causes particle deformation and the first atomised particles extrude from the edges of the crown deformation the particle assumes. For this effect, the large difference in densities is of most importance as copper is a lot denser than argon and the gas does not penetrate the liquid, but it skims it from its sides. To summarize the effect, it is the particle deformation by a high speed flow combined with its inertia and surface tension that produce the atomized particles.

The range of Reynolds and Weber numbers observed in the simulations are from particles of sizes from 55µm to 180µm for the atomised particles exhibiting velocities from 0m/s to 380m/s. Similar values for the non-dimensional numbers can be observed in other applications involving atomisation of liquid sprays, like fuel injection. The model with adequately fine meshing can potentially be altered to provide useful data for such applications as well (2.4).

Finally, the agreement of the resulting particle size distributions to the Rosin-Rammler distribution validates the simulations and demonstrates the value of the latter in predicting such distributions, especially in smaller particles that are produced. It can be concluded that CFD using VOF can be an adequate tool in gas atomization of liquids with applications to thermal spraying processes that use liquid metals. The work on this area can be extended by the addition of the heat transfer in a coupled solver in order to include the effects of temperature gradients in the overall flow and their effects on the atomization of particles.

Chapter 8: Conclusions

The three models which were presented produce data for three main stages of the plasma spraying process and provide details of the properties that affect and control the gas flow generation in the nozzle, the in fly atomisation and the particle distributions resulting from the process. The models in Chapters 6 and 7 could also be used for splat formation by setting a wall boundary condition in the outlet. The model described on Chapter 7 provides good agreement with an empirical distribution for a similar process as discussed in Section 7.5. The model on Chapter 6 compares well with experimental data and literature (Section 6.4.1). The model on Chapter 5 shows agreement with literature and while its velocity results are higher than the thermal compressible model (Section 6.4), they are at the same order of magnitude. Based on this, the MHD model (Section 5.6) supports the selection of inlet velocities for the subsequent models (Sections 6.3.1 and 7.3.1). It can enable further study of electromagnetic properties in the nozzle considering the dielectric of different materials.

In general, 3D models can provide a complete overview of a thermal spraying process, if the controlling parameters can be clearly identified and the process is separated in sub-processes that are considered as units. The same can be applied in plasma spraying process, provided it is divided into focus areas such as the ones described by the three models of this work. The theoretical background is indeed established and the current theoretical models can be adequate to give numerical simulations that produce accurate results and stand tests of experimental comparison. The plasma flow in the plasma spraying process can be studied individually, or with the interactions with liquid metal droplets, while ceramics and other materials can be studied in the

future provided their thermophysical and transport properties for all their states can be acquired by experimental data. The behaviour of the plasma arc can also be studied, but its formation produces extremely large gradients in the associated quantities, hence numerical stability and demanding mesh sizes are still issues to be considered carefully. Additionally, the mechanisms of interactions describing plasma take into account many parameters, since its formation is a result of complex phenomena. In this sense, plasma interactions cannot be described in a way that makes modelling an easy task. It can be claimed that individual metal droplets and additional dielectric presence have an effect on the plasma arc, but it may be worth investigating the effect of continuous feed of liquid metal in various streams and gun configurations, as the metal can condense the electric field, producing thicker lines, thus keeping its energy localised.

A tool like OpenFOAM which provides a programming formulation closely resembling the mathematical one can be useful for the engineering researcher. It provides the ability to add physical properties and the connections between them in a way that someone from a science or engineering background is familiar with, but this is only one step in the code development. Considering the amount of quantities that need to be defined analytically or by reference in this CFD programming framework, the analytical representation of the conservation equations can be superficial benefit, as strong programming skills are also required. Furthermore, the more variables added, the more the complexity of the solution increases. Each additional property needs to be quantified by either experimental data, which can be hard to obtain and laborious to put into data types that the solver can read, or by numerical solutions per quantity, which stress the solver more.

The use of databases with electrophysical properties of plasma can provide a very useful addition in CFD plasma models (Section 5.4). Its experimental derivation provides a direct injection of the properties that are then interpolated, thus reducing significantly computational complexity, furthermore computation time. This simplification can make models less complex and more understandable from the human point of view, without the need for analytical solutions, which require additional study and increase the chance of error.

If the mechanisms of the arc formation and sustainment can be theoretically expressed in a concise way, the properties of the arc radius and length can be simulated. Optimisations of the gun nozzle can be achieved too, by taking into account electromagnetic properties for optimised velocity and the shape and length of the electric arc.

Chapter 9: Suggestions for Further Work

As discussed earlier, modelling approaches always try to benefit from the latest technologies and theoretical tools at disposal. For the benefit of advancing the modelling capabilities for the plasma spraying process, some suggestions for future work will follow.

The experimental measurement of electrophysical properties of gases and enhancement of current databases will enable their interpolated use and reduce computational time in simulations like the ones carried through for the current work (Section 5.4, Chapter 8). The need for expanded thermodynamic tables also falls into this recommendation. Currently JANAF tables go as high as $6000K$ and the thermodynamic properties for various substances can be obtained by other individual experimental research. Data of such results is not always easy to obtain as the sources may be scattered and combination becomes an issue, since they may not always agree with each other, while the boundary values may also differ. It is important for research teams and institutions to have access to individual databases with properties they may require and to contribute references and sources in their respectful teams and institutions. As tables with thermodynamic properties are expanded, more gases and mixes of gases can be studied with the same models. This can be a next step in analysing the thermal spraying processes with the current tools, but using newly acquired properties.

A useful modelling tool would be an alternative method of determining plasma temperature. If the plasma has a unique temperature and based on this, approximations are applied on thermophysical and temperature dependent properties, modelling would be simplified.

Approximations in the form of analytical equations for heat transfer coefficients may provide an adequate relief in demanding computations. The benefit though, will only be achieved if the equations are simple. It is also worth noting that the use of more than one formula for the description of one property, where each formula applies to a sub-domain of definition of the function may be useful, but requires careful programming in CFD. It also adds additional conditions for the boundaries, which may lead to numerical instabilities.

If the arc behaviour for the radius and length can be simulated, optimisations of the gun nozzle can be produced taking into account electromagnetic properties for optimised velocity and electric arc shape and length.

Finally, as complexity in solutions is ever-increasing, the scope of each solver and its computational complexity may need to be quantified in order to be able to identify if the computational solution is viable with the computational power at the disposal of the researcher. Nowadays, solvers are measured in thousands of lines of code and are usually inherited, maintained and developed in research groups as legacy code for many years. The number of Lines of code is used as a programming metric quantity for complexity, but generally the models that have been used for complexity from code metrics have not provided accurate quantification of the defects and quality of the solution (Fenton & Neil, 1999). The addition of various programming tools and methods like abstraction, object orientation, inheritance, source control, versioning, etc, provide different degrees of usability and performance in the solvers, but may have a very steep learning curve for an engineer, even for simple models. It is also possible for a model to be developed and be numerically complete, but its solution to require a long time or a very dense mesh that had not been initially foreseen in the

design. A quantifiable solver complexity versus domain complexity may sound like the solution to this problem. But the quantification of complexities is a new science of its own and accurate metrics have not been found, at least for the computational solution. With this in mind, it is still dependent on the researcher's experience and capability to identify the properties that will play a significant part in the model and cater for them, in order to produce a model that serves its purpose: the accurate calculation and prediction of the physical phenomena it represents.

List of References

Amsden, A. A. (1966). *The Particle-in-Cell Method for Calculation of the Dynamics of Compressible Fluids.* Los Alamos: Los Alamos Scientific Laboratory report LA-3466.

Belmont, G., Grappin, R., Mottez, F., Pantellini, F., & Pelletier, G. (2013). *Collisionless Plasmas in Astrophysics.* Wiley-VCH.

Bobzin, K., Bagcivan, N., & Petkovic, I. (2011). Numerical and experimental determination of plasma temperature during air plasma spraying with a multiple cathodes torch. *Journal of Materials Processing Technology , 211* (10), 1620–1628.

Bolot, R., Coddet, C., Allimant, A., & Billieres, D. (2010). CFD modeling of the flow through the new proplasma HP gun. *Rencontres Internationales de Projection Thermique.* Lille, France.

Bolot, R., Coddet, C., Allimant, A., & Billieres, D. (2011). Modeling of the plasma flow and anode region inside a direct current plasma gun. *Journal of Thermal Spray Technology , 20*, 21-27.

Bolot, R., Planche, M.-P., Liao, H., & Coddet, C. (2008). A three-dimensional model of the wire-arc spray process and its experimental validation. *Journal of Materials Processing Technology , 200* (1-3), 94-105.

Brillo, J., & Egry, I. (2003). Density determination of liquid copper, nickel, and their alloys. *International Journal of Thermophysics , 24*, 1155.

Butler, T. D. (1964). Particle-in-Cell Fluid Dynamics on the IBM Stretch Machine. *Proc. Computer Appl. Symp. 9th.* Chicago: IIT Research Institute.

Caltagirone, J., Vincent, S., & Caruyer, C. (2011). A multiphase compressible model for the simulation of multiphase flows. *Computers & Fluids , 50* (1), 24-34.

Caruyer, C., S., V., Meillot, E., & Caltagirone, J. (2010). Modeling the First Instant of the Interaction Between a Liquid and a Plasma Jet with a Compressible Approach. *Surface and Coatings Technology* , 974-979.

CD-Adapco. (2015). Retrieved 2015 йил 11-May from Physics Documentation: http://www.cd-adapco.com/products/star-ccm%C2%AE/physics

CHAM Ltd. (2005). Retrieved 2015 йил 12-May from PHOENICS Overview, CHAM Technical Report: TR 001: http://www.cham.co.uk/phoenics/d_polis/d_docs/tr001/tr001.htm

Chang, C., & Ramshaw, J. (1994). Numerical simulation of nonequilibrium effects in an argon plasma jet. *Physics of Plasmas , 1*, 3698-3709.

Chang, J. a. (1992). Computational fluid dynamics modeling of multicomponent thermal plasmas. *Plasma Chem. Plasma Process , 12*, 299–325.

Chau, S., Hsu, K., Lin, D., Chen, J., & Tzeng, C. (2006). Modeling and experimental validation of a 1.2MW DC transferred well-type plasma torch. *Proceedings of the Conference on Computational Physics* (pp. 114-117). Computer Physics Communications.

Chen, X., & Li, H.-P. (2001). Heat transfer and and fluid flow in a high-intensity free-burning arc: an improved modeling approach. *International Journal of Heat and Mass Transfer , 44* (13), 2541-2553.

Chen., F. F. (1984). *Introduction to Plasma Physics and Controlled Fusion, Volume 1: Plasma Physics, second edition.* New York: Springer, second edition.

Choquet, I., Lucquin-Desreux, P., & Degond, B. (2007). A hierarchy of diffusion models for partially ionized plasmas. *Discrete and continuous dynamical systems. Series B , 8* (2), 735-772.

Colombo, V., Ghedini, E., & Sanibondi, P. (2008). Thermodynamic and Transport Properties in Non-Equilibrium Argon, Oxygen and Nitrogen Thermal Plasmas. *Progress in Nuclear Energy , 50* (8), 921-933.

Davis, J. (Ed.). (2004). *Handbook of Thermal Spray Technology.* Ohio: ASM International.

Dawson, J. (1962). One-dimensional plasma model. *Phys. Fluids , 5*, 445–459.

Delalondre, C., Simonin, O., Kaddani, A., & Zahrai, S. (1999). Three-dimensional modelling of unsteady high-pressure arcs in argon. *Journal of Physics D: Applied Physics , 28* (11), 2294.

Devoto, R. S. (1973). Transport coefficients of ionized argon. *Physics of Fluids , 16*, 616.

Dugdale, R. A. (1966). The application of the glow discharge to material processing. *Journal of Materials Science* , 160-169.

EDF R&D. (2015 йил April). Retrieved 2015 йил 14-May from Code Saturne version 4.0.0 practical user's guide: http://code-saturne.org/cms/sites/default/files/docs/4.0/user.pdf

Eldridge, O., & Feix, M. (1962). One-dimensional plasma model at thermodynamic equilibrium. *Phys. Fluids , 5*, 1076-1080.

Fauchais, P. (2004). Understanding plasma spraying. ,. *Journal of Physics D: Applied Physics , 37* (9), 86.

Fauchais, P., Coudert, J., Vardelle, M., Vardelle, A., & Denoirjean, A. (1992). Diagnostics of thermal spraying plasma jets. *Journal of Thermal Spray Technology , 1*, 117-128.

Fauchais, P., Montavon, G., Lima, R. S., & Marple, B. R. (2011). Engineering a new class of thermal spray nano-based microstructures from agglomerated nanostructured particles, suspensions and solutions: an invited review. *Journal of Physics D: Applied Physics* .

Fenton, N. E., & Neil, M. (1999). A Critique of Software Defect Prediction Models. *IEEE Transactions On Software Engineering , 25* (3), 1-15.

Garimella, S. V., Schlitz, L. Z., & Chan, S. H. (1999). Gas dynamics and electromagnetic processes in high-current arc plasmas - part i: Model formulation and steady-state solutions. *Journal of Applied Physics , 85* (5), 2540-2546.

Gedzevicius, I., & Valiulis, A. (2006). Analysis of wire arc spraying process variables on coatings properties. *Journal of Materials Processing Technology , 175* (1-3), 206–211.

Ghedini, E., Mentrelli, A., Bernardi, D., & Colombo, V. (2003). Three-dimensional modelling of inductively coupled plasma torches. *The European Physical Journal D - Atomic, Molecular, Optical and Plasma Physics , 22* (1), 119-125.

Greenshields, C. (2014, February 17). *OpenFOAM 2.3.0: Multiphase Modelling*. Retrieved November 11, 2016, from The OpenFOAM Foundation: http://openfoam.org/release/2-3-0/multiphase/

Guo, Z., Yin, S., Liao, H., & Gu, S. (2015). Three-dimensional simulation of an argon–hydrogen DC non-transferred arc plasma torch. *International Journal of Heat and Mass Transfer , 80*, 644–652.

Guo, Z., Yin, S., Qian, Z., Liao, H., & Gu, S. (2015). Effect of the deviation of the current density profile center on the three-dimensional non-transferred arc plasma torch. *Computers & Fluids , 114*, 163–171.

Harlow, F. H. (1957). *The Particle-in-Cell Method for Hydrodynamic Calculations.* Los Alamos: Los Alamos Scientific Laboratory report LA-2139.

Harlow, F. H. (1955). *The Particle-in-Cell Method: A combined Eulerian-Lagrangian computing method that is suitable for solving multimaterial problems involving large fluid distortions.* Los Alamos: Los Alamos Scientific Laboratory Report LAMS-1956.

Harlow, F. (1964). *Methods in Computational Physics* (Vol. 3). New York: Academic Press.

Harlow, F. (1963). The Particle-in-Cell Method for Numerical Solution of Problems in Fluid Dynamics. *Proc. Symp. Applied Mathematics 15* , 269.

Heiman, R. (2008). *Plasma Spray Coating, 2nd Edition.* Weinheim: WILEYVCH.

Herman, H., Berndt, C. C., & Wang, H. (1993). *Ceramic Films and Coatings.* Park Ridge, N.J.: Noyes Publications.

Hnat, B. (2015 йил 17-April). *Electrodynamics.* Retrieved 2015 йил 2-April from http://www2.warwick.ac.uk/fac/sci/physics/current/teach/module_home/px384/lecture_04.pdf

Huang, Y., L., S., X., L., Y., X., Y., W., J., C., et al. (2010). Hydroxyapatite coatings deposited by liquid precursor plasma spraying: controlled dense and porous microstructures and osteoblastic cell responses. *Biofabrication , 2* (4), 045003.

Hunt, J. (1998). Lewis Fry Richardson. His Contributions to Mathematics, Meteorology, and Models of Conflict. *Annual Review of Fluid Mechanics , 30*, xiii-xxxvi.

Iridis. (2015). Retrieved 11 11, 2016, from Computational Modelling Group - University of Southampton: http://cmg.soton.ac.uk/iridis

Joseph, D., Beavers, G., & Funada, T. (2002). Rayleigh-Taylor instability of viscoelastic drops at high Weber numbers. *Journal of Fluid Mechanics , 453*, 109.

Kang, C.-W., Tan, J. K., Pan, L., Low, C. Y., & Jaffar, A. (2011). Numerical and experimental investigations of splat geometric characteristics during oblique impact of plasma spraying. *Applied Surface Science , 257* (24), 10363–10372.

Karthikeyan, J., Berndt, C., Tikkanen, J., Reddy, S., & Herman, H. (1997). Plasma Spray Synthesis Of Nanomaterial Powders And Deposits. *Materials Science and Engineering A , 238* (2), 275-286.

Konstantinova, N. Y., Popel, P., & Yagodin, D. (2009). The kinematic viscosity of liquid copper-aluminum alloys. *High Temperature , 47*, 336.

Kortshagen, U. (1998). *Electron Kinetics and Applications of Glow Discharges.* New York: Springer Science & Business Media.

Koutsakis, K., Gu, S., & Vardelle, A. (2013). Three dimensional CFD simulation of liquid copper break up for the liquid precursor spraying. *Surface and Coatings Technology , 220*, 214-218.

Koutsakis, K., Shrimpton, J., & Gu, S. (2016). Multiphase Numerical Modelling in Plasma Spraying Processes atomization in argon flow. *(Submitted to) Atomization and Sprays* .

Kuper, A., Lazarus, D., Manning, J., & Tomizuka, C. (1956). Diffusion in ordered and disordered copper-zinc. *Physical Review , 104*, 1536.

Lawrence Snyder, L. H. (Ed.). (1985). *Algorithmically Specialized Parallel Computers.* Academic Press.

Lebouvier, A., Delalondre, C., Fresnet, F., Boch, V., & Rohani, V.-J. (2011). Three-Dimensional Unsteady MHD Modeling of a Low-Current High-Voltage Nontransferred DC Plasma Torch Operating With Air. *IEEE Transactions on Plasma Science, Institute of Electrical and Electronics Engineers (IEEE) , 39* (9), 1889-1899.

Leiserson, C. E., Stein, C., Rivest, R., & Cormen, T. H. (2009). *Introduction to Algorithms.* Cambridge, MA: MIT Press.

Liu, B., Zhang, T., & Gawne, D. (2000). Computational analysis of the influence of process parameters on the flow field of a plasma jet. *Surface and Coatings Technology , 132* (2-3), 202–216.

Maitland, G., & Smith, E. (1972). Critical reassessment of viscosities of 11 common gases. *Journal of Chemical and Engineering Data , 17*, 150.

Marchand, C., Vardelle, A., Mariaux, G., & Lefort, P. (2008). Modelling of the Plasma Spraying Process with Liquid Feedstock Injection. *Surface and Coatings Technology , 202*, 4458-4464.

Mariaux, G., & Vardelle, A. (2005). 3-D time-dependent modelling of the plasma spray process. part 1: flow modelling. *International Journal of Thermal Sciences , 44*, 357-366.

Matsumoto, T., Fujii, H., Ueda, T., Kamai, M., & Nogi, K. (2005). Measurement of surface tension of molten copper using the free-fall oscillating drop method. *Measurement Science and Technology , 16*, 432.

Matula, R. A. (1979). Electrical resistivity of Copper, Gold, Palladium and Silver. *Journal of Physical and Chemical Reference Data , 8* (4), 1147-1298.

Medlin, A., Morrowb, R., & Fletchera, C. (1998). Calculation of monopolar corona at a high voltage DC transmission line with crosswinds. *Journal of Electrostatics , 43* (1), 61–77.

Meillot, E., Damiani, D., Vincent, S., Caruyer, C., & Caltagirone, J. (2012). Analysis by modeling of plasma flow interactions with liquid injection. *Surface and Coatings Technology , 220*, 149-156.

Meillot, E., Damiani, D., Vincent, S., Caruyer, C., & Caltagirone, J. (2010). Analysis of the unsteadiness of a plasma jet and the related turbulence. *Surface & Coatings Technology* , 165-1170.

Meillot, E., Damiani, D., Vincent, S., Caruyer, C., & Caltagirone, J. P. (2013). Analysis by modeling of plasma flow interactions with liquid injection. *Surface and Coatings Technology , 220*, 149-156.

Moini-Yekta, S., Barad, M. F., Sozer, E., Brehm, C., Housman, J. A., & Kiris, C. C. (2013). Verification and Validation Studies for the LAVA CFD Solver. *21st AIAA Computational Fluid Dynamics Conference.* San Diego, California: American Institute for Aeronautics and Astronautics.

Mostaghimi, J., Chandra, S., Ghafouri-Azar, R., & Dolatabadi, A. (2003). Modeling thermal spray coating processes: a powerful tool in design and optimization. *Surface and Coatings Technology , 163-164*, 1-11.

Murphy, A. B., & Kovitya, P. (1993). Mathematical model and laser scattering temperature measurements of a direct current plasma torch discharging into air. *Journal of Applied Physics , 73* (10), 4759-4769.

Nasr, G., Yule, A. J., & Bendig, L. (2002). *Industrial Sprays and Atomization: Design, Analysis and Applications* (1 ed.). Springer-Verlag.

Ning, W. (2007). Development of a Next-generation Spray and Atomization Model Using an Eulerian-Lagrangian Methodology. *PhD Thesis* . Madison: University of Wisconsin.

OpenCFD. (2010). *OpenFOAM, The Open Source CFD Toolbox,User Guide, (2010),*. Retrieved 2011 йил 10-March from OpenFOAM: http://foam.sourceforge.net/docs/Guides-a4/UserGuide.pdf

Oran, E. (1992). Reactive-flow computations on a massively parallel computer. *Fluid Dynamics Research , 10* (4-6), 251.

Park, S. H., Kim, H. J., & Lee, C. S. (2009). Experimental and numerical analysis of spray-atomization characteristics of biodiesel fuel in various fuel and ambient temperatures conditions. *International Journal of Heat and Fluid Flow* , 960-970.

Park, S. H., Youn, I. M., Lim, Y., & Lee, C. S. (2013). Influence of the mixture of gasoline and diesel fuels on droplet atomization, combustion, and exhaust emission characteristics in a compression ignition engine. *Fuel Processing Technology* , 392-401.

Park, S. W., Kim, S., & Lee, C. S. (2006). Breakup and atomization characteristics of mono-dispersed diesel droplets in a cross-flow air stream. *International Journal of Multiphase Flow , 32* (7), 807–822.

Park, S. W., Kim, S., & Lee, C. S. (2006). Breakup and atomization characteristics of mono-dispersed diesel droplets in a cross-flow air stream. *International Journal of Multiphase Flow* , 807-822.

Pawlowski, L. (2009). Suspension and solution thermal spray coatings. *Surface and Coatings Technology* , 2807–2829.

Pawlowski, L. (1995). *The science and engineering of thermal spray coatings.* Wiley.

R. Turner, E. D. (1973). Compressibility and partial structure factors in the zero-wavevector limit of liquid copper-tin alloys,. *Journal Physics C: Solid State Physics , 6*, 3359.

Ramshaw, J., & Chang, C. (1992). Computational fluid dynamics modeling of multicomponent thermal plasmas. *Plasma Chemistry and Plasma Processing , 12*, 299–325.

Ranger, A., & Nicholls, J. (1972). Atomization of liquid droplets in a convective gas stream. *International Journal of Heat and Mass Transfer , 15*, 1203.

Rat, V., Pascal, A., Aubreton, J., Elchinger, M., Fauchais, P., & Vacher, D. (2002). Transport coefficients including diffusion in a two-temperature argon plasma. *Journal of Physics D , 35*, 981-991.

Rat, V., Pascal, A., Aubreton, J., Fauchais, P., Elchinger, M., & Lefort, A. (2001). Transport properties in a two-temperature plasma: Theory and application. *Physical Review E (Statistical, Nonlinear, and Soft Matter Physics) , 64*.

Rehmet, C., Rohani, V., Cauneau, F., & Fulcherind, L. (2013). 3D Unsteady State MHD Modeling of a 3-Phase AC Hot Graphite Electrodes Plasma Torch. *Plasma Chemistry and Plasma Processing , 33* (2), 491-515.

Rein, M. (Ed.). (2002). *Drop-Surface Interactions* (1 ed.). Springer-Verlag.

Restelloa, S., Boscarino, D., & Rigato, V. (2006). A study of Ti–C–N(H) and Ti:CNx(H) coatings grown with a magnetron sputtering/PECVD hybrid deposition process. *Surface and Coatings Technology* , 6230–6234.

Richard, P. (2011). Efficient Control of Thermal Spray Dust Collectors - Ensuring Operational Gains and Cost Savings. *Spraytime , 18* (2), 1-6.

Rosin, P., & Rammler, E. (1933). The Laws Governing the Fineness of Powdered Coal. *Journal of the Institute of Fuel , 7*, 29-36.

Rusche, H. (2002). Computational Fluid Dynamics of Dispersed Two-Phase Flows at High Phase Fractions. *PhD Thesis* . London: Imperial College of Science, Technology and Medicine.

Rutscher, A. (1982). *Plasmatechnik, Grundlagen und Anwendungen. Eine Einfuhrung.* Munchen, Wien: Carl Hanser-Verlag.

SAS IP, I. (2013). Retrieved 2015 *йил* 12-May from ANSYS Inc. PDF Documentation for Release 15.0: http://148.204.81.206/Ansys/readme.html

Sass-tisovskaya, M. (2009). Plasma Arc Welding Simulation with OpenFOAM. *THESIS FOR THE DEGREE OF LICENTIATE OF ENGINEERING* . Goteborg, Sweden: Chalmers University of Technology.

Selvan, B., & Ramachandran, K. (2009). Comparisons between two different three-dimensional arc plasma torch simulations. *Journal of Thermal Spray Technology, , 18*, 846-857.

Selvan, B., Ramachandran, K., Sreekumar, K., Thiyagarajan, T., & Ananthapadmanabhan, P. (2009). Numerical and experimental studies on DC plasma spray torch. *Vacuum , 84* (4), 444-452.

Shan, Y., Coyle, T., & Mostaghimi, J. (2007). 3D Modeling of Transport Phenomena and the Injection of the Solution Droplets in the Solution Precursor Plasma Spraying. *Journal of Thermal Spray Technology , 16* (5), 736-743.

Smagorinsky, J. (1963). General Circulation Experiments with the Primitive Equations. *Monthly Weather Review , 91*, 99–164.

Sturrock, P. A. (1994). *Plasma Physics: An Introduction to the Theory of Astrophysical, Geophysical & Laboratory Plasmas. .* Cambridge: Cambridge University Press.

Su, T. F., Patterson, R. D., Reitz, R. D., & Farrell, P. (1996). , 1996. Experimental and numerical studies of high pressure multiple injection sprays. *SAE Technical Paper 960861* .

Suryanarayanan, R. (Ed.). (1993). *Plasma spraying: Theory and applications.* World Scientific Publishing Co Pte Ltd.

Tien, P. K., & Moshman, J. (1956). Monte Carlo calculation of noise near the potential minimum of a high-frequency diode. *J. Appl. Phys. , 27*, 1067–1078.

Trelles, J., Chazelas, C., Vardelle, A., & Heberlein, J. (2009). Arc plasma torch modeling. *Journal of Thermal Spray Technology , 18*, 728-752.

Turner, R., Crozier, E. D., & Cochran, J. F. (1973). Compressibility and partial structure factors in the zero-wavevector limit of liquid copper-tin alloys. *Journal of Physics C: Solid State Physics , 6*, 3359.

Ubbink, O., & Issa, R. (1999). A method for capturing sharp fluid interfaces on arbitrary meshes. *Journal of Computational Physics , 153* (1), 26-50.

Utsumi, T., Kunugi, T., & Koga, J. (1998). A numerical method for solving the one-dimensional Vlasov-Poisson equation in phase space. *Computer Physics Communications , Volume 108* (2–3), 159-179.

Waelbroeck., R. D. (1998). *The framework of plasma physics, first edition.* Scranton, Pa: Westview Press.

Wan, Y., & al., e. (2003). An advanced model for plasma spraying of functionally 294 graded materials. *Journal of Materials Processing Technology , 110*, 137.

Wana, Y., Sampatha, S., Prasada, V., Williamson, R., & Fincke, J. (2003). An advanced model for plasma spraying of functionally graded materials. *Journal of Materials Processing Technology , 137* (1-3), 110-16.

Westhoff, R., & Szekely, J. (1991). A model of fluid, heat flow, and electromagnetic phenomena in a nontransferred arc plasma torch. *Journal of Applied Physics , 70* (7), 3455-3466.

Wolfendale, M. J., & Bluck, M. J. (2015). A coupled systems code-CFD MHD solver for fusion blanket design. *Fusion Engineering and Design,* .

Xiong, H. (2004). Three-dimensional simulation of plasma spray: effects of carrier gas flow and particle injection on plasma jet and entrained particle behavior. *International Journal of Heat and Mass Transfer , 47* (6), 5189-5200.

Zeng, W., Xu, M., Zhang, G., Zhang, Y., & Cleary, D. J. (2012). Atomization and vaporization for flash-boiling multi-hole sprays with alcohol fuels. *Fuel* , 287-297.

Zeoli, N., & Gu, S. (2006). Numerical modelling of droplet break-up for gas atomisation. *Computational Materials Science , 38*, 282.

Zhang, T., Gawne, D., & Liu, B. (2000). Computer modelling of the influence of process parameters on the heating and acceleration of particles during plasma spraying. *132* (2-3), 233-243.

Zhao, Y., Grant, P., & Cantor, a. B. (2000). Modelling and experimental analysis of vacuum plasma spraying. Part II: prediction of temperatures and velocities of plasma gases and Ti particles in a plasma jet. *Modelling and Simulation in Materials Science and Engineering , 8*, 515-540.

Bibliography

Harlow, F. (1964). *Methods in Computational Physics* (Vol. 3). New York: Academic Press.

Heiman, R. (2008). *Plasma Spray Coating, 2nd Edition.* Weinheim: WILEYVCH.

Nasr, G., Yule, A. J., & Bendig, L. (2002). *Industrial Sprays and Atomization: Design, Analysis and Applications* (1 ed.). Springer-Verlag.

OpenCFD. (2010). *OpenFOAM, The Open Source CFD Toolbox,User Guide, (2010),*. Retrieved March 10, 2011, from OpenFOAM: http://foam.sourceforge.net/docs/Guides-a4/UserGuide.pdf

Pawlowski, L. (1995). *The science and engineering of thermal spray coatings.* Wiley.

Rein, M. (Ed.). (2002). *Drop-Surface Interactions* (1 ed.). Springer-Verlag.

Waelbroeck., R. D. (1998). *The framework of plasma physics, first edition.* Scranton, Pa: Westview Press.